[American Journal of Science, Vol. 322, June, 2022, P. 729–794, DOI 10.2475/06.2022.01]

American Journal of Science

JUNE 2022

A GIANT SAND INJECTION COMPLEX: PROCESSES AND IMPLICATIONS FOR BASIN EVOLUTION AND SUBSURFACE FLUID FLOW

MARIO VIGORITO*,†, ANDREW HURST**, ANTHONY J. S. SCOTT***, OLIVIER STANZIONE§, and ANTONIO GRIPPA**,§§

ABSTRACT. **Giant sand injection complexes form, intricate, basin-scale fluid plumbing systems and document the remobilisation and intrusion of several tens of cubic kilometres of sand within the shallow crust in stratigraphic units 100's metres thick. This is the first detailed and extensive account of the Panoche Giant Injection Complex (PGIG), a regionally significant outcrop (>300 km^2) and part of a larger subsurface development (>4000 km^2) identified in boreholes and on seismic reflection data. Magnificent exposure of the PGIC occurs along the north western margin of the San Joaquin Valley and presents the opportunity to examine the regional geological significance of a giant sand injection complex and its origin in the context of a late Cretaceous – early Paleocene forearc basin. Between 25 and 49 km^3 of sand were remobilised and injected, at least 0.35 km^3 of which extruded onto the paleo-seafloor. Large sandstone intrusions often >10 m thick and laterally extensive on a kilometer scale formed saucer-shaped intrusions, wing-like intrusions and a variety of sill geometries along with volumetrically smaller randomly oriented dikes in a 200–300 m thick interval. Dikes prevail below and above this interval, some reaching the paleo seafloor and extruding sand. Networks of propagating hydrofractures form intensely brecciated host strata, some of which were intruded by sand. All intrusions formed in a single pulsed event in which the most intense hydrofracturing caused by supra-lithostatic fluid pressure occurred approximately 600 to 800 m below the paleo seafloor. A crudely orthogonal arrangement of dikes is preserved with most oriented normal, and less commonly oriented parallel to the oceanic trench associated with the late Mesozoic to early Tertiary North Pacific subduction. Dikes orthogonal to the trench opened against the minimum horizontal stress, which was parallel to the trench. Dikes parallel to the trench opened against the regional maximum horizontal stress along minor faults formed in extension caused by shallow crustal deformation. There is no evidence that compressional tectonics influenced the onset of elevated pore fluid pressure necessary to promote sand injection. However, tectonic compression was responsible for creating the basin physiography that locally increased subsidence and accelerated chemical diagenesis in the basin centre. PGIC outcrop, located along the basin margins, was unlikely to have experienced heating above 70 °C, equivalent about 2 km burial, so the effects of chemical diagenesis in the host strata of the injection complex had negligible potential to evolve significant pore water volume. In a deeper part of the basin approximately 150 km to the south, lateral equivalents of the host strata were subjected to heating >100 °C and would expel significant volumes of water displaced by quartz cementation**

* Equinor ASA, Exploration Norway, EXP EE GCQ – ST-FV C3, Forus, Stavanger, Norway
** University of Aberdeen, Department of Geology & Petroleum Geology, King's College, Aberdeen, AB24 3UE, United Kingdom
*** EquinorASA, Reservoir Modeling, PTEC OSL GGP - ST-FV C4, Forus, Stavanger, Norway
§ Task Fronterra Geoscience Ltd, Suit F, Kettock lodge, Aberdeen Innovation Park, Campus two, Balgownie Drive, Bridge of Don, Aberdeen, AB22 8GU, United Kingdom
§§ Aker BP ASA, Jåttåvågveien 10, Hinna Park, 4020 Stavanger, Norway
† Corresponding author: mavig@equinor.com

and clay dehydration that caused lateral pressure transfer to the north and western margin of the basin where the PGIC formed. Estimates of the total volume of water expelled from the deep basin suggest that a fluid volume equivalent to a gross rock volume reduction <1% would have provided a fluid budget sufficient to fluidise and inject the sand that forms the PGIC. In terms of areal and vertical extent, volume and architecture the PGIC shares strong similarity with the regionally developed giant injectite systems of Tertiary age in the North Sea basin. In both cases regional sand injection is genetically linked to pressure transfer toward the basin margin from more rapidly subsiding basin centres. Aqueous fluid is derived from thermally driven chemical diagenesis of thick deep water clastic sandstone and smectitic mudstone or from deeper, stratigraphically older, aquifers.

Key words: sandstone intrusions, sandstone extrusions, overpressure, regional hydrofracturing, seal by-pass, basin-scale fluid flow, paleostress

INTRODUCTION

This is the first detailed documentation of extensive outcrop of a giant sand injection complex and its extension in subsurface. Giant sand injection complexes are arguably one of the least documented basin-scale geological features of the shallow crust. Despite sandstone intrusions being recognised in Geology's formative years (Murchison, 1827), their regional scale and significance were largely unrecognised until found to contain economically significant volumes of hydrocarbons (Newman and others, 1993; Dixon and others, 1995; Hurst and Cartwright, 2007 and papers therein). Sandstone intrusions in the mudstone-dominated Hareelv Formation, Greenland (Upper Jurassic) were the first example of outcrop described as a sand injection complex (Surlyk and Noe-Nygaard, 2003); sandstone intrusions are ubiquitous wherever the Hareelv Formation outcrops in an area of ~3,850 km^2 (personal communication, Finn Surlyk, 2021). Areal variations of the thickness and internal architecture of the Hareelv injection complex, presence of extrusive sandstone (*sensu* Hurst and others, 2006) and the volume of sand injected, are unknown. Giant sand injection complexes are identified on three-dimensional seismic data from the Paleogene strata in the North Sea where they extend over thousands of square kilometres (Huuse and Mickelson, 2004; Shoulders and Cartwright, 2004; Løseth and others, 2013) and may crosscut hundreds of meters of stratigraphic section (Duranti and others, 2002; Jackson, 2007; Wild and Briedis, 2010). Sand injection complexes are however recognised from many sedimentary basins and environments globally both in the subsurface and at outcrop (Braccini and others, 2008; Huuse and others, 2010; Hurst and others, 2021a) and their geological significance is worthy of more detailed analysis.

A priori knowledge of the PGIC includes: 1) concomitant presence of clastic sills and dikes, the latter forming two dominant sets striking ENE-WSW and NNW-SSE (Smyers and Peterson, 1971; Weberling, ms, 2002, Vétel and Cartwright, 2010; Vigorito and Hurst, 2010); 2) that sand injection was a single pulsed event (Vigorito and others, 2008; Vétel and Cartwright, 2010; Vigorito and Hurst, 2010); 3) sandstone intrusions form a pervasive architecture in which most intrusions and most sandstone occur in a sill zone, which is underlain by a lower dike zone and overlain by an upper dike zone, comprising an intrusive complex (Vigorito and others, 2008; Vigorito and Hurst, 2010); 4) sand extruded onto a paleo-seafloor during the Danian (Vigorito and others, 2008; Hurst and others, 2011); 5) the PGIC sandstone was derived from multiple sandstone channels and channel complexes most of which occur in the middle section of the injection complex where both density of intrusions and volume of injected sandstone are the largest (Vigorito and Hurst, 2010; Scott and others, 2013; Hurst and others, 2017); 6) fluid to support hydrofracture and sand fluidisation was derived from the regionally extensive, thick sandstone prone fan-systems located

deeper in the section (Vigorito and Hurst, 2010). These characteristics are common to other giant injection complexes that occur in often similar sedimentary settings but in a broad range of tectonic settings, not exclusively in forearc basins. For example injection complexes are described from rift basins (Surlyk and others, 2007); intracratonic basins (Huuse and others, 2004; Briedis and others, 2007); forearc basins (Serie and Pemberton, 2021) and passive margins (Ravier and others 2015).

Mechanisms by which regional development of sand injection occurs are poorly constrained and diverse, although recognising that hydrofracturing and sand fluidisation are integral processes (Hurst and others, 2011). Defining how hydrofracture and sand fluidisation occur on a regional scale, and defining the genetic causes and controls is more problematic. A specific goal is to evaluate the influence of regional tectonics, specifically compressional tectonics associated with the North America – Pacific subduction margin, on the evolution of pore fluid pressure that in earlier work was considered a key factor in sustaining overpressure in the San Joaquin Basin (Berry, 1973 and Palladino and others, 2016) and similar strata in the nearby Sacramento Valley (McPherson and Garven, 1999). While some earlier studies proposed that the emplacement of the PGIC occurred under no imposed tectonic stress and did not provide any explanation for overpressure build-up (Vétel and Cartwright, 2010), more recent studies argued for the formation of the PGIG to be genetically linked to subduction-driven overpressure (Palladino and others, 2016). However, outcrop and subsurface data show that compressional structuration in this part of the forearc basin preceding and during emplacement of the PGIC was minor (McGuire, ms, 1988a; Bartow, 1996; Mitchell and others, 2010).

In contrast with previous studies, we infer that thermal diagenesis combined with lateral pressure transfer had a key role in elevating pore fluid pressure thus leading to basin-scale hydrofracturing and injection. In support of our hypothesis, detailed mapping and description of the entire PGIC outcrop is integrated with borehole data from the San Joaquin Valley together with existing regional (Ingersoll, 1979; Hosford Scheirer, 2007) and mineralogical data (Ramseyer and Boles, 1986; Imperato and Nilsen, 1990; Wilson and others, 1999; Hurst and others, 2017, 2021b), seismic data (Mitchell and others, 2010; Bureau and others, 2014), and basin modeling studies (Hosford Scheirer, 2007; Peters and others, 2008) to capture regional- and local-scale influences on formation of the PGIC. Although much of the outcrop area lacks evidence of significant heating since deposition (Hurst and others, 2017; Hurst and others, 2021b, 2021c) and chemical (thermally driven) diagenesis is minimal, in adjacent subsurface areas mudstone and sandstone in similar formations underwent significant chemical diagenesis (Ramseyer and Boles, 1986; Imperato and Nilsen, 1990; Wilson and others, 1999) with attendant changes in porosity and expulsion of pore fluid. Investigation herein of the distribution and burial history of the more thermally mature formations and their relevance to formation of the PGIC is original and quantitative.

Physical conditions for hydrofracturing, sand fluidization and injection are described and related to the geometry and distribution of regionally developed sandstone intrusions (Jolly and Lonergan, 2002, Vigorito and Hurst, 2010; Vétel and Cartwright, 2010; Hurst and others, 2011, Cobain and others, 2015). With the possible exception of the Hareelv Formation (Surlyk and Noe-Nygaard, 2003; Surlyk and others, 2007), other contemporary study of outcrop of injection complexes are relatively small-scale, rarely more than a few square kilometres in extent (Hurst and others, 2021a). Consequently, the regional, even local, geological context is inevitably conjectural. Because genetic and spatial relationships between parent units, an intrusive complex and an extrusive complex are numerous in the PGIC, variation in the geometry and architecture of sandstone intrusions can be related directly to the

evolution of pressure in fluidized sand during injection (Vigorito and Hurst, 2010). With reference to the combination of detailed outcrop analysis with regional data in quantitative basin modeling (Hosford Scheirer, 2007; Hosford Scheirer and Magoon, 2007a; Peters and others, 2008), evidence is evaluated for the existence and operation of the regionally developed pressure cells that drove regional hydrofracturing and sand injection. To the best of our knowledge a similar quantitative approach is not previously undertaken in the context of sand injection. Chemical diagenesis during basin fill and subsidence is investigated as an agent for the fluid expulsion and lateral transfer that triggered formation of the PGIC. This is compared with evidence for derivation of overpressure from compressional tectonics associated with active subduction to the west of the study area. Identification of the key controls of pore fluid pressure generation enables development of genetic models that, by comparison with other outcrop analogues, are globally applicable.

A different major topic of debate are the mechanical and fluid-dynamic controls on the distribution and both external and internal geometry of sandstone intrusions (Jolly and Lonergan, 2002; Duranti and Hurst, 2004; Diggs, 2007; Surlyk and others, 2007; Scott and others, 2009, Kane, 2010; Vétel and Cartwright, 2010; Hurst and others, 2011; Cobain and others, 2015; Hurst and Vigorito, 2017). Models are proposed that link *in situ* stress (and burial) to fracture opening mode (Cobain and others, 2015) and to the distribution and geometry of specific intrusive elements (for example, dikes and sills; Jolly and Lonergan, 2002; Cartwright and others; 2008; Vétel and Cartwright; 2010). These studies mainly focus on the pore-fluid pressure conditions that initiate hydrofracture, often with the assumption of a homogeneous host-strata. Although theoretically valid, the models fail to explain the concomitant occurrence of different intrusive elements and of fractures with diverse opening modes. Data presented in this paper support that distribution and geometry of sandstone intrusions are mainly controlled by the relationships between fluid pressure in the hydrofractures, *in situ* stress and the mechanical properties of the host strata. Herein, the spatial and temporal evolution of fluid pressure in hydrofractures is presented with its relationship to *in situ* stress during initiation, propagation and closure of the hydrofractures. Consideration is given to the effect of major lithological heterogeneities within the host-strata on sandstone intrusion.

Limited papers document the relationships between parent units and intrusions (Parize and others, 2007; Surlyk and others, 2007; Scott and others, 2009; Kane, 2010; Hurst and others, 2011) and the genetic events and processes that lead to the remobilization of sand, and to the modification of the internal and external geometry of a parent sandstone that remain poorly understood. Our study shows close physical association and genetic relationships between sandstone intrusions and liquefaction and fluidization of depositional sandstone at a scale previously undocumented (cumulatively at least 10's km laterally and 100's m vertically; see also Stanzione and others, 2008). Genetic association between liquefaction and sand fluidisation is widely recognised as a syn-depositional to early post-depositional process (Lowe and Lopiccolo, 1974; Lowe, 1975) and the relationships between near surface (burial < 60 m) sand liquefaction and fluidization, and sand intrusion and extrusion, are well-known (Obermeier, 1989, 1996). However, the turbiditic sandstone units in the PGIC display widespread evidence of liquefaction and sand fluidization and feeding individual intrusions (dikes) cross-cutting at least 600 m of stratigraphy. This challenges the common assumption that large-scale liquefaction and associated fluidization only occur at very shallow depth and, for the first time, the role of elevated pore fluid pressure in promoting widespread and generalised liquefaction and fluidization of depositional sand during deeper burial is documented.

Recognition of the importance of sand injection in the shallow crust has grown significantly during the past two decades, particularly when associated with the energy sector (Hurst and Cartwright, 2007; Silcock and others, 2021). Despite the excellent detail recorded in many small-scale studies, their relevance to the scale of the injection complex in which they occur is problematic, and their value in a broader tectono-stratigraphic context elusive. Opportunity to investigate local-scale characteristics of sand injection complexes are the subject of several papers (Smyers and Peterson, 1971; Vigorito and others, 2008; Vétel and Cartwright, 2010; Vigorito and Hurst, 2010; Scott and others, 2013; Hurst and others, 2017). Perhaps uniquely, because of the extensive, high-quality outcrop, abundant independent stratigraphic data, and ease of access to many sections through the entire complex, the PGIC presents the opportunity to place detailed information into a regional tectono-stratigraphic setting that is amenable to supporting interpretation of less well-exposed sand injection complexes.

METHODS

Geological mapping of lithostratigraphic units was accompanied by collection of more than 3000 geo-referenced dip-strike measurements from depositional units and sandstone intrusions. Intrusions with complex geometry required multiple measurements that were averaged to allow statistical evaluation. Pre- and post- back-rotated data are compiled as plots for the averaged dip-strike of all intrusions to constrain the *in situ* stress regime at the time of sand injection. Independently >2000 dikes were mapped on satellite images, and their strike and dip calculated by interpolation with the topographic surface using Equinor proprietary software. These data were compared with outcrop data and provide additional information from areas that were inaccessible during fieldwork.

Ten cm-scale sedimentary logs through the injection complex were collected (see Scott and others, 2013). Additional sedimentary logs were collected along strike from key outcrops to document lateral variation in the architecture of depositional and intrusive units. Logged sections were used for quantitative analyses to estimate net to gross (N:G)[1] variations. High-resolution (0.3 m) multi-spectral satellite images were used to map and correlate depositional units, sandstone intrusions and extrusions, and image analysis software was used in selected areas to estimate the N:G. These estimates were calibrated with the results obtained from sedimentary logs and to allow for extrapolation over larger areas, outside the study area and in the subsurface.

Quantitative petrographic analysis (point counting) was carried out on 350 sandstone samples from depositional and intrusive sandstone, and sand extrudites. Selected samples were analyzed using BSEM. Quantitative heavy mineralogy, including varietal mineral studies, was carried out on samples from Moreno Gulch (Hurst and others, 2017). Clay mineralogy was determined using XRD of oriented sample mounts of the <2 μm fraction. Petrographic and mineralogical data were used to confirm sediment provenance and to determine: 1) the source for both sand and fluid involved in sand injection, 2) diagenetic trends and paleotemperature versus burial relationships and 3) estimates of fluid budget.

Digitized elevation-depth maps of key horizons from Hosford Scheirer (2007) were integrated with outcrop and borehole data to produce a 3D model of the Cretaceous-Palaeocene San Joaquin Basin and of the PGIC which was used for volume calculations.

[1] Here, net to gross (N:G) is an estimate of the proportion of sandstone to other lithologies present.

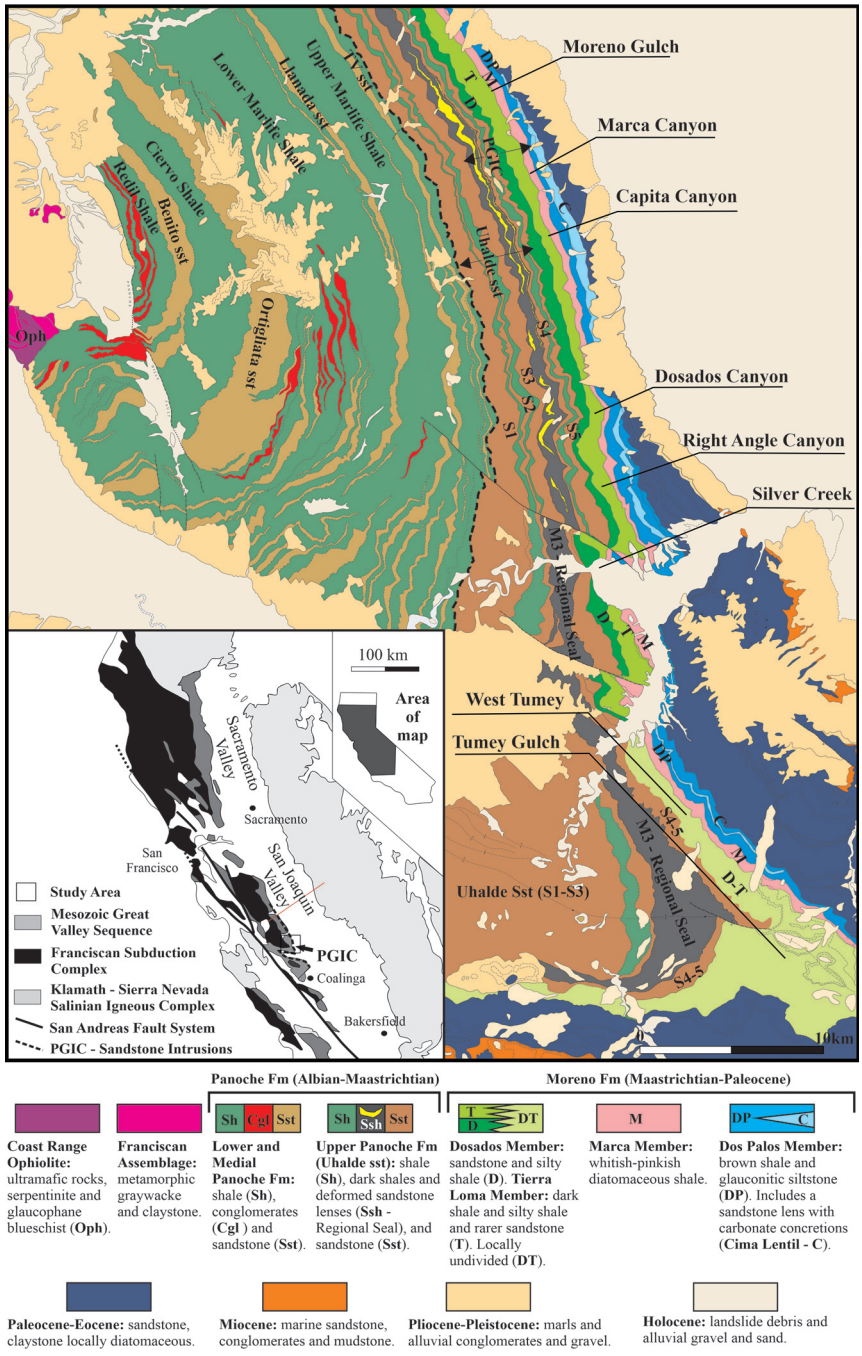

Fig. 1. Geological map of the Panoche and Tumey Hills (modified after Dibblee, 2007a, 2007b). Main lithostratigraphic units related to the Panoche Giant Injection Complex (PGIC) and the main outcrop locations are illustrated. In the inset, a general geological map of northern and central California showing the main tectono-stratigraphic units and the location of the PGIC.

GEOLOGICAL SETTING

Petrotectonic elements of the Mesozoic convergent margin, the Sierra Nevada magmatic arc, the Great Valley forearc basin, the Franciscan accretionary prism, and the Salinian Block and related sedimentary cover, dominate the geology of central and northern California (fig. 1). The first three elements formed concurrently during Pacific plate subduction beginning in the late Jurassic (Atwater, 1970). During the late Cenozoic the subduction zone evolved into a transform margin along which the Salinian Block was tectonically juxtaposed with the first three elements. There is an up to 12 km thick sedimentary fill of Upper Mesozoic and Tertiary strata forming the Great Valley Group (or Sequence; Bailey and others, 1964; Ingersoll, 1982, figs. 1 and 2). These consist of siliciclastic deposits that presently crop out in an east-dipping monocline along the eastern limb of the Diablo Range (western margin of the Great Valley) and are in faulted contact with the Franciscan accretionary complex (fig. 1).

Two formations and their litho- and tectonostratigraphic evolution are key to this study: 1) the Albian-Maastrichtian Panoche Formation (Fm) and the Late Maastrichtian to Danian Moreno Fm, which contain the parent units, the sandstone intrusions and extrusions of the PGIC (Vigorito and others, 2008; Vigorito and Hurst, 2010). In the study area, the Panoche Fm consists of ~6.5 km of sandstone-rich submarine fan deposits alternating with thick mudstone (Ingersoll 1979). Submarine fans were sourced by erosion of the Sierran magmatic arc to the east and north east and prograded westward covering most of the basin floor. From the late Maastrichtian, a basin high formed along parts of the subduction complex that was locally emergent (McGuire, ms, 1988a; Mitchell and others, 2010). During the late Maastrichtian – early Tertiary, the growth of this broad paleobathymetric high, assumed to form by west-verging thrusting, caused the ponding of the deep-water systems, which began to prograde southward parallel to the high (Mitchell and others, 2010). This shift coincided with the onset of the deposition of the Moreno Fm, which at outcrop consists of dominantly slope mudstone deposits and evolves upward into shelfal sandstone and mudstone (Anderson and Pack, 1915; McGuire, ms, 1988a, 1988b). Based on interpretation of 3D seismic data from the northern part of the San Joaquin Basin, Mitchell and others (2010) concluded that during the deposition of the Moreno Fm deltaic systems developed along the western side of the forearc basin. This implies that, west of the northern area of the San Joaquin Basin, part of the subduction complex was emergent and eroded.

LITHOSTRATIGRAPHY

The Panoche Fm is the oldest unit exposed in the study area (figs. 1 and 2) and overlies the Coast Range Ophiolite (CRO; fig. 1), which consists mostly of gabbro and basalt of mid-Jurassic age and pelagic limestone and radiolaria-rich chert. In the Panoche Hills, five major sandstone-rich lithostratigraphic units (S1–S5, figs. 2B and 3, Supplemental Material figs. S1, S2 and S3), interpreted as mid-fan deposits, are present in the uppermost 1500 m of the Panoche Fm and are termed the Uhalde Sandstone (Sst) (fig. 2B; Payne, 1962; Bartow and Nilsen, 1990). S1–S5 sandstone-rich units, typically 40 to 300 m thick, intercalate vertically with 40 to 130 m thick mudstone-dominated units (M1–M4, Ingersoll, 1982; Dibblee, 2007a, 2007b; fig. S3), which in some cases are traced with confidence throughout the study area (figs. 1 and 3). Outcrop mudstone- and sandstone-rich units in the Uhalde Sst correlate with subsurface strata in the Great Valley where they cover areas of thousands of square kilometres and form regionally developed seals and basin floor fan systems (Cherven, 1983, Nilsen and Moore 1997; Hosford Scheirer, 2007). Locally, the latter are hydrocarbon reservoirs (Hosford Scheirer and Magoon, 2007a).

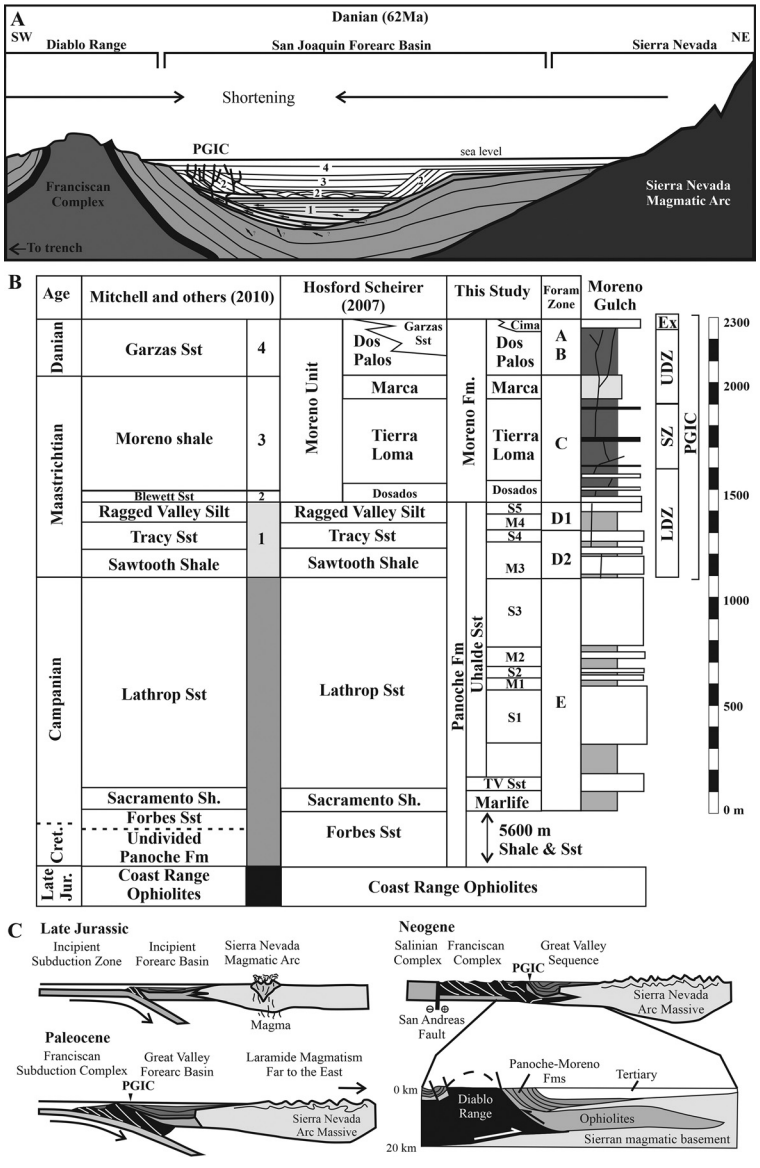

Fig. 2. A) Schematic cross-section through the northern San Joaquin Basin during the Danian (red line in the inset in fig. 1). The figure shows the architecture and stacking pattern of the depositional units that fill the Great Valley forearc basin, the modern location of the San Joaquin Basin (based on outcrop and seismic interpretation and modified after Mitchell and others, 2010). Most of the Cretaceous strata in the Panoche Fm were deformed and uplifted along the margin of the obduction complex (Franciscan Complex), tilted towards the basin axis (eastward) and are overlain and onlapped at the basin margin by deep-water fans (Uhalde Sst), and later slope and delta-slope deposits (Moreno Fm), which pass upward into shelfal deposits. These are extensively intruded by PGIC sandstone intrusions along the western side of the forearc basin. B) Correlation between the lithostratigraphic units in subsurface (Hosford Scheirer, 2007; Mitchell and others, 2010) and at outcrop (Bartow and Nilsen, 1990; this study, dating after Martin, 1964 and revision by Almgren, 1986). Lithological log from Moreno Gulch area (fig. 1), PGIC stratigraphy is shown: LDZ – Lower Dike Zone, SZ – Sill Zone; UDZ – Upper Dike Zone; Ex – Extrudites; see text for more detail. C) Mesozoic-Tertiary evolution of the Great Valley forearc basin. The PGIC formed during the Danian on the western margin of the forearc basin.

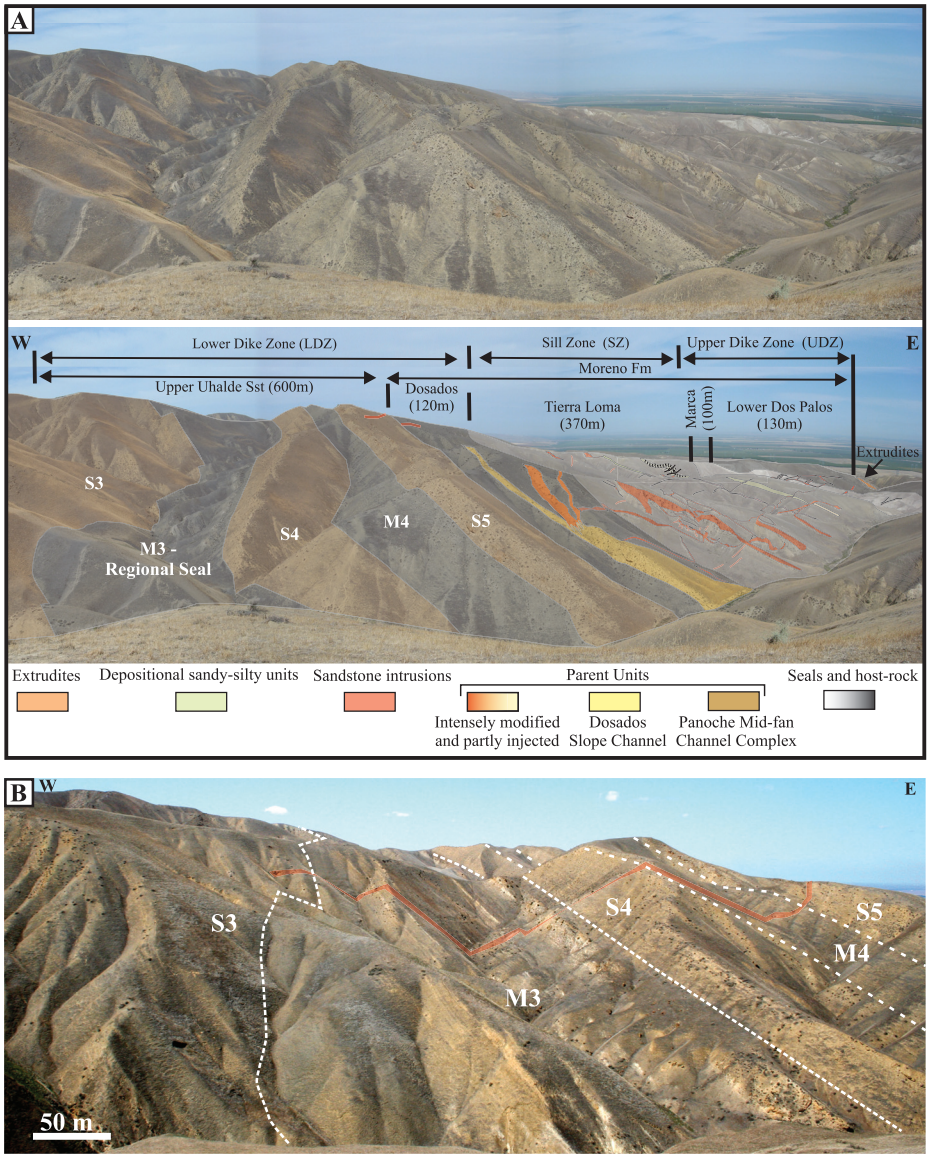

Fig. 3. A) Panoramic view of the PGIC in Moreno Gulch showing the entire injection complex from the parent units to the sand extrudites (for location see fig. 1; fig. S9). Laterally extensive sandstone-rich units (S3–S5) are present in the Uhalde Sandstone (Upper Panoche Fm), each of which is overlain by mudstone (M3, M4), and eventually Dosados Mbr (Moreno Fm) mudstone, in which laterally discontinuous sandstone channels and minor channel-complexes occur. The latter are extensively modified by sand fluidization and feed the overlying sand injection complex. Note that the deep intrusions (LDZ) are exclusively dikes, which feed both dikes and sills higher in the section. In this location sill occurrence is stratigraphically restricted to part of the Tierra Loma Mbr (see fig. 2B). Wide (up to 1m), long dikes (up to 500 m) characterize the upper part of the PGIC all of which strike N40–80 (TO, trench orthogonal). Dikes taper upward and very few dikes terminate as sand extrudites at the base of the Cima Lentil. Key lithostratigraphic units and their thickness is shown. B) Panoramic view (Capita Canyon) along the regional seal. Note the presence of irregular to well-bedded sandstone units within the M3 regional seal. The sandstones are interpreted as minor turbidite channels. A 600 m long and up to 6m wide high angle dike is highlighted in red, which is sourced from the Uhalde S3 unit and transects the entire upper Uhalde Sandstone before reaching the base of a Dosados Mbr deformed slope channel (for detailed interpretation see figs. S4 and S8).

Mudstone-rich unit M3 (60–130 m thick) is ubiquitous throughout the PGIC (figs. 1 and 2B) and is an important regional seal below which hard overpressure developed prior to sand injection (Vigorito and Hurst, 2010). In Moreno Gulch (figs. 1 and 2B), the M3 mudstone is at the base of the D2 biozone (Martin, 1964; 73.5 Ma in Hosford Scheirer and Magoon, 2007b) and correlates with the Sawtooth Shale (Campanian, Payne, 1962) in the subsurface of the San Joaquin Valley (Hosford Scheirer, 2007; Hosford Scheirer and Magoon, 2007b). M3 is the lowest stratigraphic unit intruded regularly by sandstone dikes, which are mostly sourced by diverse depositional sandstones within the S3 (300 m thick, figs. 2B and 3B) and are the deepest intrusions that are genetically related to the overlying PGIC.

Mudstone-dominated Moreno Fm overlies the Uhalde Sst (Anderson and Pack, 1915; Payne, 1951) and records a transition from a deep marine to a slope–shelfal setting (figs. 2A and B, fig. S1, Payne 1951; McGuire, ms, 1988a, 1988b). Four members are present, Dosados, Tierra Loma, Marca and Dos Palos. This progressive filling of the forearc basin is characterized by southward progradation of deltaic deposits (McGuire, ms, 1988a; Mitchell and others, 2010). Benthic forams are indicative of a base of slope environment for the Dosados Member (Mbr), and an outer shelf environment in the Dos Palos Mbr. In the study area the Dos Palos Mbr includes the Cima Lentil, a silty sandstone, locally carbonate-rich, unit (fig. 2B; Bartow, 1991, 1996; fig. S1). The Cima Lentil is interpreted to represent, in parts, the product of sand extruding at the seafloor during the emplacement of the PGIC (Vigorito and others, 2008; Vigorito and Hurst, 2010; Blouet and others, 2017), which can be therefore dated to the Danian (Minisini and Schwartz, 2007). In the study area, the Moreno Fm varies in thickness between 500 and 700 m, but in subsurface, the Moreno Fm and its equivalents are up to 4500 m thick (Hosford Scheirer, 2007).

Outcrop of the Panoche giant injection complex (PGIC)

At outcrop, the PGIC is up to 1200 m (>1500 m decompacted) thick and present over an area of >300 km^2 (fig, 1; Vigorito and others, 2008). Like other giant injection complexes the intrusions in the PGIC have tripartite architecture (Vigorito and Hurst, 2010; Hurst and others, 2011) and the PGIC has the following divisions:

1. lower dike zone (LDZ – thickness ~600 m) - characterised by sparse dikes, mostly high-angle striking ENE-WSW (N40-80) and subordinately NNW-SSE (N310-350) (fig. 2B, fig. S1);
2. sill zone (SZ – thickness ~250 m) - characterized by the occurrence of sills and random-strike oriented dikes (fig. 2B, fig. S1). With rare exceptions, sills are restricted to this interval[2];
3. upper dike zone (UDZ - thickness ~350 m) - characterised by dikes that thin and are less numerous upward with dominant strike-families oriented ENE-WSW (N40–80) and subordinately NNW-SSE (N310–350) (fig. 2B, fig. S1).

A paleo-seafloor marks the top of the PGIC that in places has lenticular sandstone bodies (Cima Lentil). Where sandstone occurs, it is interpreted predominantly as sand extrudites (Vigorito and others, 2008) although there is some evidence of depositional input (Hurst and others, 2017).

Our statistical analysis (fig. S1) reveals two dominant families of dikes striking N40–80 and N310–350; with an angle between the 2 families that varies across the study area between 60 and 80°. The dike families are orthogonal and parallel,

[2] Rare sills, generally <1 m aperture, are present deeper in the section and close to the paleo-seafloor (near the base of the Cima Lentil).

respectively to the paleo-forearc trench (see Nilsen, 1987; Bartow, 1991) and henceforth referred to as trench orthogonal (TO) and trench parallel (TP). Previous studies on dike orientation (Smyers and Peterson, 1971; Weberling, ms, 2002 and Vétel and Cartwright, 2010) are restricted mostly to the Moreno Fm and to limited transects of the PGIC outcrop. Smyers and Peterson (1971) and Weberling, (ms, 2002) have results that are consistent with our observations, whereas Vétel and Cartwright (2010) is at variance because they argue for a general random distribution of dike strike despite their data showing the dominance of the N40-80 trend (see fig. 3B in Vétel and Cartwright, 2010).

Comparison of the PGIC with other outcrop of injection complexes (Parize, 1988; Jolly and others, 1998: Diggs, 2007; Parize and others, 2007; Surlyk and others, 2007; Scott and others, 2009; Hurst and others, 2011 and references therein; Monnier and others, 2015; Cobain and others, 2015; Zvirtes and others, 2021) and subsurface examples (Dixon and others, 1995; Duranti and others, 2002; Van Rensbergen and others, 2003; Duranti and Hurst, 2004; Huuse and Mickelson, 2004; Huuse and others, 2004, Cartwright and Huuse, 2005; Hurst and Cartwright, 2007) shows that key architectural elements for injection complexes are:

1. parent units
2. host strata with seals
3. sandstone intrusions
4. sandstone extrusions.

Parent Units

Parent units are identified as sandstone from and within which sand was fluidised and injected into hydrofractures thereby forming sandstone intrusions. Sandstone S3 in the Uhalde Sst is the base of the PGIC (Vigorito and Hurst, 2010). Other parent units occur shallower in the section, mostly within the LDZ and in a stratigraphic interval 600 to 800 m thick, including the upper part of the Uhalde Sst and Dosados and Tierra Loma mbrs (figs. 2B and 3; figs. S1 and S3).

Uhalde sandstone.—Parent units in the Uhalde Sst consist of three sandstone-rich units (S3, S4 and S5), each 40–300 m thick and comprising multiple, laterally and vertically offset to partially amalgamated, high width:height sandstone-prone mid-fan channel complexes (w = 500–2500 m, h = 10–50 m, fig. 2B, fig. S3; table 1; McGuire, ms, 1988a) associated with overbank deposits dominated by interbedded, thin sandstone, siltstone and mudstone (table 1 and fig. S3B; Ingersoll, ms, 1976; McGuire, ms, 1988a; Stanzione and others, 2008). N:G in the Uhalde Sst increases gradually to the south, reaching a maximum in the Tumey Gulch area (fig 1). Evidence for de-watering is at bedset scale (figs. 4A, 4B, and 5) and although laterally and vertically discontinuous, it is pervasive throughout the study area and within each sandstone unit, transecting stratigraphic intervals from several metres up to >100 m (figs. S4 and S5). Widespread disruption of major-order bedding surfaces and primary lamination is common, and minor bedding surfaces are typically absent, inferred to be obliterated, or intensely deformed (figs. S4 and S5). Some pristine lamination is occasionally preserved in the finest-grained units. Sections of individual sandstone units 100–400 m wide, are mostly structureless and grade laterally or pass abruptly into isolated or more continuous sandstone with abundant dewatering structures and/or, pristine or slightly deformed primary depositional structures (figs. 4A, 4B, and 5; figs. S4 and S5; table 1).

Sparse, elongate (>100 m long) and wide (>1 m) aperture high-angle dikes cut the sequence, intruding units of mudstone and sandstone (figs. 3B). Minor isolated

TABLE 1

Characteristics of the main sandstone architectural elements occurring in the PGIC with criteria for distinguishing between parent units deformed by sand fluidization and injection, sandstone intrusions and sand extrudites

Element	Geometry	Sedimentary Structures	Petrography
Channel Complexes (Uhalde Sst)	4-10 km wide and up to 50 m thick mid-fan channel complexes associated with overbank fine-sand and silt-dominated deposits. Channel complexes are amalgamated or partly amalgamated and form tabular sandstone-dominated units (S1-S5) up to 300 m thick and continuous at outcrop for at least 25 km. In the subsurface the sandstones correlate with laterally extensive fan systems.	Sandstones are generally structureless or deformed by liquefaction and fluidization. Fluid escape structures are locally abundant. Deformation generally occurs at bedset-scale and locally extends through the entire stratigraphic thickness of individual Uhalde Sst units (often >100m). Major bedding surfaces are typically preserved discontinuously and primary lamination and/or minor bedding surfaces are generally intensely deformed or obliterated. In finer-grained units pristine lamination is preserved. Where pristine, channel-fills are characterised by multiple erosional surfaces, sets of compensating bedforms and locally by pebble-rich channel lags. Parallel and dune-scale cross bedding is common.	Sandstone is commonly medium and medium-fine grained and locally calcite cemented. Where fluid escape structures occur grains are more tightly packed. Little clay or mudstone clasts are present. Microfractured quartz is rare and mudstone clasts with embedded sand grains are absent. Laminae rich in debris eroded from the host-strata are locally present along upper margins of sandstone units.
Slope Channels (Dosados and Tierra Loma Mbrs)	Individual channels and minor channel complexes 100-2500 m wide and a few meters to 40 m thick, which are isolated or partly amalgamated.	Predominantly structureless. Conglomerate lags are occasionally present and contain clasts of metagreywacke, radiolaria-rich chert, and basalt. Bedding, lamination, and pristine depositional structures are rarely preserved (generally in the finer-grained units) and grade into deformed or structureless sandstone. Laterally discontinuous, lamination and dewatering structures are common.	As above.
Sills	Intrusive sandstone with slight discordance (<10°) to bedding. Stepping and branching are common and diagnostic. Splitting of sills into multiple segments that re-join laterally over distances of a few decimetres to a few 100's m. Overall saucer-shape geometry prevails.	Irregular and discontinuous (up to a few 10's metres) parallel- to cross-lamination and banding, generally sub-parallel to intrusion margins. Both banding and lamination are caused by grain segregation, concentration of clasts of host-strata or heavy minerals, and changes in the grain fabric and packing. Dish structures, consolidation laminae and pipes are locally common. Clasts (generally granule- to pebble-sized) and rafts (a few m to a few 100's m in width) of the mudstone host-strata occur. Concentrations of clasts along margins form pods of injection breccia. Elongate clasts are commonly oriented parallel to intrusion margins and locally imbricated. Flow-marks on intrusion margins are locally preserved. Normal and inverse (less commonly) grading are observed.	The margins of all intrusions enriched in sand- to mud-sized debris and clay matrix eroded from the host-strata. Mudstone-clasts with embedded sand grains are abundant. Microfractured quartz grains are diagnostic features of sandstone intrusions.
Dikes	Discordant intrusive units with angles to bedding >10°. Semi-ellipsoidal 3D geometry is typical over a range of scales (1-100's m).	As above	As above

TABLE 1
(continued)

Element	Geometry	Sedimentary Structures	Petrography
Extrusions	Mounded to tabular-bedded sandstone characterised by the presence of vents and sand volcanoes. Clastic dikes terminate at the base of the extrusion, which is locally irregular with sand-filled pockmarks. Sandstone extrudites pass laterally into dominantly carbonate seeps where dikes terminate a few metres below the paleoseafloor.	Sub-vertical vent fills, soft sediment deformation and bioturbation . Autochthonous chemosynthetic fauna are locally abundant and very abundant where sand is sparse. Internal structures are poorly preserved unless cemented. Current ripples and probable hummocky stratification are locally preserved and indicative of reworking on the paleoseafloor.	Petrographically identical to the sandstone intrusions and characterised by the presence of abundant sand-sized mudstone clasts with embedded quartz grains and intensely microfractured sand grains. Early diagenetic calcite cement is common.

sandstone-filled channels (5–15 m thick) are present within the M3 regional seal (figs. 2B, 3B and 4D). These channels are structureless or intensely deformed (fig. 4D). Occasional high-angle, and rare low-angle dikes propagate laterally from the margins of some isolated channels forming wing-like intrusions, demonstrable evidence that the channels are parent units for sandstone intrusions (fig. S6; Duranti and others, 2002; Huuse and others, 2004; Jackson, 2007).

An exceptional record of large-scale de-watering of the Uhalde Sst S5 (>70 m thick) is preserved in Silver Creek (fig. 5). Here, medium to medium-fine sandstone (typically >5 m thick) grade laterally and/or vertically from structureless to internally deformed with decimetre to a few meters-scale dewatering structures including pipes, convolute and oversteepened lamination, and pillars. A patchwork of low relief (<0.4 m high and 1m across) scallops (*sensu* Hurst and others, 2005) is locally present at the top of de-watered sandstone (fig. 5B). Intervening mudstone and interbedded mudstone and siltstone units (up to 4 m thick) are either intensely fractured and intruded by multiple high- to low-angle dikes and rare small sills (less than 1 m long and 0.1 m in aperture; figs. 5C and F), or locally pristine with ripple lamination and scours preserved in the siltstone and fine sandstone. Coarser sandstone beds (0.1 to 0.3 m thick) are variably structureless or internally deformed with local evidence of upward erosion of the overburden during sand fluidization (Hurst and others, 2011). Thinner competent mudstone and interbedded mudstone and siltstone units (typically <1m thick) are frequently brecciated or reduced to rafts within otherwise heavily deformed or structureless sandstone. Sets of normal faults strike NNW-SSE and detach on the top of sandstone heavily deformed by de-watering (figs. 5E and F). The hanging wall of the faults is a medium to medium to fine grained sandstone (>40 m thick), in which structureless facies predominate, but with local preservation of convolute bedding and lamination, pipes and pillars, as well as mudstone clasts. Large linear structures, up to 3m in aperture are present, striking NW-SE and oblique to approximately perpendicular to bedding, which resemble the lower sections of large dikes (fig. 5A; see fig. 8 in Hurst and others, 2003b).

Depositional sandstone in strata overlying the Uhalde S3 in the Uhalde Sst, Dosados Mbr and Tierra Loma Mbr are associated with sandstone intrusions that originate from, crosscut, terminate at their bases, or within them (fig. 3 and figs. S6, S7 and S8). In all cases the depositional sandstone has some degree of internal, and

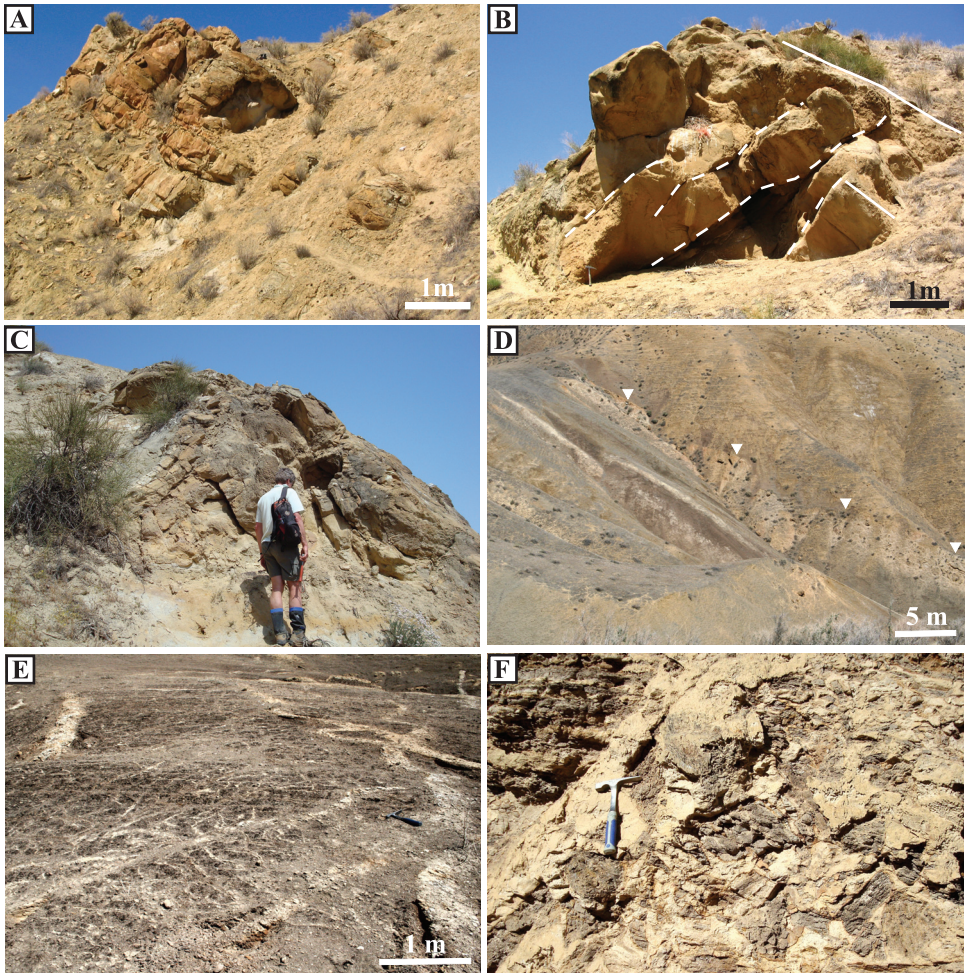

Fig. 4. A) Partly preserved Uhalde S4 turbidites passing abruptly, both laterally and vertically into structureless sandstone with patches of cemented sandstone preserving deformed bedding and lamination. B) A section of the Uhalde S4 exhibiting remains of original bedding (continuous lines) together with surfaces (dashed lines), oriented steep to bedding, interpreted as banding formed by large scale dewatering during sand injection (see fig. S4). C) An anticlinal structure in a depositional sandstone immediately adjacent to the dike in fig. 3B (see fig. S4 for detail). The base and the core of the anticline is structureless medium sand. The outer envelope is deformed laminated and stratified fine sandstone. The anticline formed when fluidized medium sandstone moved upward, dragging and deforming overlying finer sandstone that was a transient seal (person = 2 m tall). D) Isolated and largely deformed channel unit within the regional seal (Uhalde M3), north of Dosados Canyon. Note the irregular top (multiple scallops). E) Hydrofracture Belt (Tierra Loma Mbr) - the lower part of the Sill Zone (south Capita Canyon). Intensely hydrofractured mudstone with very abundant cm-scale sandstone dikes. Most of the hydrofractures are not filled with sand and some contain minor gypsum mineralization or predominantly minor unidentified oxide mineralization. F) Intensely injected and brecciated mudstone (to the right of the hammer) passes abruptly into mudstone alternating with thin-bedded sandstone and siltstone, which are less intensely sand injected (to the left of hammer). Location is shown in fig. 8A, Sill Zone - Tumey Gulch.

locally external, deformation associated spatially with intrusions (figs. 4A to C, and 6; figs. S4, S5 and S8). In general: 1) small volume depositional sandstones (generally <5 m thick and 10's to a few 100's m wide) are more intensely deformed than larger sandstones (fig. 4D); 2) the areal extent and the intensity of deformation is proportional to the aperture and length of the intrusion. Depositional sandstone from which

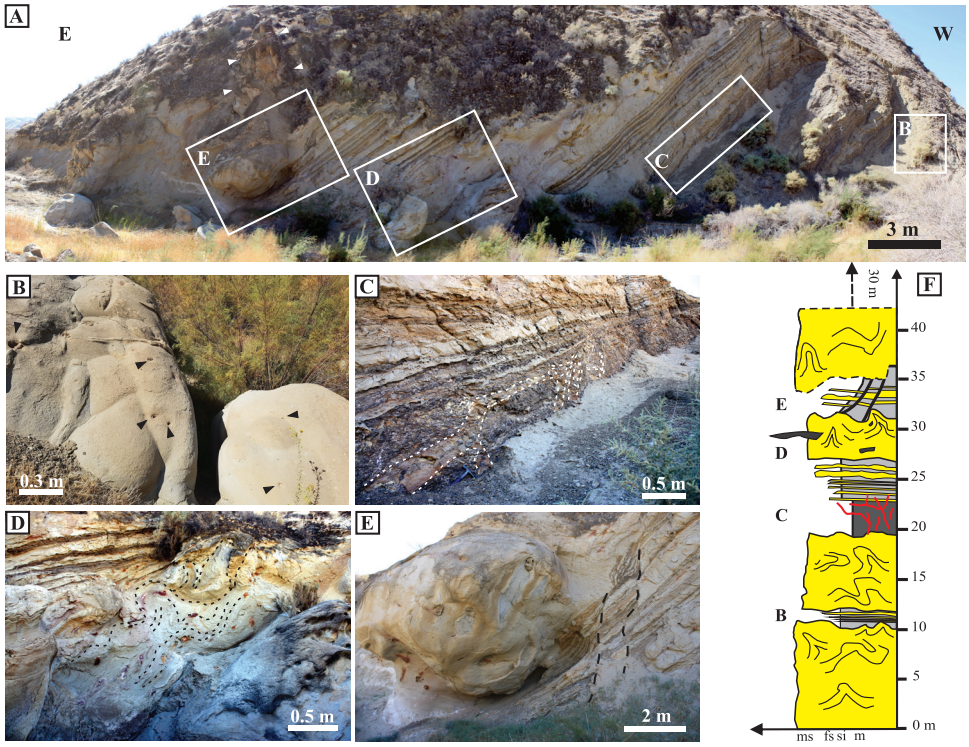

Fig. 5. A) Cross section through the lower and medial portion of the Uhalde S5 Unit (units to the left are stratigraphically younger, Silver Creek, fig. 1) showing the alternation of deformed to amalgamated thick medium-grained sandstone, thin bedded intercalated sandstone and mudstone, and mudstone. White arrows indicate the margins (characterized by high angle banding) of what is interpreted as the base of a high-angle dike. B) Shallow scallops (h <0.4 m, viewed from above) at the top of an intensely deformed bed. Black arrows indicate the presence of circular features interpreted as cross-sections of pipes. C) Mudstone intruded by sandstone dikes; D) Deformed sandstone (approx. 5m thick) with pervasive dewatering features including convolution and flames (up to 1.5 m high). E) Syn-injection faults (dashed lines) at the base of a 30–40 m thick depositional sandstone in which depositional structures are largely obliterated by sand fluidization. Formerly discrete beds are amalgamated by sand fluidization. Syn-injection faults (when back-rotated striking N320/45) are trench parallel and dip landward. Faults detach on the top of the intensely deformed unit depicted in D, which confirms genetic relationships between faulting, pervasive dewatering and sand fluidization. F) Summary log through the section in A showing locations of figures B to E.

dikes emanate are structureless proximal to the point of emanation, whereas areas more distal from dikes often preserve pristine sedimentary structures (fig. S4). Structureless sandstone is spatially and volumetrically limited (figs. S4 and S5) but deformation, including convolute bedding, pipes and pillars, dish structures and consolidation laminae are very common (figs. 4A and 5). Often the only structures preserved are high angle to vertical banding and pillars (fig. 4B).

Where crosscut by large aperture dikes, depositional sandstone adjacent to the dikes has evidence of intense internal deformation and common structureless units (fig. S4). Away from the dikes, small areas of diverse facies characterised by different styles of deformation occur without obvious organisation or relationship to sedimentary facies or lithology (fig. S4; Stanzione and others, 2008). Anticlinal structures up to 3 m high and up to a few 10's m wide occur where depositional sandstone is most deformed and crosscut by large dikes (fig. 4C; fig. S4). Core areas of the anticlinal structures are medium-grained sandstone with vertical banding, large pillars and dish

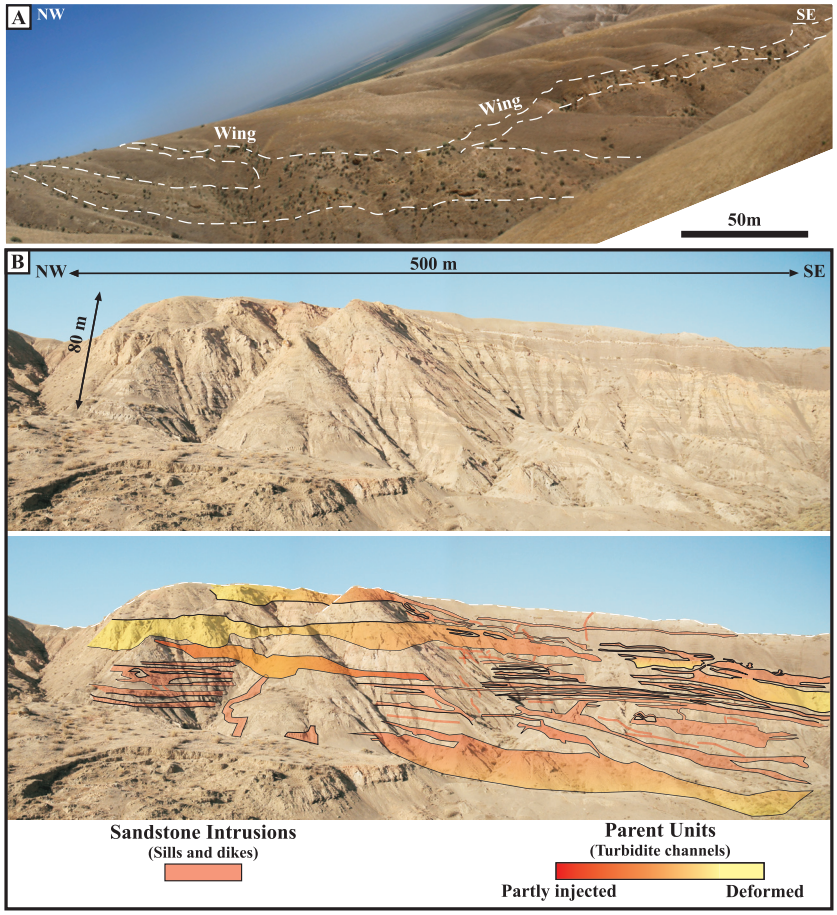

Fig. 6. A) An intensely deformed turbidite channel sandstone with a prominent wing on the left margin and a 3–4m wide low-angle dike emanating from the top of the channel. The latter feeds large sills (>100 m long and 5 m thick) and dikes (>500 m long) 50 to 70 m shallower in the section (see fig. 3A). Pristine bedding is preserved locally at the base of the channel and on the left margin, where the channel grades into thin-bedded overbank deposits (Dosados Mbr, Moreno Gulch; the picture is back-rotated to show the original geometry. B) Sill Zone of the PGIC exposed in Tumey Gulch (see fig. 1) dominated by sills and low-angle dikes. Sills intercalate with thicker (up to 20m) mostly structureless and deformed depositional sandstone. Pristine ripples and cross stratification are preserved locally (figs. 7D–E), confirming a modified depositional origin.

structures, surrounded by fine-grained sandstone, typically with internal lamination (fig. 4C).

Interpretation.—Our investigation shows that the mid-fan channel complexes in the Uhalde Sst (Ingersoll, 1979; McGuire, 1988b; Bartow, 1996) are dominantly deformed by water escape over an outcrop area of at least 100 km^2 and a total stratigraphic section in excess of 600 m, a scale not previously documented. Evidence of fluid escape is common in deep-water clastic strata, with diverse liquefaction structures developing when associated with syn-depositional or early post-depositional dewatering of gravitationally driven flows (Lowe and Lopiccolo, 1974; Lowe, 1975). Structures related to or following the deposition of gravity flows generally form within individual beds and are frequently associated at the base of beds with structures such as flames, rip-up clasts, load structures and sole marks. The tops of beds are often

truncated by erosion (Lowe, 1975, 1982). This is not the case in the Uhalde Sst in which liquefaction is persistent vertically at bedset scale up to ~100 m (fig. S4) and laterally, and is genetically associated with sand injection (figs. 3B and 5). Upper margins of sandstone units locally erode into the overburden.

During liquefaction, the overburden stress is transferred from the granular framework to the pore fluid (Allen, 1982 and references therein), which locally and momentarily attains pore-fluid pressure in excess of the fracture gradient initiating hydrofracturing and sand injection into a top seal (Obermeier, 1996; Rodríguez-Pascua, 2015; Tuttle and others 2019). Hydrofracturing and sand injection are associated with intra-stratal transfer and loss in the overburden (via hydrofractures) of pore fluid and secondarily sand, and cause changes in the geometry of the original sandstone (for example, local subsidence) and a drop in the fluid pressure. Portions of the overburden no longer supported by the grain framework nor by the fluid pressure in the underlying units, collapse into the liquefied sandstone and become deformed themselves. If the overburden is competent (for example, mudstone or consolidated or lithified siltstone), the collapse of the overburden results in normal faulting and/or, detachment of rafts and clasts (up to brecciation) from the roof of the liquefied sandstone (fig. 5D). Where the overburden is sandstone-rich the liquefaction of the underlying units promotes the collapse of the grain framework and induces liquefaction in the overburden. Normal faults detaching on the top of fluidized units and with their hanging walls in fluidized sandstone record evidence of this process (figs. 5A, E and F). In each sandstone-rich unit, liquefaction of the basal strata initiates a chain of events: 1) grain fabric collapse associated with liquefaction, 2) soft-sedimentary deformation of internal structures, and 3) obliteration of sedimentary structures associated with sand fluidization, local hydrofracturing and sand injection. These events repeat and propagate upward, causing progressive modification and obliteration of bedding surfaces and internal structures as deformation increases and individual beds merge to form internally and externally deformed sandstone units in excess of several 10's m thick. Upward transfer of overpressured fluid through hydrofractures likely contributes to reduction of the effective stress in overlying sandstone, thus increasing their propensity to liquefy.

Large-scale liquefaction and associated soft sediment deformation are often genetically associated with seismicity (Obermeier, 1996; Montenat and others, 2007; Moretti and Ronchi 2011) and subordinately other triggers (Owen and others, 2011; Shanmugam, 2016, and references therein). According to engineering studies (Seed, 1968; Seed and Idriss, 1971) that focus mainly on the very shallow overburden and hence, well-drained, non-overpressured sediment, large scale liquefaction is restricted to the first *c.* 30–60 m of burial. This is because the resisting forces to liquefaction are the confining stress and the rock stiffness (due to consolidation and lithification), which both increase with burial (Seed 1968; Allen, 1982). However, poorly consolidated to unconsolidated sandy sediment is routinely encountered in boreholes (for example, many Tertiary reservoirs in the North Sea, Ahmadi and others, 2003) to depths exceeding 2000 m where it creates challenges with control of borehole integrity, local subsidence and sand production (Mahmud and others, 2020). In addition, effective stress decreases proportionally with an increase of pore fluid pressure (Terzaghi, 1925) such that the effective stress tends to zero as pore fluid pressure approaches the overburden stress. It follows that with an increase of pore fluid pressure, a loose sediment becomes more prone to liquefaction independent of burial depth (Stewart and Knox, 1995; Allen, 1982 and references therein). In the Uhalde Sst, liquefaction is genetically associated with hydrofracturing of overlying thick mudstone units and sandstone intrusions (fig. 3B; figs. S4, S5, S6 and S8). Individual intrusions extend into the overburden for stratigraphic thicknesses of up to 600 m (fig. 3B;

fig. S8) and thus record the deposition of >600 m of mixed sedimentary facies prior to liquefaction, but if a single injection event is assumed for the PGIC (Vigorito and others, 2008; Vétel and Cartwright, 2010; Vigorito and Hurst, 2010), it is probable that liquefaction in the Uhalde Sst occurred between 1 and 1.8 km, the burial range for Uhalde Sst below paleo-seafloor. Large-scale liquefaction in similar conditions is not previously recorded, and the evidence herein shows that, under specific but not uncommon geological circumstances (for example, elevated overpressure), liquefaction occurs and may be widespread even at burial depths more than an order of magnitude deeper than previously considered.

Where dikes intrude into depositional sandstone, evidence for local pressure-driven fluid invasion is recorded by total loss of sedimentary structures or intense deformation, close to the dike walls, which abruptly pass or grade into pristine sandstone beds away from dike over distances of 10s to 100s of metres. Formation of small anticlinal structures (fig. 4C) occurs where less permeable, more competent fine-sandstone was dragged upward and folded during the emplacement of fluidized medium-grained sand concomitant with liquefaction, sand evacuation and consequent subsidence on the flanks of the structure. Sandstone intrusions in the Uhalde Sst are sparse and negligible in volume (N:G injectites <1%, see: *Lower Dike Zone*) however, the ubiquitous presence of dewatering features associated with the intrusions suggests that large volumes of fluid were expelled from the Uhalde Sst during liquefaction thus significantly contributing to the fluid budget for sand injection.

Moreno Fm - Dosados-Tierra Loma Members

In the northern area of the Panoche Hills, a few tens of meters thick mudstone in which rare dikes occur, forms the base of the Dosados Mbr, the lowermost section of the Moreno Fm (fig. 2B, figs S3B, S6 to S10). Vertically and laterally offset, or partially amalgamated, channelized turbiditic sandstone and minor channel complexes overlie the mudstone (McGuire, ms, 1988a; figs. 2B, 3 and 6; table 1; fig. S3). Sandstone in the Dosados and Tierra Loma mbrs is intensely deformed and structureless sandstone prevails. Deformation of the external geometry and internal structures is often so pervasive that detailed characteristics of the channelized origin are elusive (figs. 6, 7A, 7D, and 8A).

Wing structures develop where dikes depart from the margins of depositional units (figs. 6A and 8B). Where structureless, the tops of depositional sandstone units are enriched in sand- to granule-size clasts of host strata mudstone. Convex-upward erosion surfaces (scallops *sensu* Hurst and others, 2005) occur along the upper margins of single beds and of thicker, bedset scale units (fig. 7A). Scallops erode up to 10 m into the overburden but typically have 1 to 4 m relief. They form sharp contacts between intrusions and host strata with no significant deformation of either (fig. 7A). Where outcrop is laterally continuous, several scallops occur along the upper margin of parent units (fig. 7A). Dikes commonly emanate from the top or sides of scallops (figs. 7A and 8B). Irregular, sometimes concave-upward depressions are present proximal to scallops or dikes that emanate from the upper margins of depositional units (fig. 7A). Single sandstone beds (typically <1 m thick) may have irregular, mounded upper margins that in 2D appear diapir-like but in 3D are probably short linear dikes (figs. 7B and C). Overlying host-strata is down-faulted, deformed and rotated along the flanks of the mounded margins from which small-scale intrusions emanate (figs. 7B and C). Some channels in the Dosados-Tierra Loma Sst are faulted with displacements up to 10 m (fig. 8A). Generally, faults are injected with sand, locally forming up to 2 m wide dikes (fig. 8A) and are indicative of fault movement before or during sand injection. Most faults strike N310-350 and dip eastward, however some strike N40-80 as reported earlier (Palladino and others, 2018).

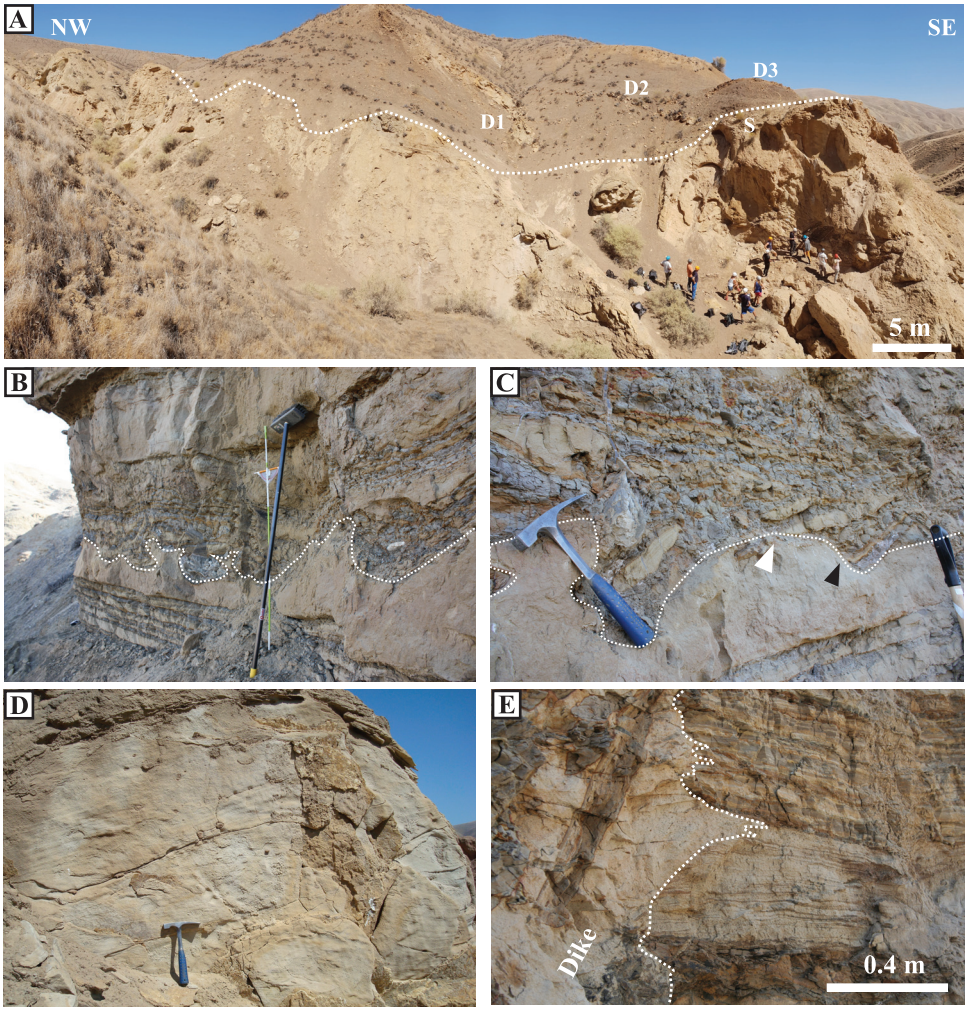

Fig. 7. A) An up to 10 m thick slope channel, extensively modified and deformed by sand remobilization forming the uppermost parent unit in Tumey Gulch. High and low angle dikes depart from the top, which is an irregular margin formed by scallops that document erosion of overburden diagnostic of sand fluidization and injection. The most prominent scallop (S - see also fig. 8B) has a relief of about 5 m with two dikes (D2 and D3 departing from the top). It is separated from the next scallop (to the left) by a shallow depression with an additional dike (D1) departing from the center (see also fig. 8B). B) Thin bedded turbidites at the base of a slope channel (Dosados Mbr). Beds are locally deformed, have an irregular top and exhibit evidence for liquefaction and fluidization. C) Detail of B; deformed sandstone with an irregular top and structures resembling small diapirs with shallow overhangs, these are short dikes in 3D. Fractured host-strata is intruded and locally brecciated. Minor listric faults with decollement developed at the top of the deformed sandstone (black arrow) to accommodate a sinking body of host-strata into the underlying liquefied sand. Thin low-angle dikes depart from the top of the scallops (white arrow). D) Original cross-bedding locally preserved in a slope channel deformed by sand remobilization. The latter corresponds to the uppermost modified depositional unit in fig. 6B. E) 0.75 m wide dike (left side) cutting through thin-bedded and laminated overbank deposits at the base of the deformed channel in (A). Large mudstone and siltstone clasts are present and, where elongate, are oriented parallel to the dike wall. Cm-scale sills depart laterally from the dike and intrude along bedding between laminated fine sandstone and silty mudstone.

Interpretation.—Intense deformation of internal structures in sandstone, including obliteration and partial obliteration of primary sedimentary structures is attributed to sand fluidization and injection. Bedding surfaces are rarely preserved, giving an

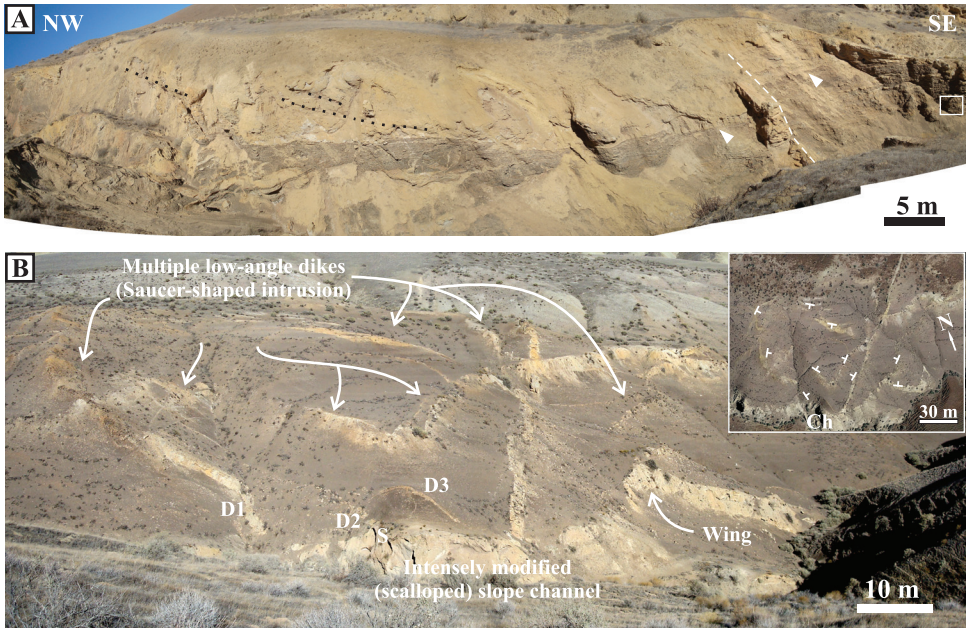

Fig. 8. A) Dosados-Tierra Loma Mbr - Tumey Gulch (fig. S11); base of a 10–15 m thick channel with discontinuous relics of original bedding (black dotted lines) in otherwise structureless sandstone. A 2 m wide dike is emplaced along a fault striking N150 (trench parallel, TP, white dashed line) that displaces the base of the channel (white arrows). Note the irregular intrusions in the mudstone below the channel; the box at the far right is the location of injection breccia in fig. 4F. B) Dike swarms with overall saucer geometry emanate from the top of the intensely-modified channel sandstone. The latter has a convex-upward, scalloped top (fig. 7A); a minor wing-like injection departs from the top of the unit. The low-angle dikes form a composite saucer-shaped intrusion. The insert shows an approximately plan view section of the same outcrop, note orientation of the intrusions. Low-angle dikes are arranged concentrically around a focal point toward which they dip. The focal point is the top of the deformed slope channel, which is the parent of the saucer-shaped intrusion. See fig. 7 for detail about the scallop S and dikes D1 to D3.

amalgamated appearance. Sandstone intrusions emanating from the upper and lateral margins are common (figs. 6, 7A, and 8B; figs. S3A, S3B, S6, S9 and S11). Dikes are traced up to 700 m through the overlying mudstone, transecting the sill zone (SZ), continuing into the upper dike zone (UDZ), and finally reaching the paleo seafloor (Vigorito and Hurst, 2010). This is direct physical evidence that the Dosados Mbr is the main parent unit for sand injected into the PGIC, a relationship confirmed independently by mineral provenance (Hurst and others, 2017).

Occasional depressions and concave-upward surfaces near dikes that emanate from the upper margins of parent units are evidence of sand evacuation into the intrusive network (figs. 7A to C, and 8B). Some, often extreme, modification of the external geometry of parent units is caused by the combination of sand evacuation, disaggregation of the overburden margin by hydrofracturing and gravitational collapse into liquefied or fluidized sandstone, and further modification by erosion caused by turbulence in fluidized and injected sand-water mixtures (figs. 5, 7A, and 8A). Similar erosion formed scallops along the upper margins of parent units (figs. 7A to C), which confirms a turbulent flow regime and is diagnostic of sand fluidization and injection (Duranti and Hurst, 2004; Hurst and others, 2005; Scott and others, 2009; Hurst and others, 2011). The combination of hydrofracturing and erosion that forms scallops increases the proportion of sand- to granule-size mudstone clasts within them (Scott and others, 2009, table 1). Enrichment in mudstone-clasts and mud

matrix, occur almost exclusively adjacent to the upper margins of parent units, whereas in sills similar concentrations occur near upper and lower margins, and along layers within them (see *Sill Zone*). Near the base of parent units, collapse of the grain fabric suppresses erosion because of insignificant particle movement. By contrast, near the top of parent units, sand-laden fluidized flow eroded the overburden. In sills, fluidized sand flows and erodes along both the basal and upper surfaces (the fracture margins), forming laminae enriched in host-strata clasts adjacent to both margins, the identification of which are criteria for distinguishing parent units from sills.

Sand injected along normal fault planes accommodates the deformation caused by the evacuation of both sand and fluid from parent units, either by reactivation of pre-existing faults or syn-injection faulting. Fault orientation is most commonly N310-350 (TP) and subordinately N40-80 (TO) and is indicative of the regional tectonically-controlled stress regime, which will be discussed later.

Mudstone Host-Strata and Seals

Mudstone is the predominant host strata for sandstone intrusions in the PGIC. M3 is the thickest mudstone (fig. 3, figs. S1 and S2), and its subsurface equivalent is the regionally developed Sawtooth Shale present throughout most of the San Joaquin Basin (Hosford Scheirer and Magoon, 2007a, 2007b). Smectite dominates the clay mineralogy of mudstone outcrop from the Uhalde Sst (Scott, ms, 2009), which is locally enriched in organic matter (Hosford Scheirer and Magoon, 2007a). In the subsurface of the Sacramento Basin, the stratigraphic equivalent mudstone is illite dominated (Strongin 1981; Mertz, 1988; Smith and Berry, 1988; Imperato and Nilsen, 1990).

Smectite is the dominant clay mineral also in the Moreno Fm mudstone (Ramseyer and Boles, 1986; Lewan and others, 2014; Hurst and others, 2021c), which is locally organic-rich, for example, in the Tierra Loma Mbr (McGuire, ms, 1988a; Fonseca-Rivera, ms, 1997; Hosford Scheirer, 2007), diatomaceous in the Marca Mbr, and slightly more kaolinitic upward throughout the Dos Palos Mbr (Hurst and others, 2021b). Most of the PGIC sandstone intrusions are hosted by the Moreno Fm (>90%; fig 2; figs. S1, S2 and S12; Vigorito and others, 2008; Vigorito and Hurst, 2010), which is locally intensely hydrofractured (for example, in Tierra Loma Mbr), however >95% have no sand fill (figs. 4E and F). There is localised evidence for injection into depositional sandstone and siltstone (figs. 3B, 7E, 8A, 9C; fig. S4) as well as in the unconsolidated mud that was present at and immediately below the seafloor at the time of injection.

Interpretation.—Mudstone in the Uhalde Sst is a basin-floor deposit formed during transgressive events when the forearc basin was starved of sand. In this perspective, the M3 and its subsurface equivalent the Sawtooth Shale, form a basin-wide condensed section that records a major transgressive event at ~73 Ma (Nilsen and Moore, 1997; Hosford Scheirer and Magoon, 2007a). Mudstone in the Moreno Fm is dominantly a slope deposit that records the southward progradation of late Cretaceous to early Paleocene deltaic systems (Cherven, 1983; McGuire, ms, 1988a, 1988b).

The smectite-rich mineralogy of the mudstone, suggests that these are mostly weathering products of volcanic ash derived from the paleo-Sierra Nevada and that, in the outcrop area, burial temperature never reached 60 °C. In similar strata elsewhere burial temperature exceeded 100 °C, such as in deep areas of the Sacramento Basin, where illite prevails (Mertz, 1988; Smith and Berry, 1988; Imperato and Nilsen, 1990). Above 60 °C thermally driven decomposition of smectite occurs with concurrent growth of illite (Nadeau, 2011). Analogous burial and temperature conditions existed over large areas of the San Joaquin Basin during the final phases of deposition of the Moreno Fm (Hosford Scheirer, 2007; Peters and others, 2008).

Paucity of intrusions and the very small volume of injected sand in the Uhalde Sst (<1% of the entire PGIC), suggest that prior to formation of the PGIC, limited overpressure above the fracture gradient was present in S3, below the regional seal M3. Prior to sand injection and higher in the section in S4 and S5, pore fluid pressure was below the fracture gradient although likely above hydrostatic (see section: *Hydrofracturing and Vertical Fluid Pressure Evolution During Sand Injection*).

Above the M3 regional seal, sand intruded mudstone and subordinately sandstone and siltstone in the Uhalde Sst and Moreno Fm, which were *transient seals* (Deming, 1994) that failed in tension and locally in shear (Vétel and Cartwright, 2010) as they were unable to transmit migrating pore fluid at rates equivalent to the fluid influx. Most of the rapid fluid influx was transmitted by major dikes that connected the regionally overpressured aquifer in the Uhalde Sst S3 and its subsurface equivalent (Vigorito and Hurst; 2010). While accepting that all seals leak, the *transient seal* concept has specific relevance to the intense hydrofracturing that occurred at between ~600 to 800 m burial in the poorly consolidated Moreno Fm, where fractures propagated very rapidly (figs. 4E and F and 7E). Organisation of sandstone intrusions in the PGIC records evolution of pore-fluid pressure relative to the lithostatic gradient (σ_v) with pressure in the hydrofractures exceeding the fracture gradient below the SZ (dike formation in LDZ), pervasive supra-lithostatic pressure in the SZ (intense hydrofracturing, sill and dike formation), and return to sub-lithostatic pressure in the UDZ (Vigorito and Hurst, 2010). Complete breaching of the Moreno Fm seal was achieved when dikes reached the paleo-seafloor (Vigorito and Hurst, 2010).

Sandstone Intrusions

Sandstone intrusions are sand-filled hydrofractures and are here classified as: 1) sills, close to bed-concordant intrusions (<10° to bedding) and 2) dikes, bed-discordant intrusions (>10°; tables 1 and 2). Intrusion margins are generally sharp though irregularities such as flow-marks and evidence for modification by erosion are locally common (Scott, ms, 2009; Hurst and others, 2011). Internally, sandstone intrusions can be structureless, or display varied suits and associations of internal structures, microstructures and grain fabrics (tables 1 and 2; Scott, ms, 2009; Hurst and others, 2011; Scott and others, 2013). Orientation of the intrusions is important when determining the *in situ* stress at the time of injection (discussed in the *Distribution and trend of sandstone intrusions*), whereas internal structures provide insights on the mechanical, hydrodynamic and sedimentary processes during emplacement of sandstone intrusions, which is the focus of the *Injected Flows: Characteristics, Fluid Dynamic Behaviour and Sedimentary Record.*

Lower Dike Zone (LDZ).—The LDZ is the lowest part of the PGIC and extends upward for 400–600 m from the base of the regional seal (M3) to the base of the SZ in the Tierra Loma Mbr (fig. 2; Fig. S1).[3] It includes most of the depositional parent units (from Uhalde S3 to the lower portion of Tierra Loma Mbr; fig. 2). In the deepest part of the LDZ intrusions are sparse high-angle dikes, generally >70° to bedding. Dikes become progressively more common higher in the LDZ between the Uhalde Sst S3 and S5, and some terminate at the base of the Dosados Mbr (figs. S2, S6 and S8).

Dikes in the Uhalde Sst include some of the widest aperture (~6 m) and longest (~700 m) present in the PGIC (fig. 3B; figs. S4 and S8). Typically, dikes transect

[3] One, exceptionally long, high angle dike (1250 m in outcrop length and >1 m aperture), is mapped west of Right Angle Canyon. It cross cuts the entire lower Uhalde (S1 to M2) and terminates at the base of the S3 unit (fig. S2). Given the sporadic occurrence of dikes deeper than the S3 unit and discontinuity of exposure, any genetic relationship with intrusions above in the section cannot be proved.

TABLE 2

Geometry and internal structures in the main geometric elements of the sand injection complex, the pore pressure at which they formed, and other factors that influenced their emplacement

Intrusive element	Description	Associated features	Interpretation
Staggered sills	Composite intrusions of multiple 1-10 m long and typically <1m thick sill segments that are laterally and vertically offset and separated by short (typically <5 m) dikes.	Found in close association with randomly-oriented dikes and intensely hydrofractured host strata including narrow (<5 mm) sandstone dikes, gypsum veins and open fractures characteristic of the hydrofractured belt.	Staggered sills and their associated features were emplaced when fluid pressure in the injected flows was supralithostatic and exceeded the overburden stress. A high density of fractures in the hydrofractured belt compared with adjacent strata is indicative of formation when the pressure difference between injected fluids and lithostatic pressure was at its maximum.
Stepped Sills	Laterally continuous (10-100's m), and up to 12 m thick, characterised by multiple steps, and locally by erosional upper margins (scallops *sensu* Hurst and others, 2005). Overall wing geometry is common.	Typify intervals immediately above the hydrofractured belt and associated with wide (up to 2 m) and long (10 to 100's m) dikes. Stepped sills may form segments of saucer-shaped intrusions.	Stepped sills and associated intrusions (dikes and minor sills) tend to be thicker and more widely spaced than staggered sills. This records supralithostatic fluid pressure during emplacement but at slightly lower fluid pressure than in staggered sills. During sand injection it is energetically more favourable to open and dilate a few major fractures than many shorter ones.
Multilayered sills	Sills with composite sets of multiple thin (0.05 – 0.3 m) discontinuous to laterally continuous (10's to 100's m) intrusions that are irregularly stratified with fragmented host strata. High-angle dikes are generally the lateral feeders to the sills.	Multilayered sills occur only where the host-strata are lithologically heterogeneous with thinly bedded alternations of mudstone, siltstone and sandstone. Multilayered sills are generally fed laterally by one or more oblique- or high-angle dikes	Presence of interlayered heterogeneity (for example mudstone-sandstone alternations) is a key requirement for the formation multilayered sills. Bed contacts conceivably form lithological and mechanical planes of weakness that represent surfaces along which the tensional strength of the host-strata is greatly reduced. In turn this favours the emplacement of multiple ~bedding-concordant intrusions.

multiple stacked depositional units (up to 100 m thick) and mostly are high angle and belong to the TO and subordinately TP trends. Among the high angle dikes only TO dikes are longer than 80 m. This dike-strike distribution pattern is consistent throughout the study area, but dikes are not as numerous as in the Moreno Fm. Dikes in the

TABLE 2
(continued)

Intrusive element	Description	Associated features	Interpretation
Low angle dikes	Up to 15 m wide discordant intrusions that cut the host strata at angles between 10 and 25° though nearly bed-concordant and steeper segments (up to 45°) locally occur. Dip to bedding of low-angle dikes is controlled by proximity to the SZ with shallower dip within and close to the SZ.	Generally low-angle dikes occur in the SZ and within the first 100-150 m below (LDZ) and above (UDZ) the SZ. Deeper in the section (100-250 m below the base of the SZ) high-angle basal segments occur. Within the SZ these may transform into sills or have bed-concordant segments. Major low-angle dikes transform rapidly into high-angle dikes as they approach and/or intersect the top of the SZ.	Low-angle dikes are most common and largest (a ~ 15 m and L = 750 m) within a stratigraphic interval which extends from 100 m below to 100 m above the SZ. This specific stratigraphic distribution suggests formation of low-angle dikes was promoted by supralithostatic or near-to-lithostatic pressure conditions in injected flows.
Oblique and high angle dikes	Dikes that intrude the host-strata at angles >25º to bedding are ubiquitous in the PGIC and form the numerical majority of sandstone intrusions. Oblique dikes are inclined <60º and high angle dikes are >60º to bedding.	Oblique and high-angle dikes in the LDZ and UDZ belong to two dominant strike groups (TO – N40-80 and TP - N310-350). The vast majority of large dikes (w >1 m and l >50 m) belong to the TO and TP with TO dikes steeper than 70º and TP dikes commonly dipping 45-75° easterly.	High-angle dikes are widespread throughout the PGIC. Although abundant in the SZ the emplacement of a high-angle dike does not require supralithostatic pore-pressure to propagate fractures. The presence of two distinct groups of dikes indicates the presence of imposed tectonic stress during emplacement.
Saucer-shaped intrusions	Composite intrusions with crudely circular to horseshoe plan-view geometry and low-angle saucer shape in cross-section. Composites of stacked sills (aperture of 2 to 5 m but up to 15m) and low-angle dikes with apertures of (a = 2 to 15 m) form saucer-shaped intrusions. The saucers are up to 2300 m in diameter, crosscut up to 230 m of stratigraphy and have cumulative sand thicknesses up to 50 m. The maximum estimated sandstone volume for an individual saucer-shaped intrusion is 0.04 to 0.06 km^3 (West Tumey).	Saucer-shaped intrusions occur mainly within the SZ but may extend into the UDZ. Close to bedding-concordant segments occur exclusively in the SZ while above it they cut the stratigraphy at angles of 35° to 70° to bedding (the dip increases with distance from the SZ). Swarms of high-angle dikes are common at the margins of the saucer-shaped intrusions. Intrusions within the area of saucers are less abundant and randomly oriented. Secondary saucers may occur in the core areas of larger features. Jack-up and force-folding of host-strata is characteristic.	Although tops of the saucer-shaped intrusions may extend beyond the SZ into the UDZ, the fact that most of saucer-shaped intrusions are developed within the SZ indicates that supralithostatic conditions in the injected flows are necessary to the form them. Jack-up and force folding of the host-strata is indicative of supralithostatic fluid pressure.

SZ = sill zone, LDZ = lower dike zone and UDZ = upper dike zone.

Uhalde Sst tend to occur in isolation or in clusters within ~10–200 m wide strike sections. Seven large-aperture (2–6 m), long (100–600 m) high-angle dikes, sourced from the S3, are present deep in the section in the Panoche Hills (fig. S12A). These dikes are 700 to 1500 m apart (1300 m on average) however, more than fifty dikes (up to 1m wide and 40 m long) are present in the M3 mudstone regional seal in Silver Creek (fig. 1) in an area of 200 x 200 m.

LDZ dikes originate from, crosscut, and abruptly terminate within depositional sandstones. Where dikes terminate at the base of a depositional sandstone, it is often possible to observe one or more new dikes emerging from the top of the same sandstone unit (figs. S6 and S10). In these cases, the dikes at the base and top have horizontal offsets of a few metres and up to 700 m. In general, the largest offset occurs where depositional sandstone is thickest. Shallower in the section, dikes are progressively more abundant and diverse in terms of both strike and dip, specifically in the Dosados and Tierra Loma mbrs, as they approach the SZ (fig. 2; fig. S1; see *Distribution and trend of sandstone intrusions*). Where Dosados Mbr parent units are present deeper in the section, for example, in the northern part of the Panoche Hills (figs. 2, 3A, and 6A), large aperture (up to 3 m wide) dikes emanate from parent units at angles >40° to bedding and over a vertical distance of approximately 200 m become more gently inclined (<25°). Eventually they transform into sills as they enter the SZ (Vigorito and Hurst, 2010; fig. S8). In the southern PGIC (south Panoche Hills and Tumey Hills), parent units are located closer to the base of, or within the SZ, and the number of intrusions emerging from parent units increases. Their orientation is more varied with a larger proportion of low-angle dikes and sills (fig. 6B; compare figs. S9 with S11). In the uppermost part of the LDZ, large aperture (>1 m), long (>30 m) intrusions are commonly low-angle dikes with varied strike and TO high-angle dikes.

Interpretation.—Scarcity of sandstone intrusions in the LDZ and their distribution are indicative that the regional seal M3 was breached in several focused areas where large aperture dikes emerge from the underlying S3 sandstone. The focused areas are on average 1.3 km apart and are the origin of individual branches of the intrusive network, with each branch propagating into the overburden by upward branching and areal spreading. Branching and spreading of sandstone intrusions is analogous with that described from Gas Point, Sacramento Basin (Jolly and others, 1998). The general absence of sills and the occurrence of large intrusions dominated by TO high-angle dikes is interpreted to record the vertical orientation of the maximum stress at the time of injection, thus disfavouring the formation of sills. Minimum horizontal stress was oriented NW-SE, trench parallel, and maximum horizontal stress was oriented perpendicular to the trench, hence the dominance of the TO dikes that opened against the minimum stress. High-angle dikes (mostly TO) characterise the LDZ, but in the upper part, dikes become more varied in both strike and dip. This is interpreted to reflect a change in the relationship between fluid pressure in the hydrofractures and the prevailing *in-situ* stress in the host-strata, which was controlled by the regional stress field (Vigorito and Hurst, 2010). As hydrofractures and intrusions propagated upward, fluid pressure within them approached lithostatic pressure that when exceeded led to formation of sills. The base of the SZ is estimated to be ~700 to 800 m below the paleo-seafloor at the time of injection (fig. 2B; Vigorito and Hurst, 2010).

Sill Zone (SZ).—The SZ is the stratigraphic portion of the PGIC where the highest volume of sand is found and most sills, saucer-shaped intrusions and wing-like intrusions are concentrated (figs. 2B, 3A, 6B, and 9A; Vigorito and others, 2008). In the study area, the SZ is a restricted stratigraphic interval present between ~270 m (± 30

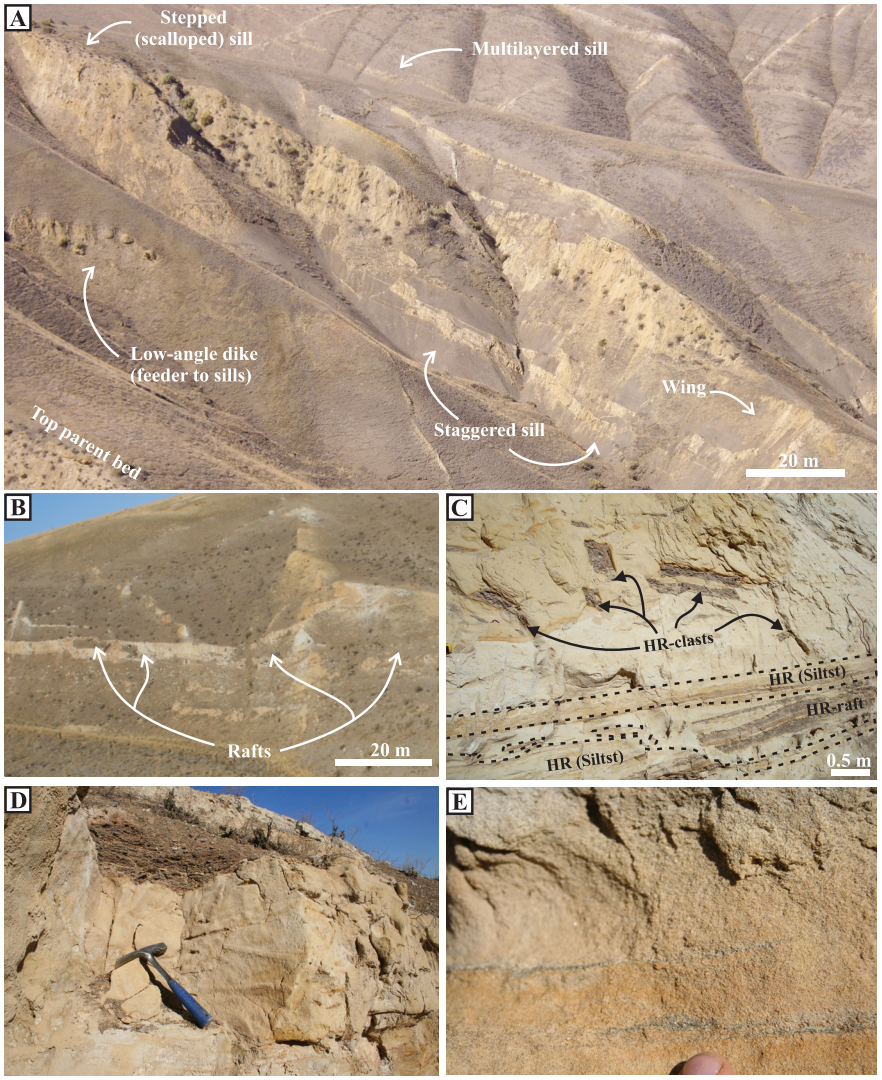

Fig. 9. A) Panoramic view of the sill-dominated section of the PGIC in the Dosados and Tierra Loma mbrs in Moreno Gulch (MG in figs. 1, 3A). A well-developed wing on the lower-right margin of the staggered sill with an overall saucer-shaped geometry. B) A staggered sill with short sill-segments offset both laterally and vertically by intervening dikes. Rafts and boulders of host strata are enclosed within the sill. C) Detailed view of a multilayered sill that includes rafts of mudstone and laminated silty sandstone. Some intrusions are wedge-shaped (fracture tip or leading wedge) that intrude along and split bedding. D) Internal structures from the staggered sill in (B) showing the presence of well-developed cross and parallel banding. E) Internal grading and presence of discontinuous laminae enriched in sand- to granule-sized clasts of mudstone (grey) from the sill in B.

m) and ~20 m (± 10 m) below the base of the Marca Mbr, (Vigorito and Hurst, 2010; fig. S1).

In the north of the study area, host strata in the lowermost (30–60 m) part of the SZ, and almost the entire SZ in the southern area, is intensely hydrofractured (figs. 4E and F) and is termed the Hydrofractured Belt. Random fracture orientation is apparent on bedding planes (fig. 4E). Where adjacent to dikes or sills some fracture alignment sub-parallel to intrusion margins occurs. Although laterally continuous

throughout the PGIC, the intensity of fracturing varies spatially, being most intense and widespread adjacent to large sandstone intrusions. Where hydrofracturing is intense the host mudstone forms mainly clast supported breccia, but is matrix supported where injected by sand (fig. 4F). Breccia clasts are angular and typically coarse gravel- to less commonly boulder-sized. Clasts are often rotated between ~5° and 20° to bedding. Where best developed (for example Tumey Gulch), injection breccia forms pods, 10's to a few 100's m wide but <10 m thick. Breccia pods pass laterally and vertically into intensely-fractured and intruded host-strata (fig. 4F) or, alternatively, into more pristine host-strata with minor intrusions, these transitions are either gradual or sharp (fig. 4F). Pods of injection breccia are restricted to areas where relatively thin (<10 m) packages of mudstone are sandwiched between intensely deformed parent units (fig. 8A) and/or, large aperture sills ($a > 3$m). Throughout the PGIC, intense fracturing locally associated with injection breccia, occurs proximal to abrupt changes in strike or dip associated with large aperture intrusions ($a > 1$m). Breccia is common, though limited in volume, at intrusion margins and subordinately within large aperture intrusions (typically $a > 1$ m; fig. 7E). Along the margins or within sandstone intrusions, matrix supported injection breccia has angular or rounded clasts rotated at diverse angles relative to bedding that when elongate have long axes parallel to intrusion margins (fig. 7E). Mudstone clasts are locally imbricated and exotic clasts (not derived from adjacent host strata) may occur.

Sill geometry has three characteristic styles: staggered, stepped and multilayered (table 2; Vigorito and others, 2008). Staggered sills are dominant in the lower part of the SZ, whereas stepped and multi-layered sills occur mainly in the upper part of the SZ (figs. 3A, 9A, and B; Vigorito and Hurst 2010). Where exposure is laterally continuous all the large-scale sills (10's to 100's m wide) have shallow concave-up or saucer-shape geometry with margins that often extend into steeper segments or "wings" (figs. 9A, 10A, 11A, and 11B), or are bounded by sub-vertical dikes (fig. 11A). Sills are characterised by stepping, splitting and convergence of individual sill segments (figs. 9A and B, and 10A) and internally can be structureless or, more often, have distinctive sedimentary structures (figs. 9C to E, table 2).

Within the SZ, swarms of low-angle dikes and sills form composite intrusions with an overall saucer-shaped geometry in cross-section (figs. 8B and 10; fig. S6; Vigorito and others, 2007; Hurst and Vigorito 2017, Grippa and others 2019). The largest saucers in the PGIC are km-scale and have dimensions and geometry analogous to hydrocarbon fields in the North Sea Basin (table 2). From 3D seismic data these intrusions are known to have crudely circular to elliptical, or horseshoe, planar geometry (Huuse and others, 2004; Shoulders and Cartwright, 2004; Shoulders, ms, 2005; Huuse and others, 2014). Above saucers the overburden is uplifted (jacked-up) and/or folded with the height of jack-up or the fold approximately equal to the cumulative thickness of sandstone in the saucer-shaped intrusion (fig. 10B; Hurst and Vigorito 2017; Grippa and others, 2019).

Sills are associated with abundant dikes that have random strike-distribution but within which, both TO and subordinately TP strike-oriented groups are most common (fig. S1). In the lower part of the SZ, dikes are generally short (from several decimeters to a few tens of meters) and steep with $a < 0.5$ m. In the medial to upper part of SZ dikes tend to be wider ($a = 0.5$ to 2 m), longer (several 10's to 100's m) and more laterally continuous (fig. 3A; figs. S6 and S10). Sometimes major high angle dikes crosscut most of the Moreno Fm (up to 700 m through the upper LDZ, SZ and UDZ, fig. 3A). These major dikes belong exclusively to the TO group (fig.11A; figs. S2 and S9). Large aperture, low-angle dikes ($a = 3$–8 m; fig. S10) are present. Major low-angle dikes are 100 to 800 m long and laterally transition into steeper segments (35 to 60° to bedding) that cut and taper upward through the UDZ for up to 130 m (fig.

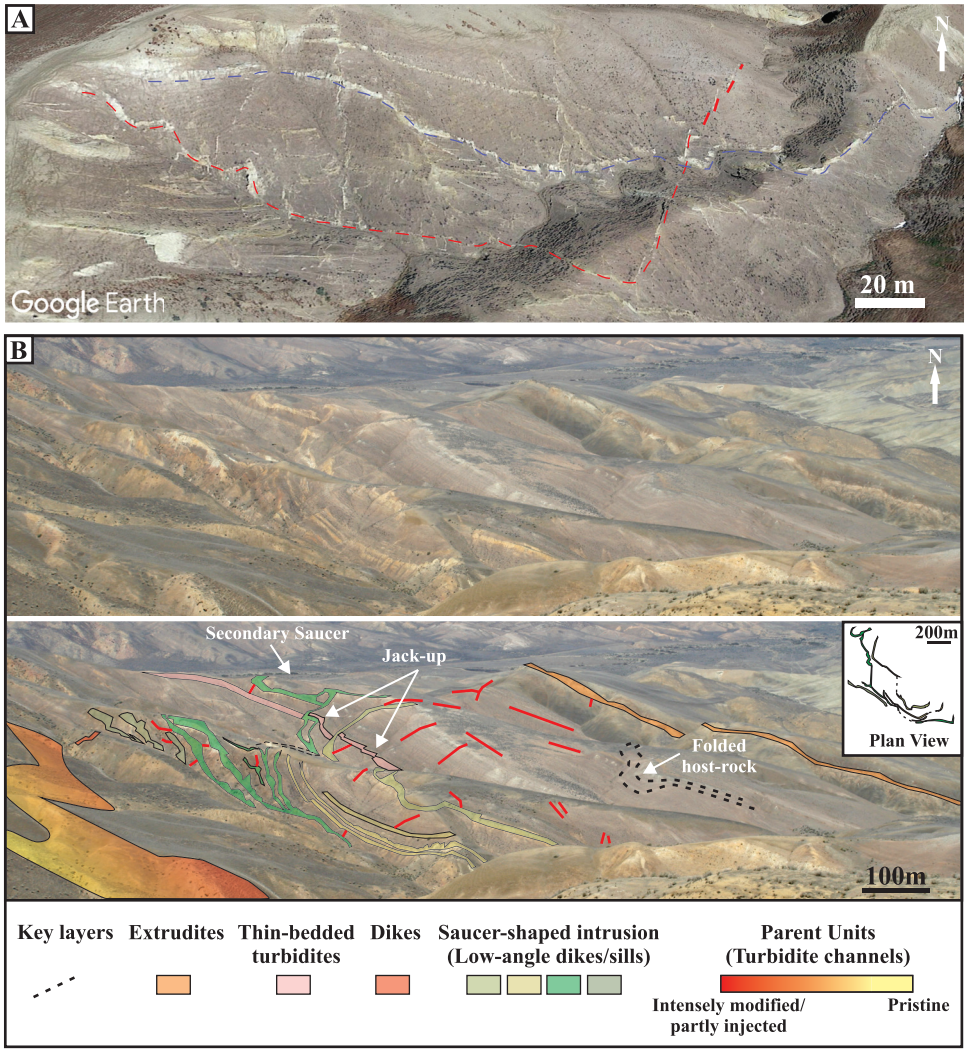

Fig. 10. A) Vertically stacked and partly nested sills (dashed lines) with an overall saucer-shaped geometry, Dosados Canyon (fig. 1; see fig. S10). B) Panoramic view of the saucer-shaped intrusion in West Tumey (fig. 1), a composite intrusion consisting of vertically-stacked sills and low-angle dikes with a minimum cumulative thickness of ~50 m. Forced folding and jack-up occur in the overlying mudstone. Mudstone in the central area above the intrusion contain thin, widely-spaced dikes with diverse strike. A ~100 m diameter secondary saucer is present at the top of the northern wing (to the left).

10B; figs. S7 and S10). Occasional decimeter- to meter-scale shear-folds are present in the SZ: 1) between closely spaced sills or low angle dikes; 2) close to steps in major sills and low angle dikes, 3) in front of the tips of intrusions (Vétel and Cartwright, 2010).

Interpretation.—Occurrence of sills with low- and high-angle dikes records fluid pressure that exceeded the vertically oriented maximum principal stress. Pore fluid pressure within the propagating hydrofractures was at its maximum level above the maximum *in-situ* stress, and numerous hydrofractures formed with diverse strike, in places creating intense hydrofracturing (fig. 4E and F; Vigorito and Hurst, 2010). Under these pressure conditions, fractures opened in all directions and sand intruded

in random trajectories (fig. S1; see *Distribution and Trend of Sandstone Intrusions*). Brecciation is *in-situ*, overwhelmingly clast-supported and subordinately sand matrix-supported where hydrofractures were injected with sand. This differs from injection breccia within sandstone intrusions in which clast-oriented fabric, grain imbrication and segregation, and the presence of exotic clasts, are indicative of sediment transport.

Staggered, stepped and multilayered sills tend to occur in that sequence from deep to shallow in the SZ (fig. 9A) and formed in response to the relative pressure difference between the fluid pressure in the hydrofractures and the lithostatic pressure at specific depths (table 2; Vigorito and Hurst, 2010). Staggered sills (generally a = 1–5 m thick; figs. 9A and B), occur only in the hydrofractured belt and generally a few meters above intensely deformed parent units. They formed by intrusion into multiple fractures initiated in response to the highest fluid overpressure relative to the local overburden stress. Vertically offset fractures with staggered geometry combine with abrupt variations of sill thickness (fig. 9A and B) that formed in response to irregular deformation of the host mudstone caused by sand fluidization and evacuation from underlying parent units. Staggered sill formation and geometry have no relationship to heterogeneity in the host strata.

Stepped sills are generally thicker (a = 1 to 12 m; fig. 10A) than staggered sills and occur mainly in the upper part of the hydrofractured belt or above it. They form by repeated dilation and intrusion along a single fracture, or several stepped fractures, that are slightly discordant to bedding. Supra-lithostatic fluid pressure is inferred, but with a lower pressure differential than for formation of staggered sills. Note that it is more efficient to dilate a single fracture (the tensional strength of the host-strata is overcome only once) rather than multiple fractures of similar length (as for staggered sills). Stepped sills are typically layered with common banding and lamination that records continuous but pulsed fluid flow (fig. 9D and E; Scott and others, 2009; Hurst and others, 2011).

Multilayered sills require the lowest pressure differential to form and exploit multiple bedding surface heterogeneities in host strata (fig. 11C). Typically, they form where lithological and grain size contrasts form weaknesses in the tensional strength of the host strata that promotes lateral propagation of hydrofractures. Where the sand injection process is pervasive and multiple pulses of sand injection occurred, what was a thin-bedded depositional sandstone or siltstone intercalated with finer grained strata can become a thick amalgamated sandstone (>8 m thick) with rafts and clasts of host strata (fig. 9C). In concurrence with Vétel and Cartwright (2010) the occasional presence of shear-folds associated with sills implies that, at least in the SZ, some hydrofractures opened because the host strata locally failed in shear.

Irrespective of size, most sills have an overall saucer-shaped geometry, which is broadly analogous to magmatic intrusions (Pollard and others, 1975; fig. 10, figs. S6 and S10). Right Angle Canyon and West Tumey are the only known outcrop of km-scale saucer-shaped intrusions (figs. 1 and 10B; fig. S6; Vigorito and others, 2007; Hurst and Vigorito, 2017; Grippa and others, 2019). Jack-up and folding (fig. 10B; forced folding *sensu* Cosgrove and Hillier, 2000; Shoulders and Cartwright, 2004) of the host strata is recognised and demonstrates a correlation between height of the jack-up and the thickness of the underlying sandstone intrusion, a relationship often inferred in subsurface interpretation. Geometric and volumetric similarity between these outcrops and subsurface examples proves their value as analogues in subsurface interpretation (Hurst and Vigorito, 2017; Grippa and others, 2019).

Upper Dike Zone (UDZ).—The UDZ is dike dominated and extends vertically for 350 to 450 m from the top of the SZ (~20 m below the base of the Marca Mbr) to the base of the Cima Lentil (figs. 2, 3A, and 11A; figs. S1 and S6 to S11). Dikes have commonly a = 0.3 to 2.5 m and are up to 700 m long with a general semi-ellipsoidal

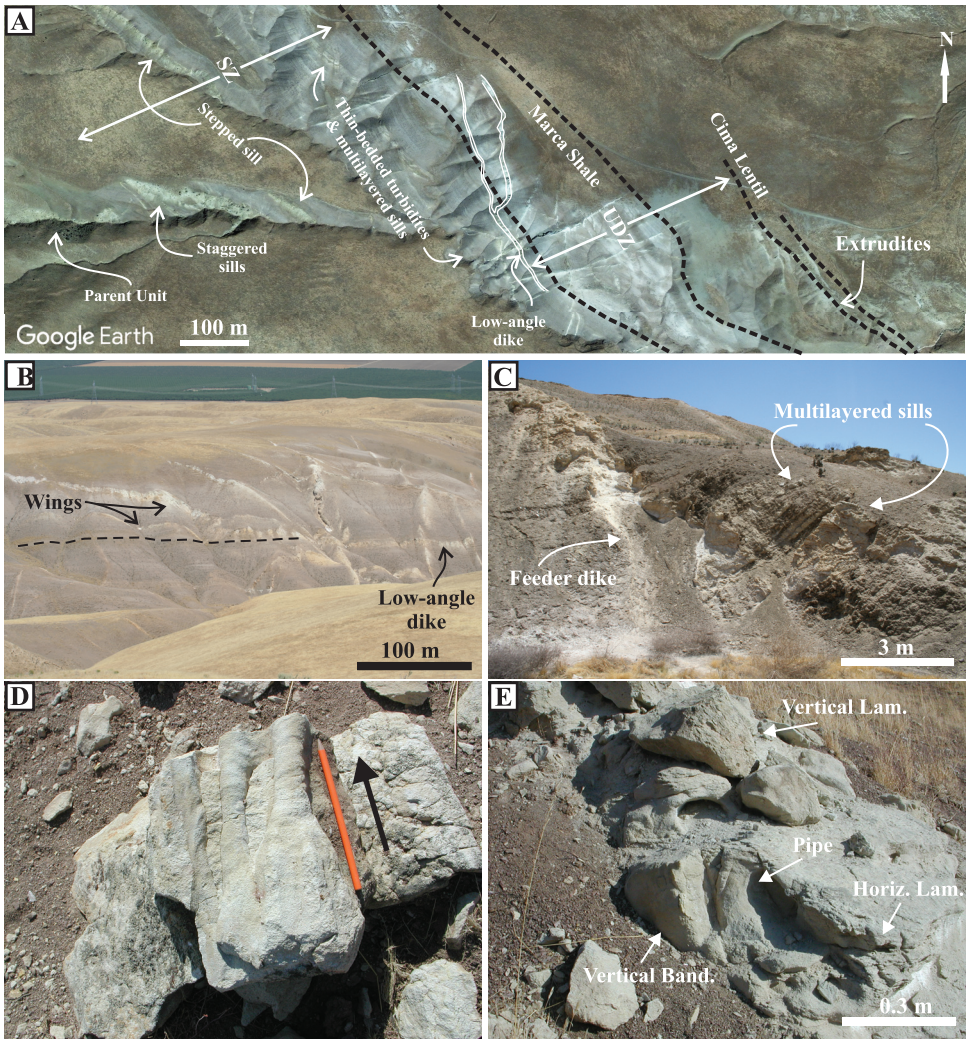

Fig. 11. A) Satellite image of the medial and upper part of the PGIC in Marca Canyon, showing the sill-dominated lower portion (SZ) and dike-dominated upper portion (UDZ). A 5 m thick low-angle dike with a saucer geometry (detail in B) is present, which to the NW (left) has two well-developed wings the largest of which cross cuts ~90 m of stratigraphy (see fig. S7). B) Detail of the low-angle dike (10–15° to bedding – dashed line) and the associated wings (20–50° to bedding). The low-angle dike has approximately the same strike as the bedding (dashed line) and is thus viewed in strike section and appears more bed concordant than in reality. C) Multiple minor sills (multilayered sill) emanating laterally from a major dike; Lower Tierra Loma Member – SZ. D) Cluster of pipes in a major high-angle dike, Marca Member - UDZ. The sample is from the margin of a high-angle dike and the arrow indicates the way up. E) Internal structures associated with a major high-angle dike (aperture = 0.7 m), Marca Member – UDZ.

geometry inferred from dip-strike distribution across single intrusions (Vétel and Cartwright, 2010). The dominant groups of dikes, TO and TP, create a crudely orthogonal pattern, which is particularly evident in the northern area (fig. 11A and B; figs. S7 and S10; Smyers and Peterson, 1971). Upper segments of large-aperture ($a = 5$ to 12 m) low-angle dikes present in the SZ transect part of the UDZ and are often associated with swarms of high-angle dikes (figs. 11A and B, fig. S6).

Dikes are either, continuous and linear, or have en echelon segments, and are characterised by series of lateral steps (fig. 11B; Vétel and Cartwright, 2010). Higher

in the UDZ, dikes tend to taper and bifurcate upward. Where dikes cross lithological boundaries, for example between diatomaceous (paler) and clay mineral-rich (darker) mudstone in the Tierra Loma and Marca mbrs, they typically segment with higher horizontal offsets, locally coupled with branching (figs. 11A and B; fig. S9).

Dike margins are typically sharp lithological boundaries although locally they preserve hackles and plumose markings, flute casts and other flow-marks such as grooves and scours (Scott, ms, 2009). Low aperture (a <0.2 m) dikes often lack internal structures, while more complex associations of structures characterise the inner parts of wider (a >0.2 m) dikes (fig.11D and E, table 2).

Most dikes terminate within the first 10 to 40 m of the diatomaceous Marca Member, some terminate <5 m below the base of a 5 to 15 m thick concretionary horizon in the upper part of the Marca Mbr (Minisini and Schwartz, 2007), and relatively a few reach the paleo-seafloor at the base of the Cima Lentil (figs. 3A, 11A, 12A, and 12D). The upper 100 to 150 m of the UDZ in the Dos Palos Mbr is characterised by a low density of dikes (fig. 12A, figs. S6, S7, S9, S10 and S11). Rare narrow (generally a <0.1 m) sills occur within 5 m below the paleo-seafloor (Vétel and Cartwright, 2010; Blouet and others, 2017).

Interpretation.—The UDZ records the emplacement of sandstone intrusions when fluid pressure was above the fracture gradient but below the lithostatic gradient. Dikes thin and branch upward, have semi-ellipsoidal 3D geometry and a segmented outer fringe at their periphery similar to magmatic intrusions (Pollard and others, 1975). In common with magmatic intrusions, the segmented outer fringe suggests that hydrofracture propagation occurred as a set of relatively short and commonly offset individual fractures that progressively amalgamate as the intrusion grows (compare with Vétel and Cartwright, 2010). In magmatic intrusions (Pollard and others, 1975; Schofield and others, 2016) variations in the mineralogy and mechanical properties of host-strata cause abrupt changes in fracture propagation velocity, which explains why dikes commonly segment coincident with lithological boundaries in host strata. Erosion along dike margins is often observed and confirmed by petrographic evidence. Together with the presence of grading and grain segregation (table 2) this confirms prevailing turbulent flow as recognised in other sandstone intrusions (Taylor, 1982; Diggs, 2007; Surlyk and others, 2007; Scott, ms, 2009; Scott and others, 2009; Hurst and others, 2011 and references therein).

Consistent cross-cutting relationships between the dikes are absent and TO and TP dikes are interpreted to have emplaced synchronously (Vigorito and others, 2008, Vétel and Cartwright, 2010; Vigorito and Hurst, 2010). Controls on dike orientation are discussed in detail later.

Rare occurrences of thin sills very close to the paleo-seafloor record situations where maximum and minimum stresses are approximately equal and low, and where the vertical and horizontal tensile strength of the host strata control intrusion geometry. Occurrence of shallow sills does not therefore imply supralithostatic fluid pressure throughout the PGIC hydrofracture system as concluded by Vétel and Cartwright (2010) and is recorded also in sandstone intrusions in the Miocene Santa Cruz Mudstone (Hurst and others, 2011) and probably in the Ordovician Rosroe Fm (Jolly and Lonergan, 2002).

Sandstone extrusions (Extrudites).—Dikes in the upper part of the UDZ terminate abruptly at the base of, or gradually within, the first a few metres of the Cima Lentil, a mixed clastic and carbonate unit within the otherwise mud-silt dominated Dos Palos Mbr (figs. 2, 3A and 12; Bartow, 1996, Schwartz and others, 2003, Minisini and Schwartz, 2007). Sandstone in the Cima Lentil varies in thickness from 0 to ~30 m and tends to be thicker in the Panoche Hills (~30 m thick in Right Angle Canyon) and thins to the south in the Tumey Hills (~6 m in West Tumey, fig. 1; fig. S1). Very

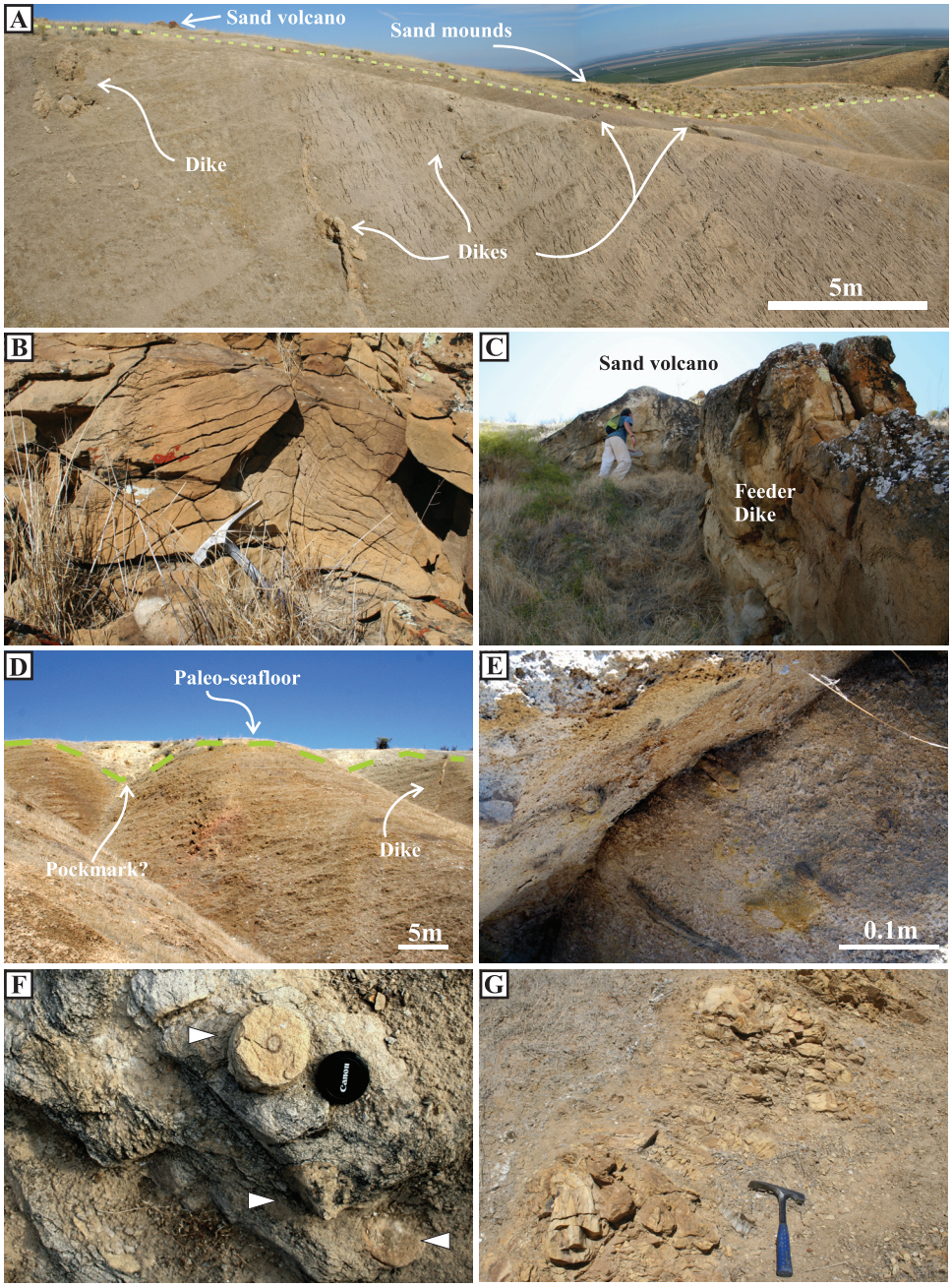

Fig. 12. Sand extrusions, Cima Lentil. A) Multiple dikes terminate at the paleo-seafloor (dashed green line) and feed sand mounds one of which contains a sand volcano, Marca Canyon. B) Detail of the sand volcano in A. C) A 2.2 m high sand volcano directly fed by a 0.5–0.7 m wide high angle dike, Marca Canyon. D) A dike terminates at the paleo-seafloor where there is an irregular basal contact (dashed green line). The shallow sand-filled depression on the right side is interpreted as a pockmark, Rosetta Canyon. E) Sub-horizontal burrows in Cima Lentil sandstone. F) A sandstone mound with multiple sand-filled vents (white arrows), Cima Lentil extrusions, Capita Canyon. G) A 0.4 m wide dike located immediately below the paleo-seafloor containing abundant clasts of pale grey host mudstone, Marca Canyon.

poorly consolidated fine- to medium-grained sandstone predominates in the northern area from Moreno Gulch to immediately south of Dosados Canyon (figs. 1). The top few meters (<10 m) of the unit are often carbonate cemented. Locally, the base of the sandstone fills low-relief depressions (up to 10 m wide and 2 m deep) that are commonly associated with underlying dikes (fig. 12D). Where best preserved and carbonate cemented, the sandstone is parallel to low-angle cross stratified and bioturbated (fig. 12E), with soft-sediment deformation, convolute lamination, pipes, consolidation laminae and dish structures, as well as occasional ripples and rare hummocky cross stratification. Clusters of mounded features (up to 1,5m high and 20m wide) with single or multiple cylindrical conduits (vents; fig. 12F) similar to abraded sand volcanoes (van Loon and Maulik, 2011) are preserved along with cross sections through sand volcanoes (up to 2 m high and 30 m wide, figs. 12B and C).

The sandstone-rich Cima Lentil coincides with areas where dikes are common in the underlying strata, or unusually large dikes (a >1 m) breach the paleo-seafloor (figs. 12A, C and D). Proximal to the paleo-seafloor dikes often contain host strata mudstone clasts (fig. 12G) thus providing evidence for local brecciation during hydrofracture propagation. Where dikes terminate just below the sea-floor, for example immediately north of Right Angle Canyon, discrete sandstone units are absent, sand and silt are sparse, and the Cima Lentil is predominantly rich in micritic carbonate characterised by mounds and pavements rich in chemosynthetic benthic fauna including bivalves, worms, deep-water solitary corals and bryozoans (Schwartz and others, 2003, Minisini and Schwartz, 2007). Further south in the Tumey Hills, carbonate and sandstone are laterally and vertically interbedded but are clearly segregated with predominantly micritic or bioclastic carbonate mounds with very little siliciclastic content.

Interpretation.—Previously interpreted as shelf-slope deposits (McGuire, ms, 1988a; Bartow, 1996, Schwartz and others, 2003, Minisini and Schwartz, 2007), the sandstones in the Cima Lentil were re-interpreted as predominantly sand extrudites (Vigorito and others, 2008; Vigorito and Hurst, 2010). Sandstone-filled depressions are interpreted as pockmarks (fig. 12D) that formed when the paleo-seafloor was breached by hydrofractures and filled by sand extruded onto the seafloor, typically via multiple vents that formed sand volcanoes. As vent activity varied and migrated through time the extruded sand aggraded and migrated forming extrudite facies (*sensu* Hurst and others, 2006). Large pockets and more laterally continuous sheets of sandstone formed that were locally reworked by bottom currents and waves. Extrudites with similar characteristics are observed in the Miocene of the Santa Cruz area, California (Bohem and Moore, 2002; Hurst and others, 2006; Hurst and others, 2011).

Dikes that did not reach the seafloor, hence not associated with venting of sand, became conduits through which migrating fluid diffused through the shallowest a few metres of underlying mud, and carbonate cold seeps formed (Minisini and Schwartz, 2007; Blouet and others, 2017). Prolonged seepage (up to 2 Ma, Minisini and Schwartz, 2007) of methane-rich fluid migrated through the underlying injection complex although the thermogenic or biogenic origin of the methane is unresolved (Minisini and Schwartz, 2007; Blouet and others, 2017).

PGIC: SUBSURFACE

Sandstone intrusions are observed in outcrops of late Cretaceous to early Paleocene age, along the western margin of the San Joaquin Basin, from north of the San Luis Reservoir to Coalinga (>180 km; figs. 1, 13, and 14) and are likely to extend into the subsurface of the San Joaquin Basin. This hypothesis is confirmed by reports of intrusions from the sparse core data, the recognition of saucer-shaped intrusions in 3D seismic data (Huuse and others, 2014) and, with lower confidence, from borehole petrophysical logs (figs. S13, S14, S15 and table S16). By integrating these data it is

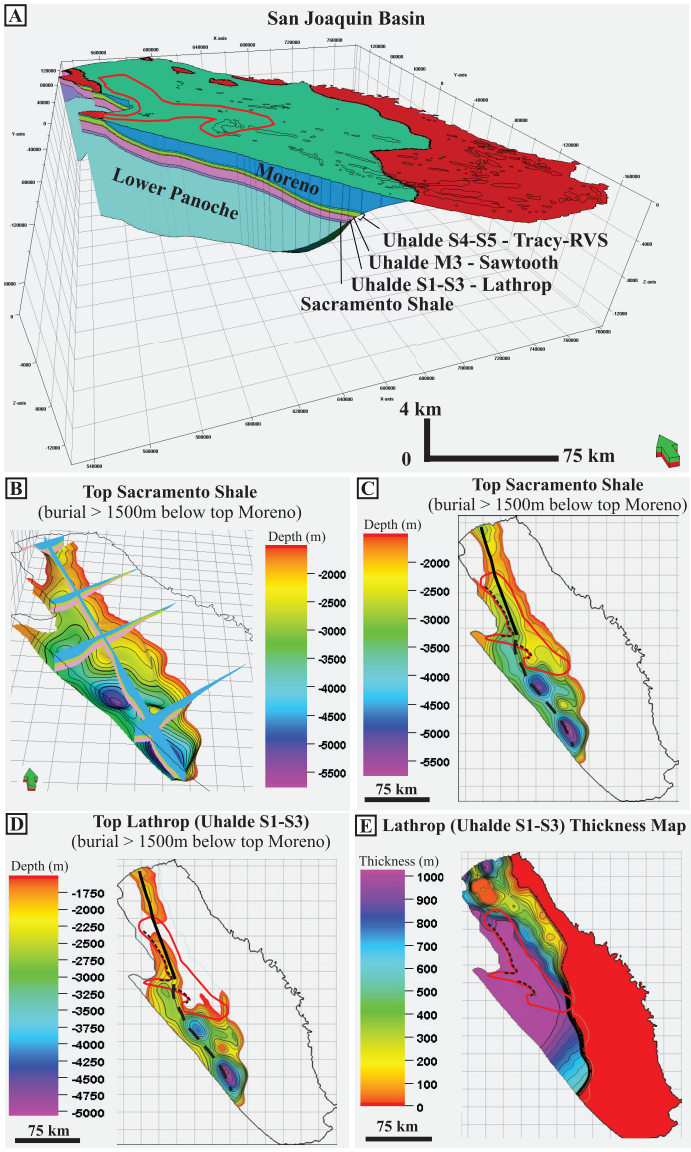

Fig. 13. San Joaquin Basin. A) 3D structural model. The red outline is the PGIC as defined at outcrop and subsurface in fig. S15. The outline of gas and oil fields is in black; B) Fence diagram with longitudinal and transverse sections across the 3D structural model displayed at the top Sacramento shale and base Lathrop (Uhalde S1–S3 Unit). C) and D) Structure maps truncated at depths shallower than 1500 m (present depth below the paleo-seafloor and corresponding to the first occurrence of quartz cement, equivalent to T_{max} ~70 °C) for the base (C) and top (D) Lathrop unit. These surfaces correspond to base and top of the Uhalde S1–S3 interval and define the maximum area and volume of the pressure cell subject to silica diagenesis in the Danian. Dotted lines are locations of intrusions at outcrop (Panoche-Tumey Hills to the north and Cantua Well-Coalinga to the south); the outline of the PGIC is in red. The black line represents the approximate location of the axis of the forearc basin in the Maastrichtian and the dashed line indicates the boundary between areas with high confidence sediment thickness data (to the east) and areas with increased structural complexity and lower confidence (to the west). The latter are excluded from volumetric calculations. E) Isopach map of the Lower Uhalde (S1–S3) – Lathrop unit. Note that the PGIC (red outline) overlies the thickest area of the Lower Uhalde-Larthop.

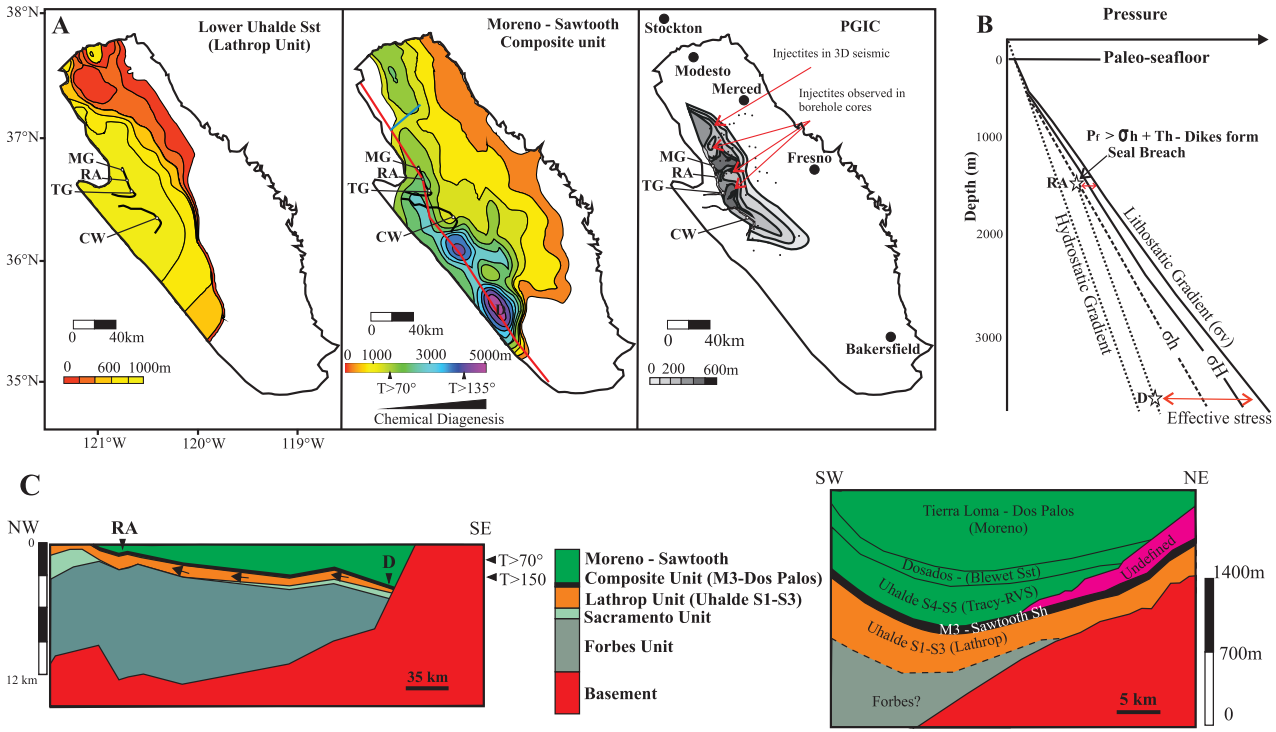

Fig. 14. A) Isopach maps from left to right: the Lower Uhalde Sst (Uhalde S1–S3, equivalent to the Lathrop unit), Moreno-Sawtooth composite unit (equivalent to the stratigraphic extent of the PGIC), and the sandstone-rich part of the PGIC above top Panoche Fm (fig. S15). All maps integrate outcrop, well and seismic data. Isopach map of the Lower Uhalde and Moreno-Sawtooth units modified after Hosford Scheirer (2007) and integrated with outcrop data. Red and blue lines are traces of the cross sections in C. Thick lines show trends of exposure, key outcrops are labelled (MG: Moreno Gulch; RA: Right Angle Canyon; TG: Tumey Gulch; CW: Cantua Well). Estimated temperature at burial from geothermal gradients in Peters and others (2008). B) Effect of lateral pressure transfer within the Lower Uhalde (Lathrop Unit) from the depocenter (D) to the study area (RA). Only minor overpressure at depth translates to hard overpressure and largely reduced effective stress at the basin margins. C) Cross sections through the San Joaquin Basin. To the left, a section through the western margin (red line in A); to the right, a section (blue line in A) west of San Luis Reservoir interpreted from a seismic line (fig. 3 in Mitchell and others, 2010). Both sections are flattened at the top Moreno Fm. South of the outcrop areas, and within large portion of the Maastrichtian-Danian basin, the lower Uhalde (S1–S3) and deeper units were buried deeply enough to experience T_{max} >70° and underwent some chemical diagenesis.

TABLE 3

Gross Rock Volume (GRV) and area for various lithostratigraphic units in the San Joaquin Basin models

Lithostratigraphic unit	Present GRV Volume	Area
Lower Uhalde Sst (S1-S3) / Lathrop Sst	7.2* to 8.4** x 10^3 km^3	1.08 x 10^4 km^2
Upper Uhalde Sst (M3-S5) / Tracy Sst and Ragged Valley Siltstone	4.8 x 10^3 km^3	1.1 x 10^4 km^2
Moreno Fm	1.8 x 10^4 km^3	1.1 x 10^4 km^2
PGIC drainage polygon GRV above base Uhalde Sst – Lathrop unit	3.0 x 10^4 km^3	1.37 x 10^4 km^2
PGIC drainage polygon GRV above base regional seal (Uhalde Sst M3)	2.2 x 10^4 km^3	1.37 x 10^4 km^2
PGIC gross rock volume	613 km^3	4.5 x 10^3 km^2
PGIC volume of remobilised and injected sand	25 to 49 km^3 (grain volume = 19 to 37 km^3, assuming 25% average porosity)	4.5 x 10^3 km^2

Calculations are derived from the Petrel 3D structural model; * and ** are the minimum and maximum estimates for the GVR of the Lower Uhalde Sst (S1-S3) – Lathrop unit within the thermal diagenesis window with top set at 2200 m (Smith and Berry, 1988) and 1500 m (first occurrence of quartz cement at outcrop, respectively (see: MINERALOGY AND PETROGRAPHY) of present burial below top Moreno Fm. The PGIC drainage polygon corresponds to the limit of the area where the Sacramento Shale is buried deeper than 1500 m, excluding the areas of increased structural complexity and with larger uncertainty on sediment thickness (see fig. 13).

possible to constrain the subsurface extent of the PGIC (fig. S15) and to estimate the gross rock volume of the PGIC in the San Joaquin Basin (table 3).

Elevation maps of key horizons from Hosford Scheirer (2007)[4] are integrated with our outcrop data, geo-referenced and imported into Petrel™ to construct a 3D structural model of the San Joaquin Basin flattened on the top Moreno Fm (fig. 13A to D). This model is used to make volumetric calculations (table 3) and to generate isochore maps for key intervals (S1-S3-Lathrop Sst, M3 – Sawtooth Shale, S4-S5 - Tracy Sst and Ragged Valley Silt and Moreno Fm, figs. 13A and 14), which provide information on the paleophysiographic evolution of the San Joaquin Basin during the Campanian to Danian. By comparing the position of the PGIC with the physiography of the basin at different times it is possible to make some key-observations: 1) the mapped extent of the PGIC overlies the thickest part of the Lathrop deep-water system (equivalent to Uhalde S1-S3; fig. 13E); 2) the PGIC is located at the top of paleophysiographic highs, updip of the main depocentres and along plausible migration routes for fluid flow when expelled from deeper parts of the basin (figs. 13C, 13D and 14A); 3) the areal extent of the PGIC coincides with areas where at the time of the injection the Moreno Fm was <1000 m thick (fig. 14A).

PETROLOGY, POROSITY AND PALEOTEMPERATURE

Sandstone

The paleo-Sierra Nevada is the predominant source terrane for sand deposited in the Uhalde Sst and Moreno Fm (Ingersoll, 1979, McGuire, ms, 1988a). More recent

[4] Hosford Scheirer (2007) distinguishes areas of structural complexity, coinciding with the western-central and western-southern areas of the basin, with a higher degree of uncertainty. In the outcrop areas south of the Vallecitos Syncline and extending along the Diablo Range into the Coalinga area, thickness of units as defined in the model does not match those observed at outcrop. These areas are excluded from our volume calculations hence our estimates are conservative.

evaluation of outcrop and seismic data identified a periodically active western source terrane within parts of the Coast Range Ophiolites, potentially from the Franciscan Subduction Complex and any overlying sedimentary cover exposed along the western margin of the forearc basin (Mitchell and others, 2010; Greene and Surpless, 2017). Presence in the upper Uhalde Sst (S4 and S5) of heavy mineral assemblages, in which minor glaucophane (blueschist terrane) is persistent (Hurst and others, 2017) as well as of Dosados Mbr conglomerate with clasts of metagreywacke, radiolaria-rich chert, and basalt (table 1) support the presence of a contemporaneous western source terrane. This coincides with switching from a largely unconfined basin floor fan setting, typical of older sections of the Panoche Fm, to the shallowing-upward slope environment that characterises the Moreno Fm (McGuire, ms, 1988a; Mitchell and others, 2010). Most sandstone intrusions are concentrated in the Moreno Fm (SZ and UDZ) and these have demonstrable spatial association with the depositional Dosados Sst. Mineral-chemical analysis confirms that most of the sand in the PGIC intrusions is derived from the Dosados Sst and that the Uhalde Sst contributed an insignificant sand volume (<1%) to the PGIC intrusions. Uhalde Sst provenance is limited to the sparse LDZ intrusions (Hurst and others, 2017) that formed conduits for fluid migration from the regional pressure cell below the M3 into the Moreno Fm when the PGIC formed.

Sandstone is generally poorly consolidated with traces (< 2% by volume) of quartz cement, the only evidence of thermally driven chemical diagenesis, in the deepest parts of the Uhalde S3 unit. Porosity ($\emptyset$) varies in accord with variations in average grain size and packing, and abundance of cement (table 4). Calcite and secondarily gypsum, are the main cements present. Calcite forms concretions and more continuous cemented layers that preserve both pristine depositional and sand fluidization structures, and their transition to injectites, thus constraining the timing of calcite precipitation to predominantly post sand injection. Absence of clasts of carbonate cemented sandstone in sandstone intrusions further supports that most of the carbonate cementation occurred after sand injection.

Where uncemented, the range of sandstone $\emptyset$ = 0.10 to 0.34 (Scott, ms, 2009)[5], with the lowest porosity in facies with tightly packed de-watering structures, and the highest porosity in the thickest sills (table 4). Depositional sandstone has more grain size variation and in general, a more diverse porosity distribution (table 4). By contrast, PGIC sandstone intrusions are pervasively fine to medium grain sand with $\emptyset$ = 0.2 to 0.34 (Scott, ms, 2009; Wu and others, 2018). Porosity range and distribution observed in the PGIC are similar to values derived using density logs from boreholes located close to the outcrop that have similar burial history to the PGIC outcrops (Grippa and others, 2019), and with sandstone porosity in nearby gas fields, $\emptyset$ = 0.35 to 0.26 at depths ranging from ~1000 to ~2500 m respectively (table 4). A general decrease in porosity with depth occurs and we conclude that porosity was initially controlled by the combination of depositional texture (grain sorting), post-depositional remobilisation and injection (grain packing), and subsequent mechanical compaction. Emplacement of sandstone intrusions created a permeable network that favoured persistent post-injection dewatering and focused fluid flow, which in turn, favoured the precipitation of carbonate cement.

A geothermal gradient of ~25 °C/km is inferred from basin modeling and temperature history matching of exploration and production wells in the San Joaquin Basin (Wilson and others, 1999; Peters and others, 2008). A T_{max}[6] of ~40–45 °C is estimated for the base of the Moreno Fm, which has a decompacted thickness of

[5] Where sandstone is cemented, original porosity, immediately after the emplacement of the PGIC, is estimated as the sum of present porosity plus carbonate and gypsum cements.

[6] Maximum temperature during burial.

TABLE 4

Porosity ranges for different elements of the PGIC including depositional sandstone with pristine depositional structures(S); sandstone with extensive dewatering structures (D); structureless sandstone (SL)

Porosity (%)					
Element	**Point Counting**	**NMR**	**Helium**	**Density logs**	**Grain size (mm)**
Parent Units	22-28-34 (S) 10-16-22 (D-SL)				
Lower Uhalde	10-18-25 (mostly D-SL)				0.10-0.37
Upper Uhalde	10-18-25 (D-SL) 15-24-32 (S)			15-20-25	0.10-0.37
Moreno Fm	15-22-34 (SL-S)	29–30-31	29–30 –31	20-28-35	0.10-0.40
Injectite	20 – 27 - 34			20-25-30	0.10-0.20
Dikes	20-25-30	23-26-34	24-27-33		0.10-0.20
Sills	24-30-34	26-29- 30	29-30-32		0.10-0.20
Extrudites	21-22-24			28-30-36	0.10-0.16

Sandstone Reservoir Analogues – Gas Fields, San Joaquin Basin

Field	**Pool**	**Formation**	**Geologic Age**	**Depth (m)**	**Porosity (%)**
Ash Slough Gas	Blewett	Moreno	Late Cretaceous	1676.4	30.0
Chowchilla Gas	Garzas	Moreno	Late Cretaceous	1021.1	39.0
Chowchilla Gas	Garzas	Moreno	Late Cretaceous	2438.4	26.5
Merrill Avenue Gas	Blewett	Moreno	Late Cretaceous	2011.7	27-34
Mint Road Gas	Blewett	Moreno	Late Cretaceous	1966	35

Porosity is estimated using different types of data. Note that low porosity is commonly associated with dewatering structures such as pipes, pillars, consolidation lamina and convolute lamination, and, in the Uhalde Sst, with structureless sandstone closely associated with dewatering structures. In the Moreno Fm, structureless sandstone may have locally higher porosity. In general, porosity decreases with burial with the lowest porosity in the Lower Uhalde. Porosity from point counting assumes that diagenetic cement (mostly calcite) precipitated post sand injection (see main text for details), hence porosity estimates are the sum of observed primary porosity and the volume of carbonate cement (when present). Porosity encountered in stratigraphically equivalent reservoirs from gas fields in the San Joaquin Valley are provided for comparison.

800–1000 m and paleotemperature at the sediment-water interface[7] of approximately 20 °C (Peters and others, 2008). Blouet and others (2017) estimate temperatures between 32 and 45 °C for the Moreno Fm at a burial depth of 800 m. Independent mineralogical evidence from the Moreno Fm in the Panoche Hills suggests T_{max} <40–45 °C (Hurst and others, 2017[8]; Hurst and others, 2021b). T_{max} was >70 °C at

[7] By the end of the deposition of the Moreno Fm (Dos Palos Mbr and Garzas Sst) shelfal conditions extended over much of the early Paleocene San Joaquin Basin with water depths likely shallower than 150 m (McGuire, ms, 1988a, b; Minisini and Schwartz, 2007).

[8] Persistence of titanite and Ca-amphibole (Hurst and others, 2017), which are typically unstable during early burial diagenesis, is consistent with T_{max} < 40–45 °C (Morton and Hallsworth, 2007).

approximately 250 m below the base of the M3 regional seal (burial depth ~1800–2000 m) when sand injection occurred, which is within the top of the thermally driven silica diagenesis window (Nadeau, 2011), and is consistent with the global occurrence of the onset of quartz cementation in sandstone (Walderhaug and others, 2001). Toward the basin axis to the south and east, the Moreno-Sawtooth composite unit, the lithostratigraphic section occupied by the PGIC, is up to 5 km thick (fig. 14A), and T_{max} >150 °C existed in the M3 regional seal and underlying sandstone (fig. 14A; Peters and others, 2008). It is implicit that in the more deeply buried parts of the basin, where higher T_{max} prevailed, chemical diagenesis occluded pores, lowered permeability, and expelled pore fluid (Oelkers and others, 2000; Walderhaug and others, 2001; Nadeau and others, 2002b).

Mudstone (Host Strata)

Clay mineral- and locally organic-rich, mudstone and subordinate siltstone, occur in the Uhalde Sst and Dosados and Tierra Loma mbrs. Whole-rock XRD analysis shows that illite (including mica) and smectite predominate (21.9–63.4%) (Scott, ms, 2009; Hurst and others, 2021c). Clay fractions (<2 μm) are dominated by dioctahedral, often almost pure (85–98%) smectite with subordinate kaolinite, illite and chlorite. Some organic-rich samples have hydrocarbon source rock potential (Hosford Scheirer and Magoon, 2007b).

In all mudstone samples $\emptyset$ <0.25, which by comparison with independent laboratory data from mudstone with similar porosity and mineralogy, is equivalent to permeability <1 nD (Mondol and others, 2008). Excellent seal quality is inferred. During the early Paleocene in the deeper part of the basin to the southeast T_{max} >150 °C was reached in mudstone in the Uhalde Sst at depths likely up to 6 km (fig. 14A and C; Peters and others, 2008). Consequently, large parts of the basin had T_{max} >60 °C, temperatures at which smectite decomposes and illite forms (Nadeau, 2011). Because illite forms smaller crystals than smectite (lower surface area to mass ratio) it compacts forming tighter micro-pores thereby enhancing seal quality (Nadeau and others, 2002a; Schneider and others, 2003). Smectite-illite transformation is associated with expulsion of water that, combined with fluid expulsion caused by thermally driven porosity reduction in sandstone, causes hard overpressure (Nadeau, 2011). This concurs with the observation from subsurface data from the San Joaquin Basin where illitization in mudstone stratigraphically equivalent to the Uhalde Sst is reported (Strongin, 1981). Confirmation of the excellent seal quality of mudstone in the Uhalde Sst in the deep basin comes from a borehole in the Kettelman Dome area (~90 km south east of the Panoche Hills) where hard overpressure in the range of 0.86 of the lithostatic pressure was recorded in equivalents of the Uhalde Sst at ~4000 m depth (Strongin, 1981).

Salinity and isotopic analyses of formation water from the Cretaceous and Miocene strata in the San Joaquin Basin indicate effective water expulsion after illite formation, and inferred shale dehydration (Strongin, 1981; Wilson and others 1999). A paucity of well penetrations in late Cretaceous strata prevents better constraint of the burial diagenetic history. Extensive illitization (diagenetic growth of illite) and quartz diagenesis in abnormally overpressured sandstone reservoirs are reported from the late Cretaceous turbidite systems in the adjacent Sacramento Basin (Mertz, 1988; Imperato and Nilsen, 1990) with illitization and quartz cementation starting at T >80 °C, equivalent to 2200 m burial (Smith and Berry, 1988). The Sacramento and San Joaquin basins have similar geological history throughout the Cretaceous, so data from Smith and Berry (1988) are consistent with our model. In the San Joaquin Basin, overpressure caused by illitization is documented at depths >2.5 km in Miocene strata with the highest overpressure observed at >4 km where illitization and shale dehydration reached their peak at temperatures >100 °C (Ramseyer and Boles,

1986; Wilson and others, 1999). It is inevitable that the highly smectitic mudstone throughout most of the PGIC undoubtedly contributed significantly to the development of hard overpressure concurrent with illitization, such as in the deepest part of the basin to the SE of the outcrop.

VOLUME OF SANDSTONE INTRUSIONS AND EXTRUSIONS

Mapping of the outcrop combined with mineralogical and petrographic data (Scott and others, 2013; Hurst and others, 2017) strongly support that sandstone in the Dosados Mbr is the main parent unit for the PGIC intrusions and extrusions. The remarkable implication is that at least 0.35 km^3 of sand, the estimated minimum volume of sandstone extrusions at outcrop, was transported within the shallow crust, through at least 600 m (the average vertical distance between Dosados Mbr and Cima Lentil) of mudstone-dominated section and vented onto the paleo-seafloor. The total volume of injected sand in the study area[9] of approximately 25 km^2 (Panoche and Tumey hills) is estimated as ~2 km^3 (table 5). This, however, is only a fraction of the volume of remobilised and injected sand in the PGIC (table 3, fig. S15). The gross rock volume of the PGIC, as traced at outcrop and in the subsurface of the San Joaquin Valley (fig. S15), is 613 km^3. Scott and others (2013) estimated an average N:G = 0.08 for the injected and remobilized sandstone in the Moreno Fm of the study area as observed at outcrop, however, N:G varies greatly from area to area (in general intrusion volume decreases away from the study area, especially towards the north). Here, a more conservative N:G range of 0.04 to 0.08 is used in our volume calculation.

Subsurface giant injection complexes are always associated with basin-scale aquifers, often deep-water turbidite systems (Huuse and others, 2004; Hurst and others, 2005; Huuse and others, 2005; Serié and Pemberton, 2021; van Oorschot and others, 2021), which represent the source of fluid necessary to form regionally developed hydrofractures and injectite complexes. It is thus reasonable to assume that the presence of a very large aquifer is a pre-requisite for the formation of a giant sand injection complex. We are unaware of previous studies that investigated the fluid-sand budget at basin scale, although, at meso-scale, the fluid-sand budget is reasonably well constrained with sedimentological and numerical models (Duranti, 2007; Scott, ms, 2009; Vigorito and Hurst, 2010; Hurst and others, 2011; Cobain and others, 2015). Constraints to the physics of injected flows and their hydraulic behaviour demonstrate that the fluid budget must be at least approximately equal to the sand volume but is most likely three to nine times larger, with grain concentration (C) in injected flows ranging from 0.1 to 0.54 (Scott, ms, 2009; Vigorito and Hurst, 2010; Hurst and others, 2011; Cobain and others, 2015). The volume of injected and remobilised sand in the PGIC is estimated as 25–49 km^3 (grain volume = 19–37 km^3, assuming 25% average porosity; table 3) and at least 16 (C = 0.54) to 171 km^3 (C = 0.1) of fluid was required to fuel the processes that led to emplacement of the PGIC.

Using the 3D model of the San Joaquin Basin (based on earlier work by Hosford Scheirer, 2007; fig. 13) and integrated with our outcrop data, it is possible to estimate the sand-fluid budget involved in the emplacement of the PGIC. The main source of fluid in our model is the lower part of the Uhalde Sst (S1–S3), which in the subsurface coincides with the basin-scale fan systems of the Lathrop Sst (fig. 2, Ingersoll, 1979; Cherven, 1983; Bartow and Nilsen, 1990). Quartz diagenesis in sandstone combined with quartz and silicate diagenesis in associated mudstone, initiate at T ~70 °C, here

[9] In the area under consideration the total outcrop length in the study area is ~25 km and the average outcrop width is ~1 km.

TABLE 5

Present-day granular and pore-fluid volumes, $V_{granular} = V_{tot}\,(1 - \Phi)$ and $V_{fluid} = V_{tot}\,\Phi$, respectively from sandstone in the PGIC

	Total rock volume (V_{tot})	**Granular volume ($V_{granular}$)**	**Fluid volume (V_{fluid})**
Uhalde Sandstone (present day)	S1-S5: 19.5 to 22.8 km^3 S4-S5: 3.7 to 5.2 km^3 S3: 4.5 to 6 km^3	S1-S5: 15.6 to 18.2 km^3 S4-S5: 3 to 4.2 km^3 S3: 3.6 to 4.8 km^3	S1-S5: 3.9 to 4.6 km^3 (for $\Phi = 0.2$) S4-S5: 0.7 to 1 km^3 S3: 0.9 to 1.2 km^3
Intrusions (present day)	1.28 km^3	0.96 km^3	0.32 km^3 ($\Phi = 0.25$)
Extrusion (present day)	0.35 km^3	0.26 km^3	0.09 km^3
Uhalde Sst – pre-injection	S1-S5: 16.7 to 26 km^3 (for $\Phi = 0.30$) S4-S5: 4.6 to 6.4 km^3 (for $\Phi = 0.35$) S3: 5.1 to 6.9 km^3 (for $\Phi = 0.30$)	S1-S5: 11.7 to 18.2 km^3 S4-S5: 3 to 4.2 km^3 S3: 3.6 to 4.8 km^3	S1-S5: 5 to 7.8 km^3 (for $\Phi = 0.30$) S4-S5: 1.6 to 2.2 km^3 (for $\Phi = 0.35$) S3: 1.5 to 2.1 km^3 (for $\Phi = 0.30$)
Sand and fluid volume involved in sand injection		1.22 km^3 (present day granular volume of intrusions + extrudites)	1 to 11 km^3 (fluid volume estimate for grain concentrations of 0.54 and 0.1 in injected flows).

Total sandstone, injected sandstone and depositional sandstone volumes are the sum of the relative volumes calculated for each outcrop in the Panoche Hills over a 14 km transect (see section: *Volume of Sandstone Intrusions and Extrusions*). Pre-injection V_{tot} and associated V_{fluid} are included. Estimates of pre-injection V_{tot} were made by keeping present-day $V_{granular}$ constant and by using an average pre-injection porosity of 0,3 and 0.35 (estimated pre-injection porosity from thin sections). Additionally, the table has estimates of the $V_{granular}$ and V_{fluid} involved in the formation of the PGIC. Note that fluid volume loss in the Uhalde Sandstone, from pre- to post-injection, ranges from approximately equal to about x3 the $V_{granular}$ of the intrusions and extrudite combined. This concurs with our volumetric considerations for fluid/solid mass-balance during sand injection. These estimates only consider the potential local source of fluids and do not include any contribution from the Dosados and Tierra Loma depositional sandstone and adjacent portions of the basin.

equivalent to ~2000 m burial depth[10] (with T_{max} >100 °C at 3200 m burial). A volume of 7200–8400 km^3 of the lower Uhalde Sst (S1–S3 and equivalents, fig. 2; table 3) underwent quartz and silicate diagenesis that occluded primary porosity thereby expelling aqueous fluids that raised pore fluid pressure and later caused sand injection.

Loss of $\emptyset$ = 1% from the gross volume of the Uhalde S1–S3 – Lathrop Sst unit sources a fluid volume of 72–84 km^3, which is greater than or equal to twice the maximum estimated grain volume of sand remobilized and injected in the PGIC. Published porosity-depth curves for mudstone and sandstone (Chuhan and others, 2003; Mondol and others, 2008; Bruijn and Almqvist, 2015, Yeseul and others, 2018) show that for a burial increase from 2000 to 6000 m, the maximum thickness of the late Cretaceous-Danian sequence above base Uhlade Sst - Lathrop Sst, a porosity loss between 10% and 20% is expected hence, the fluid budget for injection was likely to be more than an order of magnitude greater than the 84 km^3 estimate. Widespread evidence for pervasive sandstone liquefaction in the Uhalde Sst (<2000 m burial and T_{max} <70 °C, figs. 4A, B and 5; figs. S4 and S5) suggests that where poorly consolidated, grain fabric re-arrangement into tighter packing following liquefaction was an additional source of fluid during sand injection. Upscaling the estimates of the fluid budget derived from sandstone outcrop for the Uhlade S4–S5 and Dosados-Tierra Loma Mbr (table 5) to the entire PGIC area (fig. S15), the fluid contribution from this unit to sand injection is at least 115 km^3.

There are at least three demonstrable limitations to the estimate of the fluid budget: underestimation of gross rock volume, overestimation of burial depth (and thereby T_{max}), and overestimation of fluid volume. Gross rock volume calculations are based on present day thickness (strata already dewatered and compacted), which if unaccounted for causes underestimation the fluid volume expelled per unit of porosity loss. Estimation of burial depth of the Uhalde S1–S3 – Lathrop is compromised because it includes part of the Danian section (<200 m) above the inferred paleo-seafloor (Upper Dos Palos Mbr, part of the Garzas Sandstone). Fluid volume is overestimated because no consideration is given to seepage through the overburden, which is an inevitable continuous fluid loss through geologic time, but problematic to quantify; even in exceptionally low permeability seals (< 1 nD) seepage occurs.

DISCUSSION

Hydrofracturing and Vertical Fluid Pressure Evolution during Sand Injection

Increasingly common and widespread knowledge of giant sand injection complexes globally (Hurst and Cartwright, 2007; Braccini and others, 2008; Huuse and others, 2010; Hurst and others, 2021a) provides insight into the origin, geometry and distribution of regional hyrdrofracture networks in the shallow crust. In sand injection complexes, hydrofractures are "sand-propped" and form sandstone intrusions that are easily resolved at outcrop (figs. 6 to 11; Hurst and others, 2011; Hurst and Vigorito, 2017; Grippa and others, 2019) and using subsurface data (Huuse and others, 2004, 2007; Jackson, 2007; Lonergan and others, 2007; Schwab and others, 2015; Satur and others, 2021). It is entirely possible that regionally developed hydrofracturing occurs in the shallow crust but in the absence of sand injection is difficult to discern in fine grained strata. Hydrofracture propagation is driven and sustained by the pressure gradient established between the base of the fracture, in the PGIC the top of a parent sandstone, and the tip or leading edge of the fracture where stress concentrates

[10] At outcrop first indications of quartz cement occur at ~1500 m below the paleo-seafloor, hence we limit our volume estimate to the sections of stratigraphy presently buried at least 1500 m below the top of the Moreno Fm.

(Brenner and Gudmundsson, 2004). Once formed, hydrofractures remain open and propagate so long as the fluid pressure in the fracture exceeds the *in-situ* stress normal to the fracture. Hydrofracture in homogeneous, isotropic rock at constant overpressure produces elliptical opening profiles (Sneddon and Lowengrub, 1969) with apertures that vary regularly along the profile with overpressure (Valkó and Economides, 1995). In layered strata the aperture variation of hydrofractures is, in general, much greater and depends on the mechanical contrast between layers (Brenner and Gudmundsson, 2004).

Heterogeneity in the Uhalde Sst and Moreno Fm reflect: 1) distinctive changes in composition and grain size of the mudstone and 2) alternation with depositional sandstone and siltstone. Both are related to the evolution of the depositional environment from basin floor to shallowing upward to the shelf edge (McGuire, ms, 1988a; Bartow and Nilsen, 1990; Bartow, 1996; Nilsen and Moore, 1997). Evidence for extensive liquefaction and fluidisation confirms that, at the time of injection, the depositional sandstone was poorly consolidated while the adjacent mudstone, although weakly lithified, was cohesive and mechanically stiffer. Sandstone intrusions that intersect lithological boundaries are observed to change in aperture and/or dip, bifurcate, or arrest as they approach or cross lithological boundaries (fig. 11A and B, figs. S6 to S9, Vétel and Cartwright 2010). Intrusions intersecting thick sandstone (typically t >5m) tend to arrest or increase in aperture and/or become less steep (fig. S4, Vétel and Cartwright, 2010). Exceptionally long high-angle dikes (vertical length H >200 m) occur in mudstone dominated strata above the Dosados and Tierra Loma mbrs (figs. 3, 11A and figs. S6, S7 and S9), which concurs with earlier studies that show hydrofractures are more likely to propagate vertically in stiff than in soft layers (Brenner and Gudmundsson, 2004 and references therein). Contrast in the stiffness of adjacent lithologies controls fracture aperture, which is greater in soft layers, and controls fracture tip geometry. In soft strata fracture tips become blunt, stress concentration is reduced, and fracture propagation may stop (Brenner and Gudmundsson, 2004). Blunting of fracture tips and consequent arrest of the propagation of the leading edge also occurs when fractures intersect high permeability intervals, for example, depositional sandstone, that induce rapid leak-off of fluid (Dong, 2010) and hence a drop in fluid pressure. An additional influence on the opening mode of fractures is caused by changes in Young's modulus in adjacent layers that induces transition between tensile and shear opening and generates abrupt changes in fracture dip and aperture (Brenner and Gudmundsson, 2004; Dong, 2010).

In the Danian, when pore fluid pressure below the regional seal in the Uhalde Sst exceeded the minimum horizontal stress plus the tensional strength of the host strata, hydrofractures began to form in the M3 (figs. 3A and 15). Overpressured fluid opened and propagated fractures in focused areas where long, steep and isolated dikes formed (LDZ, fig. 3B and figs. S2 and S12) mainly perpendicular to the minimum horizontal stress (TO group). Simultaneously, some pre-existing fractures and faults dilated along which the tensional strength of the host strata was low and possibly zero (for example TP group). Focusing of hydrofracturing to form localised dikes discouraged the clustering of hydrofractures (Jolly and others, 1998) in the M3 regional seal. From their points of origin in the M3, dikes become more abundant upward and form an interconnected network (fig. 15A). Genetic, spatial and temporal relationships between the various branches of the PGIC are discussed later.

Along the track of a single propagating fracture, fluid pressure within the fracture decreases following a gradient depending on the density of the fluids and on the concentration (C) of the solid particles ($0 < C < 0.54$) and is always less than the overburden (fig.15C). It follows that the magnitude of overpressure, relative to the *in-situ*

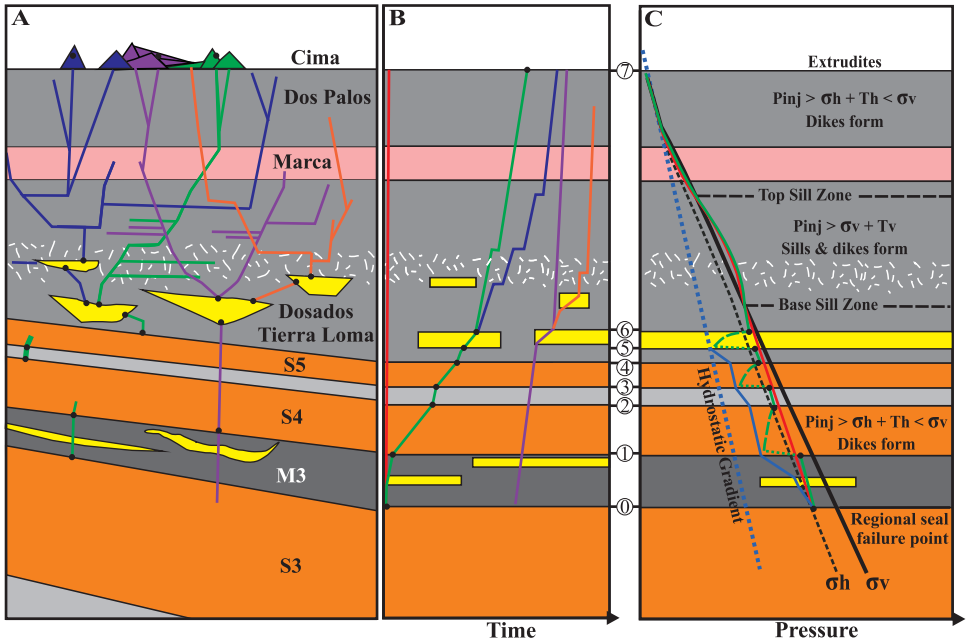

Fig. 15. A) Distribution of sandstone intrusions in the PGIC. Different color lines represent different branches of the PGIC. Black dots represent points where intrusions depart from and terminate in depositional units. B) Relative timing of propagation of intrusions along individual branches (thick lines in A). The red line represents propagation of a single vertical hydrofracture from the base regional seal to the seafloor. C) *In situ* stress conditions (black lines), hydrostatic gradient (dotted blue line), idealized pore fluid pressure conditions pre-injection (thick blue line) and pore fluid pressure evolution during injection in an idealized single vertical hydrofracture (red line in B and C) and along a branch of the PGIC (thick green line in A, B and C). Intrusions originate in sparse focused areas and propagate upward becoming more numerous and widespread. The highest density of intrusions is reached in the sill zone and more specifically in the Hydrofractured Belt (white dashes) where overpressure in the fracture network attained its maximum value above the *in situ* stress (C). As intrusions propagate into the overburden, multiple branches form each characterized by different complexity, tortuosity and velocity of propagation (B), hence formation of cross-cutting relationships (A). Intersection of hydrofractures with thick depositional units (for example, points 1, 3 and 5) that are aligned on a lower pore fluid pressure gradient, causes an abrupt pressure drop (dotted part of the green line), that may stop propagation of hydrofractures, pressure is transferred and fluids may vent into the depositional sandstone. Because of the drop in pressure at the tip of the fracture, flow velocity in the fracture increases and sand may entrain into the flow. As pressure transfers from the underlying unit, pore fluid pressure in the formation progressively increases (pressure build up phase – dashed green line) until it exceeds the fracture gradient at the top of the depositional unit and new hydrofractures form (for example, points 2, 4 and 6). The time interval represented by a pressure build up phase depends upon the volume of the depositional unit and the original overpressure (B). Phases of pressure build up in large volume sandstones are probably the largest time lapses in the emplacement of an injection complex (B).

stress, grows with upward fracture propagation and fluid pressure approaches the intermediate and maximum stress (fig. 15C).

Distribution and Trend of Sandstone Intrusions

Hydraulic fractures form when $P_f > \sigma_n + T$, where P_f = fluid pressure, σ_n = component of the confining stress normal to the fracture and T= tensile strength of the host strata. Vertical dikes form when $P_f > \sigma_{|h|} + T_h$ and sills form when $P_f > \sigma_v + T_v$, where $\sigma_{|h|}$ and σ_v are the horizontal (perpendicular to the orientation of the fracture) and vertical component of the confining stress, and T_h and T_v are the horizontal and vertical tensile strength of the host strata. In poorly consolidated mudstone T is

generally very small (Hill and Marsters, 1990; Bell, 2000; Gudmundson, 2011), and when strata are buried deeper than a few 100's m, values of T are generally negligible when compared with the confining stress (Jolly and Lonergan, 2002). Sandstone intrusions are natural hydraulic fractures propped open by injected sand. It follows that the distribution and orientation of sandstone intrusions is primarily controlled by the relationship between P_f in the propagating hydraulic fractures and *in-situ* stress.

To constrain this relationship structural data for both sandstone intrusions and sand-filled pre- and/or syn-injection faults, are back-rotated to their position at the time injection occurred. Using the base of the Cima Lentil (paleo-seafloor) as the datum, the structural data were rotated 35° to the SW along an axis striking N330 (figs. 16A and B). After back rotation, the TO dikes strike N40–80 and the TP N300–340. In the well-defined tripartite architecture of the PGIC, the LDZ and UDZ are dominated by steep dikes, but dikes become progressively less steep in proximity to SZ. This characteristic of the architecture of the PGIC is easily visualized when the dip of the dikes is plotted in relation to their stratigraphic position (fig. 16C). Concentration of sills in the SZ, in association with dikes with diverse strike and dip, implies that, when P_f was supra-lithostatic and sills formed, the pressure in the propagating hydrofractures overcame the confining stress and opened fractures in all directions. This, together with the fact that in both the LDZ and UDZ sills are extremely rare and that major dikes are >75° steep, is indicative that throughout the vertical extent of the PGIC (the shallowest 1.5 km of the forearc sedimentary sequence), the principal regional stress at the time of intrusion was vertical (σ_v), and the intermediate and minimum stresses were in the horizontal plane (Vigorito and Hurst, 2010), respectively σ_H maximum horizontal stress and σ_h minimum horizontal stress.

Because high-angle dikes open mainly against the horizontal stress, analysis of their trends helps determine the orientation of the intermediate and minimum stress and highlights stress variations present within the injection complex when it formed. TO and TP dikes respectively represent 43% and 18% of all high angle dikes and they are best represented in the LDZ and UDZ. If only major (length > 100 m) dikes are considered, the significance of the TO group is very clear (fig. 16A). The trend of major dikes is less affected by local variations in the stress field and stress perturbations caused by the presence of other sandstone intrusions and their strike is more likely to be controlled by the regional stress field at the time of injection (Bohem and Moore, 2002). When the azimuthal trend of the dikes is plotted versus aperture and length, both increase toward two defined strike intervals N50–70 and N240–260 (fig. 16E), which is consistent with a maximum horizontal stress oriented N65 (±10°). This approximates the direction of main compressive stress for the western margin of the San Joaquin Basin during the Early Paleocene (Bartow, 1991) and confirms that TO fractures opened against the minimum horizontal stress with an opening direction parallel to the orientation of the trench. It follows that, the high angle dikes in the TP group opened mainly against the maximum horizontal stress (fig. 16A).

Dikes in the TO group are almost exclusively near vertical, whereas dikes in the TP group vary in dip, mainly between 45 and 80 degrees, and 82% dip eastward (landward) (figs. 16A and D). Emplacement of the TP group was favoured by extensional stress and probably occurred along minor fractures and faults caused by shallow gravitational tectonics promoted by: a) uplift of the subduction complex to west and the consequent tilting to the east, and b) landward gravitational collapse of the western (seaward) margin of the forearc basin. The uplift of the subduction complex during the late Campanian and Maastrichtian time, and the consequent formation of a topographic high along the west margin of the basin (Bartow and Nilsen 1990, Mitchell and others 2013), were likely associated with important local perturbation in the regional stress field (Martel, 2016; Bird, 2017) which promoted local extension. A SW-

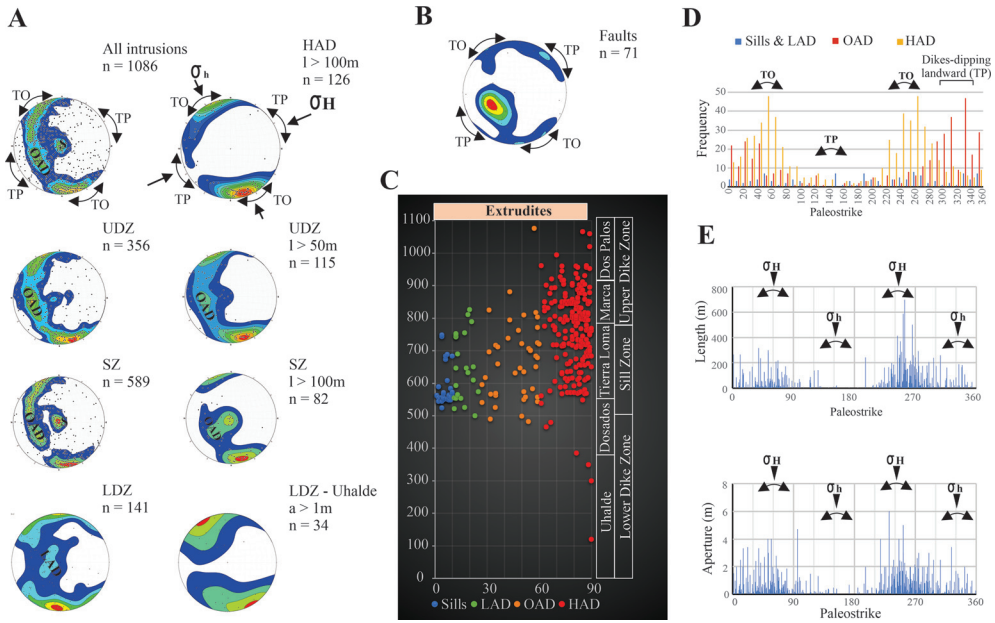

Fig. 16. Statistical analysis of the sandstone intrusions and faults in the PGIC. Structural data are back-rotated 35° anti-clockwise (to the W) along an axis trending N330°. S: sills; LAD, OAD and HAD: low, oblique and high angle dikes respectively. A) Orientation of sandstone intrusions at the time of injection (paleo-strike). Plots of the poles of the sandstone intrusions (lower hemisphere projection) for the entire dataset and in the three stratigraphic zones of the PGIC. The plots show a well-defined structural trend with a high density of poles belonging to two groups: 1) trench orthogonal (TO – strike N40 to 80) and 2) trench parallel (TP – strike N300 to 340). Major intrusions (for example, length $l > 50$ m or aperture $a > 1$ m) are dominantly high angle dikes striking TO and subordinately oblique angle dikes striking TP and dipping landward. Major high angle dikes (length $l > 100$ m) are almost exclusively TO. Principal *in-situ* stress is vertical, maximum and minimum horizontal stress are respectively (σ_H = N65 and σ_h = 155N). B) Plot of poles of pre- and syn-injection faults with TP landward dipping faults most common. Displacement is generally low (< 2 m) but occasionally up to 10 m. C) Intrusion paleodip vs true stratigraphic position (depth below the paleo-seafloor). Deep in the section intrusions are sparse and high angle (LDZ). Dikes become less steep upward as they approach the SZ. Sills are almost entirely restricted to the SZ and co-occur with dikes with diverse dip. In the UDZ dikes are dominantly high angle. Data from a transect of the PGIC extending from Moreno Gulch to Capita Canyon. D) Frequency of intrusions and their paleo-strike. TO dikes dominate and are mostly high angle. Landward dipping TP dikes are common and mostly oblique angle (OAD). E) Dike length and aperture vs paleostrike, show that dike length and aperture increase toward and reach their maximum values between N50–70 and N240–260. These clusters of large dikes have a weighted average corresponding to an azimuth N65, which confirms the orientation of the maximum horizontal stress (σ_H). TO dikes open against the inferred minimum stress (σ_h = N155) hence favoring their formation. They tend to be high angle and larger (in aperture and length) than dikes in other orientations. Long, wide TP dikes dip exclusively landward (mostly to the NE) and probably formed by sand injection into pre-existing extensional faults and fractures.

NE oriented extension is confirmed by the presence of pre- and syn-injection normal faults (for example fig. 8A) that dominantly strike NNW-SSE and tend to dip ENE at oblique- to high-angles (fig. 16B), these faults show a strong affinity, in trend and dip, with the TP intrusions (fig. 16A). The orientation of these faults concurs with earlier studies (Palladino and others, 2018) that document the presence of NNW-SSE oriented sandstone-filled normal faults but neglected the regional structural control.

Random orientation of sandstone dikes throughout the Moreno Fm was proposed by Vétel and Cartwright (2010), from which they infer an isotropic stress regime in the horizontal plane, *in situ* stress dominated by vertical loading under the K_0 condition and emplacement of the PGIC in the center of the forearc basin. Most of their data are from a stratigraphic interval coincident with the SZ (mostly correspondent with the Tierra Loma Mbr, fig. 3 in Vétel and Cartwright, 2010) in which dikes are randomly oriented. Despite UDZ and LDZ being recognized (fig. 18 in Vétel and Cartwright, 2010) and demonstrably different than the SZ, UDZ and LDZ data are merged uncritically with SZ data into a single distribution. This introduces a strong statistical bias that in turn invalidates their analysis and conclusions regarding the regional stress regime and the inferred location of the PGIC in the forearc basin at the time of sand injection.

The active Kumano forearc basin, located above the modern Nankai subduction zone of SW Japan, is proposed as an excellent analogue for the structural setting of the PGIC (fig. 17). It is characterised by multiple normal faults, both trench-orthogonal and trench-parallel (more abundant and mostly dipping landward) in the seaward portion of the basin onlapping the subduction complex (Moore and others, 2013). In the Kumano Basin faulting is associated with thrusting in the underlying accretionary prism, but noticeably absent within the forearc basin (fig. 17), and with formation of intra-wedge highs created by rugosity on the subsiding oceanic plates and consequent uplift of parts of the basin. This caused flexure, tilting and gravitational tectonics with concomitant faulting and landward extension within the seaward portion of the forearc basin fill, whereas toward the basin centre extensional faults are scarce or absent (Sacks and other, 2013; Saffer and others, 2013; fig. 17). Extensional faults have small displacements (10 to 20 m in general), no evidence of growth, and are thought to be short lived (Moore and others, 2013). In the same part of the forearc basin, reverse faults and thrusts are absent. It is inferred that the compressive stress, which characterises the overall deformation in the accretionary prism, does not propagate into the overlying forearc sedimentary basin, in which only extensional regimes and structures are recorded (Moore and others, 2013; Sacks and other, 2013; Saffer and others, 2013; see also: Fuller and others, 2006 and Mannu and others, 2016). Seismic data interpretation validates this hypothesis, and the results of leak-off tests provide evidence of stress decoupling between the accretionary prism and the overlying sedimentary basin (fig. 17; Chang and others, 2010). In the seaward part of the Kumano Basin a sharp angular unconformity separates the sedimentary sequences from the underlying deformed accretionary prism. Below the unconformity the maximum horizontal stress is oriented orthogonal to the trench (parallel to the main compressive stress) with the overburden the intermediate stress (fig. 17). In the forearc sedimentary basin, maximum stress is vertical, and the maximum and minimum horizontal stresses are, in general, trench orthogonal and parallel, respectively (Chang and others, 2010). Maximum horizontal stress rotates from trench-orthogonal in the basin centre (site C009; fig. 17) to trench parallel toward the seaward margin of the basin (over a distance of 20 km, site C002; fig. 17). This is consistent with the location and trend of the normal faults which are more abundant in the seaward-most part of the Kumano Basin and mostly strike parallel to the trench (Saffer and others, 2013). Also, it suggests that stresses in the landward portion of the basin and upper wedge are mainly

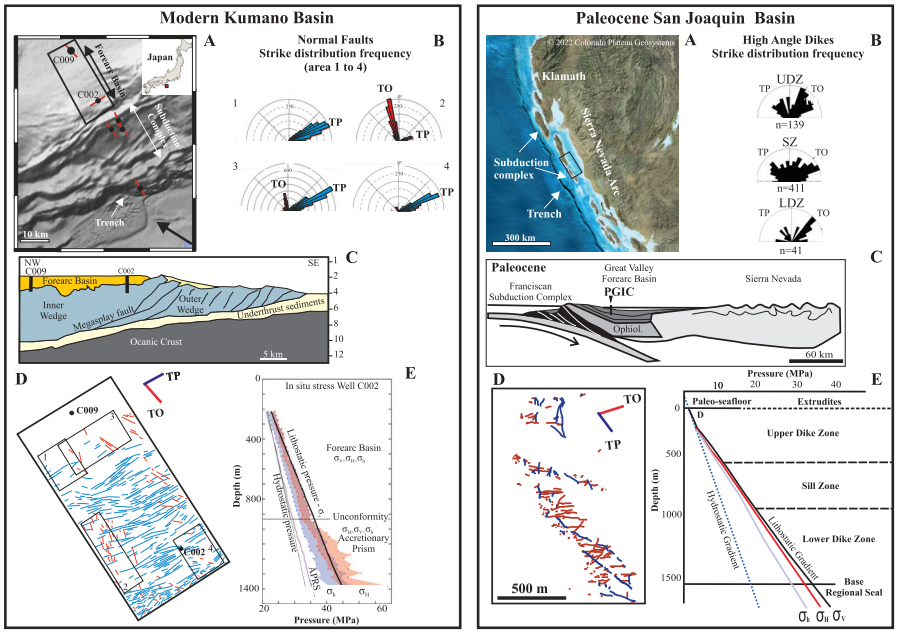

Fig. 17. Comparison between the Kumano and San Joaquin forearc basins. Kumano Basin: A) Seafloor map showing the main physiographic elements of the seaward portion of the basin. Location of 3D seismic data (black box) and IODP wells (C009 and C002) are shown. Red lines indicate the orientation of the maximum horizontal stress (modified from Chang and others, 2010). B) Frequency and orientation of trench orthogonal (TO) and trench parallel (TP) normal faults mapped from 3D seismic. C) Geoseismic section across the subduction complex and the overlying forearc basin. D) Map of extensional faults occurring in the shallow section of the forearc sequence. E) Variation of the orientation of the *in situ* stress with depth in well C002. In the upper section, above the unconformity that marks the boundary of the deformed subduction complex, the principal stress is vertical and the intermediate and minimum stresses are in the horizontal plane, oriented perpendicular and parallel to the trench. Below the unconformity the principal stress is horizontal and oriented perpendicular to the trench, the overburden is the intermediate stress and the minimum stress is oriented parallel to the trench. San Joaquin Basin: A) Paleogeographic map of the San Joaquin Basin in the Danian with the approximate location of the study area (black box). B) Orientation and frequency of high angle dikes in the LDZ, SZ and UDZ of the PGIC. C) Geological section across the forearc basin in the Danian showing the approximate location of the outcrop area. D) Orientation of the large high angle dikes in Right Angle Canyon showing the abundance of trench parallel and trench orthogonal intrusions. E) *In situ* stress distribution is derived from the distribution of the sandstone intrusions in the shallowest 1500 m of the basin. Intrusions are only present in the undeformed section, above any significant compressional structures of Paleocene age or older. There is no indication of reversal of the principal stress from vertical to horizontal.

controlled by the regional tectonic processes whereas, along the seaward margin stresses reflect local effects of topography or slip on the shallow megasplay fault (Saffer and others 2013).

Validation of the Kumano Basin analogy in the PGIC is demonstrated by evidence for basinward tilting of the forearc basin (figs. 18A and B), absence of pre-injection evidence for compressional deformation, and little evidence for any other deformation, combined with analysis of the distribution and orientation of the intrusions (figs. 16A and 17). In this context intrusions formed preferentially parallel to the maximum horizontal stress, oriented orthogonally to the trench, whereas less abundant intrusions formed parallel to the trench by dilating pre-existing fractures (mostly small faults dipping landward) associated with uplift and tilting of the seaward margin of the basin. Accordingly, TP intrusions are predicted to be more sparse or absent in the LDZ and UDZ present in the PGIC in subsurface and located toward the basin centre. Assuming a similar regional stress regime, a basin-centre setting can be inferred for the sandstone intrusion at Gas Point in the Upper Cretaceous of the Sacramento Basin (Jolly and Lonergan, 2002), which only has TO high-angle dikes. Because our statistical strike-distribution data are from a limited transect of the PGIC (roughly 35 km), it is likely that the local stress field, and consequently intrusion strike distribution, vary commensurately in response to local controls. These include changes in the physiography of the margin of the forearc basin, presence of structural elements such as faults or folds and topography.

It is worthy of note that dominant dike sets striking NE-SW (TO), and implicitly a maximum compressional stress oriented in the same direction (parallel to the main compressive vector along the plate margin), are observed in different injection complexes of northern-central California: in the Turonian of Sacramento Basin (Jolly and others, 1998) and in the Miocene of Santa Cruz Basin (Bohem and Moore, 2002). This confirms the strong control of super-regional tectonic stresses, associated with North Pacific subduction, on the trend of sandstone intrusions.

Onset of Overpressure: Causes and Timing

Location of the PGIC in a forearc basin makes compression an initially attractive regional structural control that can generate fluid overpressure (Berry, 1973). In the Sacramento Basin, numerical modeling was used to infer that recent (<1 Ma) tectonic compression coupled with burial diagenesis are likely the cause of present-day high overpressure in many hydrocarbon exploration and production wells with reservoir of Upper Cretaceous age (McPherson and Garven, 1999). Tectonic compression caused by proximity to an active subduction zone was adopted as the likely driving mechanism for overpressure build up prior to the emplacement of the PGIC (Palladino and others, 2016). Our evaluation considers the role of burial diagenesis combined with lateral pressure transfer, occurring along regional fluid flow vectors controlled by the structural setting, as prominent to the development of hard overpressure.

During the late Cretaceous to early Danian, shortening and deformation were concentrated within the subduction complex to the west of the study area whereas, to the east and within the forearc basin, contemporaneous sequences are relatively undeformed and lack evidence of contemporaneous large-scale compressional structures of late Cretaceous - early Palaeocene age (Anderson and Pack, 1915; McGuire, ms, 1988a; Bartow, 1996; Dibblee, 2007a, 2007b; Mitchell and others, 2010). During the Danian, nappe geometry was characterised by predominantly westward verging major thrusts, and the sedimentary fill of the forearc basin dipped eastward (Dickinson and Seely, 1979; Wentworth and others, 1984; Dickinson, 2002; Constenius and others, 2014). Consequently, large-scale fluid flux during tectonic compression was westward toward the trench (fig. 2A) and not eastward toward the forearc basin as suggested by

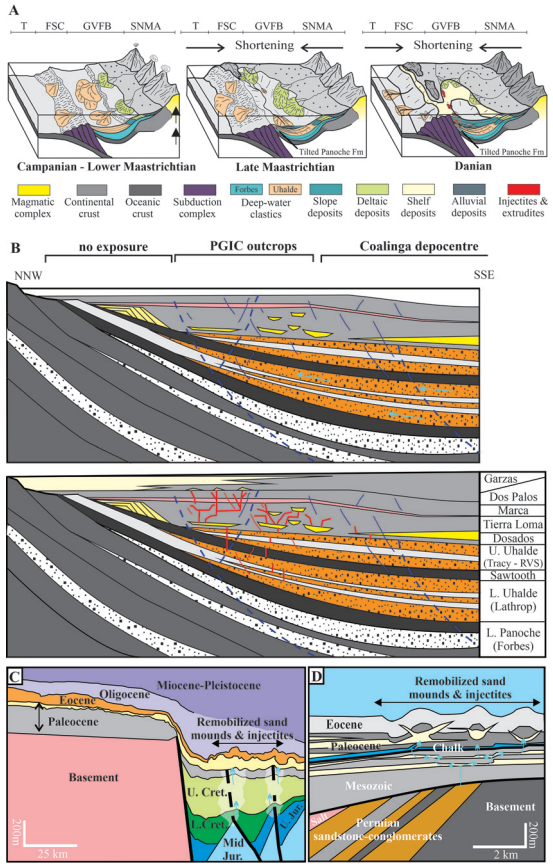

Fig. 18. A) Tectono-sedimentary evolution of the San Joaquin Basin in the Campanian-Maastrichtian. Most of the Great Valley Basin is covered by deep-water fan deposits (Uhalde Sandstone/Lathrop-Ragged Valley Silt units; see fig.2) sourced from the E and NE by the erosion of the magmatic arc of the Sierra Nevada. In the late Maastrichtian major tectonic compression caused shortening of the forearc basin and the formation of a structural high on the western margin of the basin. The structuration was associated with the deformation and uplift of the Panoche Fm and the underlying Coast Range Ophiolites, which were locally exposed and sourced E to SE progradation of deltaic systems. During this period the Moreno Formation deposited and onlaped the basin margins, generally prograding southward. In the Danian tectonic compression and consequent uplift of the subduction complex to the west, led to progressive uplift and tilting of the western portions of the Cretaceous fan systems and to the formation of trench-parallel extensional faults (blue lines in B). Deeper in the basin the lower Uhalde and older rocks were heated enough during burial to undergo chemical diagenesis. This tectono-stratigraphic framework favored expulsion of formation fluids from the basin center and their migration toward the margins where hydrofracturing ensued and emplacement of the PGIC occurred. T: Trench; FSC: Franciscan Subduction Complex; GVFB: Great Valley Forearc Basin; SNMA: Sierra Nevada Magmatic Arc. B) During the Danian, overpressure increased progressively below the regional seal (Sawtooth Shale) that covered much of the basin. Cyan arrows indicate inferred migration pathways for fluids expelled from areas, deeper in the basin, undergoing thermally-driven chemical diagenesis. Hydrofracturing and sand fluidization and injection occurred at the structurally higher parts of the deformed fan-systems where hard overpressure developed within the Lower Uhalde sandstone due to lateral pressure transfer. When pore fluid pressure below the regional seal, exceeded the fracture gradient, hydrofractures formed and propagated upward, progressively filling with sand that formed sandstone intrusions. Frequency of intrusions and their orientation was controlled by the magnitude of pressure above the *in situ* stress, and most frequently intrusions formed by opening fractures against the minimum horizontal stress (TO group) or by dilating pre-existing fractures (TP group). C) Geoseismic sections across the Frigg Delta and Balder-Grane area (North Sea Basin). Both areas have extensive sand injection intrusions into Paleocene and Eocene strata that overlie Mesozoic and Paleozoic structural highs and where the Cretaceous regional seal (both shale and carbonate) have strong indications of fluid leakage (probably associated with faults). Cyan arrows indicate pre- and syn-injection migration pathways for overpressured fluids sourced deeper in the section. Thermally-driven chemical diagenesis is the main cause for overpressure.

Palladino and others (2016). Likelihood of significant eastward fluid migration was further compromised by approximately 6.5 km of Upper Cretaceous sedimentary fill with thick, regionally extensive mudstones in the Panoche Fm (Payne, 1951) that formed additional barriers to eastward fluid migration (compare figs. 2 and 18, with fig. 18 in Palladino and others, 2018). Consequently, tectonic compression as a significant cause of overpressure in the forearc basin by pervasive eastward fluid migration to form the PGIC is unlikely.

Independent of tectonic setting, thermally driven chemical diagenesis (Bjørkum and others, 2001; Walderhaug and others, 2001; Nadeau, 2011) and concomitant lateral pressure transfer (Swarbrick and Osborne, 1998; Robertson and others, 2013; Gao and Flemings, 2017) are the main causes of elevated overpressure in sedimentary basins globally. Emergence and erosion of the subduction complex during the late Campanian to early Maastrichtian (fig. 18A) was associated with shortening (up to a few 10's km; Mitchell and others, 2010) of the forearc basin, progressive deformation and uplift of sedimentary strata, including the entire Panoche Fm and underlying Coastal Range Ophiolite, and rapid shifts of the main sediment-routing systems and depocentres (Mitchell and others, 2010). On the seaward (west) margin of the forearc basin, this progressive uplift and tilting changed the Uhalde Sst from west-dipping to east-dipping (fig. 18A; Mitchell and others, 2010) and led to an increase in the subsidence rate in the forearc basin. This led to the deposition of >5000 m of strata that include the Sawtooth Shale (equivalent to the regional M3 seal), the upper Uhalde Sst (from S4 to S5) and the entire Moreno Fm (that together form the Sawtooth-Moreno Composite Unit in fig. 18; Hosford Scheirer, 2007). During the late stages of deposition of the Sawtooth-Moreno Composite Unit, which hosts the PGIC (figs. 18A and B), large portions of the lower part of the Uhalde Sst (S1–S3 – Lathrop Unit) were buried to between 1500 m and 6000 m (present compacted thicknesses, figs. 13B and C, and 14; Hosford Scheirer, 2007), equivalent to T_{max} between 70 °C and >150 °C. In this thermal window quartz and silicate diagenesis prevail with the twofold effect of, 1) expulsion of pore-fluid caused by quartz cement occluding pores and clay dehydration (Walderhaug, 1994, 1996), and 2) decrease of permeability because of changes in the pore-size distribution and the overall lowering of porosity by mineralogical reactions such as illite crystallization (Oelkers and others, 2000; Walderhaug and others, 2001; Nadeau, 2011). Via illitization, mudstone permeability is reduced by three orders of magnitude, from μD to nD, and seal capacity is significantly enhanced (Nadeau and others, 2002a and b; Schneider and others, 2003).

Comparison with independent experimental data (Mondol and others, 2008) the smectitic mineralogy of mudstone in the Uhalde indicates that M3 was probably a high quality seal when buried to 1000–1500 m, and an even better seal deeper in the basin where illite prevails (Mertz, 1988; see section: MINERALOGY AND PETROGRAPHY). The kinetics of temperature-driven reactions mean that they proceed at higher rates at higher temperatures, for example quartz cement precipitation is five times faster at 120 °C than at 80 °C (Walderhaug, 1994, 1996; Walderhaug and others, 2001). Consequently, the rate of expulsion of formation fluids caused by chemical diagenesis reached its peak at the end of deposition of the Moreno Formation, when in a large area of the basin T_{max} >100 °C. Diagenetically evolved fluid would be expelled from sandstone in the lower Uhalde Sst (S1–S3 - Lathrop Unit) below the M3-Sawtooth regional seal in the deep basin (fig. 14), thereby raising P_f to moderate to hard overpressure (point D in fig. 14B and C). Lateral transfer of overpressure toward the basin margin where the same stratigraphic units were shallower, raised P_f to exceed the minimum horizontal stress and the fracture gradient, thereby causing regional hydrofracturing, and sand fluidization and injection (figs. 14B and C, 18A and B).

Combination of subsurface data (Hosford Scheirer, 2007) with outcrop data, and our interpretation of relevant borehole data, shows that pressure transfer occurred laterally over at least 80 km, and probably >150 km, through an estimated ~700 m thick sedimentary section, between the deep basin and the location of the PGIC on the northwest basin margin.

Rejecting compressional tectonics as the prominent cause of the hard overpressure that drove emplacement of the PGIC is a significant change in interpretation of large-scale subsurface fluid flow. Compressional tectonics were, however, instrumental in creating the basin physiography in which increased subsidence promoted temperature-driven chemical diagenesis. A similar interpretation is relevant to formation of the Upper Cretaceous, Gas Point sand injection complex in the northern Sacramento Valley (Jolly and others, 1998) and the late Eocene Tumey Giant Injection Complex of the San Joaquin Basin (TGIC, Zvirtes and others, 2021), which have similar geological settings and evolution to the PGIC, characterised by increased tectonically-driven subsidence with consequent uplift along the basin margins (Bartow, 1991; McPherson and Garven, 1999). It is important to note that rapid subsidence of the basin centre relative to its margins is not restricted to compressive geodynamic settings but characterises diverse sedimentary basins globally where evidence for regional scale hydrofracturing and sand injections is identified (Huuse, 2008; Hurst and others, 2021a).

Regional Sand Injection and Basin Scale Fluid Flow

Because the Uhalde Sst and its subsurface equivalents (fig. 2) are regionally developed aquifers, they can generate very large fluid volumes with only minor pressure drops. When a network of hydrofractures established hydraulic connectivity between the regional aquifers and the smaller volume depositional sandstones in the Moreno Fm, and ultimately the paleo-seafloor (figs. 15, 18A and B), pressure gradients were maximised and the volume of fluid expelled from the Uhalde Sst promoted extensive remobilization and injection of sand from the Dosados and Tierra Loma members (Vigorito and Hurst, 2010). It is conceivable that such large aquifers together with post-injection compaction and de-watering of adjacent mudstone, had the capacity to provide fluid charge for the prolonged (2 Ma) seepage of methane-rich fluids documented within the Cima Lentil (Schwartz and others, 2003; Minisini and Schwartz, 2007).

Overpressure in the range of 7–10 MPa, equivalent to a gradient of 0.015–0.016 MPa/m, is estimated for the PGIC below the M3 regional seal prior to injection (Vigorito and Hurst, 2010). These gradients are 0.85 and 0.90 of the estimated lithostatic gradient $\Delta\sigma_v$ = 0.018 MPa/m; (Vigorito and Hurst, 2010) and are similar to gradients presently observed in boreholes along the western margin of the Great Valley in stratigraphic intervals from the Cretaceous to the Miocene (for example 0.85 lithostatic in Upper Cretaceous sandstones in North Kettleman Dome, San Joaquin Valley; Strongin, 1981). If our model is correct, pore fluid pressure of ~52–55 MPa was present at ~4500 m burial during the early Paleocene (point D in fig. 14C). In that area, this fluid pressure was largely below the fracture gradient and explains the absence of sandstone intrusions in borehole data but equates with fluid pressure of 22–25 MPa at ~1500 m along the western margin of the basin where fluid pressure exceeded the fracture gradient, for example at point RA (fig. 14C).

The rock volume in which the PGIC was emplaced (fig. 14 and fig. S15), covers an area that is located above the thickest package of Uhalde Sst-Lathrop Sst (fig. 13E) and overlies structural highs located immediately updip of main depocentres where chemical diagenesis was highly active. Continuity and connectedness within the Lathrop Sst provided excellent migration routes for fluids expelled from the basin centres (figs. 13C and 13D, 14A and 14C) to these structurally higher areas where

overburden was at its thinnest thus minimising the pressure differential between pore fluid pressure in the Uhalde Sst-Lathrop Sst and the overburden stress (low effective stress) and maximising the potential for hydrofracturing and sand injection (RA in fig 14B).

Injected Flows: Characteristics, Fluid Dynamic Behaviour and the Sedimentary Record

A pressure gradient develops between the tips of newly formed hydrofractures and their point of origin in an underlying pressure cell (Vigorito and Hurst, 2010). During upward fracture propagation the pressure difference between the base and the top of the hydrofracture network, and the level of overpressure relative to *in-situ* conditions increases. This is caused by fluid pressure in the hydrofractures decreasing upward relative to fluid density in the hydrofractures, and hence grain concentration, whereas the in–situ stress decreases concomitantly along the lithostatic gradient (fig. 15C; Jolly and Lonergan, 2002; Vigorito and Hurst; 2010). If host strata are homogeneous, pressure difference increases progressively until the hydrofractures reach a free surface at which point the maximum pressure gradient occurs. In the PGIC this is represented by the paleo-seafloor (fig. 15C). Sand entrainment occurs when flow velocity exceeds the minimum fluidisation velocity for sand, which initiates migration of sand into the fracture network (Vigorito and Hurst, 2010). It is implicit that during the early stages of an injection event hydrofractures contain only water (Vigorito and Hurst, 2010; Bureau and others, 2014).

Given the regional scale of the PGIC, the intricacy of the hydrofracture network and the heterogeneity and thickness of the host strata, including the presence of sandstone, it is reasonable to assume that sand entrained into the flow in different areas at different times during propagation of the hydrofracture network and likely before hydrofractures reached the paleo-seafloor. It follows that grain concentration in the injected flows varied temporally and spatially during the emplacement of the injection complex. A consensus is that the maximum concentration for fluidized flow, C = 0.54 was never exceeded (Leva, 1959; Allen, 1982; Hurst and others, 2011). Estimation of the average velocity of injected sand is 0.5–0.7 m/s (Duranti and Hurst, 2004; Gallo and Woods, 2004; Levi and others, 2008). Using the minimum settling velocity of mudstone clasts in PGIC sandstone intrusions, estimates of the average velocity for fluidized sand are in the range of 0.28–0.7 m/s and that peak velocity may locally and temporally be much higher (9.43 m/s, Scott, ms, 2009). Assuming that injected flows are analogous to fluid flow in fractures, flow velocity is mainly controlled by the pressure gradient, fracture aperture and fluid density. Fracture aperture controls the permeability of the fracture and fluid density is largely represented by the concentration (C) of sand (Lyons and others, 2016). Because hydrofractures are propped open by fluid it follows that when fractures form and propagate, average propagation rate and average flow velocity are similar. Propagation rates of mantle-derived dikes in low-viscosity magma are estimated to be in the range of 0.1–10 m/s (Rubin, 1995).

Because natural geological systems are inherently heterogeneous and complex the rate of hydrofracture propagation and flow velocity of injected fluid differs significantly temporally and spatially. Given this spatial and temporal variability, and the limited information preserved in the geological record, estimates differ widely for Reynolds numbers (Re) for injected flows in ostensibly similar sandstone intrusions. In the PGIC, Scott (ms, 2009) estimates Re $\gg$2300 and inferred dominantly turbulent flow that concurs with independent estimates from other locations (Duranti and Hurst, 2004; Duranti, 2007, Scott and others, 2009; Ross and others, 2014). This is at variance with Cobain and others (2015) who, using a similar approach, estimated Re $<$2300 and inferred laminar to transitional flow.

Perturbation of fluid pressure gradients and flow velocity occur whenever hydrofractures intersect permeable units, including pre-existing faults and fractures, with different pore fluid pressure conditions (fig. 15C; see Dong, 2010). Fracture aperture increases and decreases with changes in fluid pressure whereas local variations in fluid pressure and flow velocity occur when hydrofractures stop propagating and start to close and expel fluid, or where new hydrofractures form and dilate, and via lateral leak off along fractures (Germanovich and Murdoch, 2010). It is therefore likely that regional sand injection is characterised by pulsed rates of fracture propagation, and concomitant changes in fracture aperture, flow velocity and upward directed rates and volumes of fluid discharge. Changes in fracture aperture and the flow velocity influence flow regime temporally and spatially, and within sandstone intrusions form internal sedimentary structures such as lamination, banding, grain segregation, and flow markings and erosion surfaces (Hurst and others, 2011 and references therein). Pulsing of flow complicates estimation of average and peak velocities of fluidized sand that often differ and span over two orders of magnitude, and likely is the reason why evidence for different flow regimes is reported from injectite analogues (Scott, ms, 2009; Hurst and others, 2011; Cobain and others, 2015).

Duration of Sand Injection

Emplacement of the PGIC was a single injection event that produced non-systematic cross-cutting relationships between sandstone intrusions, sills distributed within a well-defined stratigraphic interval throughout the study area, and a single stratigraphically constrained sand extrudite (Vigorito and others, 2008; Vétel and Cartwright, 2010; Vigorito and Hurst, 2010). Non-systematic cross-cutting of sandstone intrusions records the emplacement of different parts of the PGIC at slightly different times during the single injection event (Vétel and Cartwright, 2010). Assuming a velocity of 0.28 m/s (average for the PGIC; Scott, ms, 2009) for a fluidised sand grain derived from a parent unit in the Dosados Mbr, it would take ~47 minutes to reach the paleo-seafloor if a direct vertical conduit was available (red line in fig. 15B). This estimate is unlikely to be representative as is recorded by the complexity of the architecture of the PGIC, which demonstrates that hydrofractures propagated upward along indirect paths creating multiple intrusions with ranges of aperture, orientation and dip. Consequently, fluidized sand took a variety of routes to the paleo-seafloor independent of actual fluid velocity in a specific hydrofracture and caused fluidized sand to reach different levels in the host strata at different times (fig. 15B).

Sandstone dikes usually stop at the base, or within the basal section, of depositional sandstones especially if more 5m thick, although exceptions occur (Capita Canyon; fig. 3B, fig. S8). Intrusions that emerge from the top of depositional sandstones are generally laterally offset up to several 10's to 100's m from the underlying dikes (fig. 15A), a geometry that records that the hydrofracture intersected the base of depositional sandstone (with lower pore fluid pressure compared to the hydrofracture) stopped propagating and began to transfer pressure by local venting of fluid into the sandstone (Brenner and Gudmundsson, 2004; Dong, 2010). A consequent phase of pore-fluid pressure increase occurred in the depositional sandstone until it exceeded the fracture gradient and new hydrofractures formed along its upper margin (fig. 15A and C). This process is commonly observed in sandbox experiments (for example, Rodrigues and others, 2009) where the phase of pressure build-up corresponds to the lag time between the onset of fluid pumping and the initiation of hydrofracturing. During the period of pressure build-up, fluid and overpressure are transferred from an external source, in the PGIC case from a deeper overpressured sandstone. In the upper part of the Uhalde Sst and the Moreno Fm, depositional sandstone has varied areal and vertical distribution, internal lateral and vertical

connectivity and permeability, that in combination create baffles to the upward propagation of hydrofractures (fig. 15; Brenner and Gudmundsson, 2004; Dong, ms, 2010). It is likely that the active propagation of individual hydrofractures and branches proceeded in pulses separated by phases during which pressure above the fracture gradient had to re-establish following local pressure drops (fig. 15C). Phases of pressure build up would represent periods during which the rate of propagation of the hydrofracture network has locally and temporarily declined. On a local scale their duration was proportional to the volume of the depositional sandstone (it would take more time to pressure charge a large channel complex in the Uhalde Sst than an isolated channel in the Dosados Mbr) and inversely proportional to rate of influx of fluid from the aquifer below and to the level of overpressure of the depositional sandstone.

Non-systematic, cross-cutting relationships of intrusions and the formation of various sedimentary structures in them (Duranti and Hurst, 2004; Scott and others, 2009; Kane, 2010; Hurst and others, 2011) requires that pore-fluid pressure and the velocity of propagation of hydrofractures varied temporally and spatially during their emplacement. In the PGIC parts of the injection complex propagated while others did not (fig. 15B, Vétel and Cartwright 2010). This intrinsic diachroneity explains why the emplacement of any regionally developed sand injection complex proceeds in spatially and temporarily variable pulses despite being a single event. Despite the high velocity of injected flows, we infer that, because of the regional-scale intricacy of the fluid migration routes caused by the combination of depositional sandstones and hydrofractures, the emplacement of the PGIC occurred during a period of at least several days or weeks.

We are unaware of modern analogues for sand extrusions fed by overpressured aquifers at depth (burial >100 m) hence duration of sand injection and rate of sand extrusion are unknown. Analogy with modern, often catastrophic events, of sand (mostly seismogenic) or mud extrusion is unclarified but can add some perspective to the discussion. Between 2010 and 2011, a total of approximately 500,000 tons (191×10^3 m^3, Villemure and others, 2012) of sand and silt were extruded by four discrete earthquakes in the Canterbury area of New Zealand. Active extrusion of sand occurred from 1000's of sand blows over an area of several 10's km^2 and lasted cumulatively for a few hours. By contrast, the Lusi mud volcano, Indonesia, erupted 73×10^6 m^3 of mud over 3 years, with an initial solid particle concentration C = 0.2–0.4 (Tingay, 2010). Mud erupted from a single main conduit and at least 200 additional ephemeral vents mostly aligned along two intersecting faults within a radius of 4.5 km from the main vent (Tingay, 2010). Extruded granular volume of sand estimated for the PGIC is 280×10^6 m^3 over 25 km^2 of outcrop. This is at least three orders of magnitude greater than the volume of sand associated with Canterbury earthquakes. Assuming a concentration in the extruded sand-water mixtures C = 0.3 for the PGIC, the extruded sand volume is approximately an order magnitude greater than the mud volume erupted by the Lusi mud volcano.

PGIC and Subsurface Interpretation

Without oil industry subsurface data, recognition of occurrence of giant sand injection complexes and their distinctive geometry would probably have remained an elusive geological backwater (Hurst and Cartwright, 2007). Three-dimensional seismic surveys used in hydrocarbon exploration and oilfield development enabled identification of the regional significance of sand injection complexes with sandstone intrusions forming distinctive bedding discordant features (Duranti and others, 2002; Huuse and others, 2004; Huuse and others, 2005). The PGIC outcrop assumed a significant analogue role in interpretation of subsurface sand injection complexes (Hurst and others, 2005; Briedis and others, 2007; Hurst and others, 2016). More generally, because most steep (>45°) sandstone dikes are undetected on seismic surveys

dikes may constitute "invisible" fluid leakage systems. If unpenetrated in boreholes, or penetrated and unrecognized as sandstone intrusions, they pose hazards for gas or fluid sequestration projects that assume undisturbed fine-grained strata with intrinsically low vertical transmissivity. A natural example of this is seepage through the injectites in the PGIC that is estimated to have fed seafloor cold-seep carbonate communities for almost 2 Ma (Minisini and Schwartz, 2007). In a mudstone-prone interval identified as prospective for sequestration, but where sandstone dikes are present and undetected, when fluid is pumped into the formation it will preferentially flow through sandstone intrusions relative to the much less permeable mudstone. The net effect is that pore-fluid pressure will transfer rapidly to the shallowest levels in the injection complex, thus increasing the risk of causing hydrofracturing shallower in the formation.

Parts of giant sand injection complexes in Paleogene of the Frigg area and the central area of the Utsira High (fig. 18C and D; Briedis and others, 2007; Wild and Briedis, 2010) occur on the western and eastern margins, respectively of the North Sea Basin (UK and Norway). In both cases, the injection complexes are developed within and above large sandstone-rich deepwater fan systems below which the regional seal (carbonate- and mudstone-prone Cretaceous sequences) has evidence for fluid leakage (for example, gas chimneys in figs. 18C; see also Wild and Briedis, 2010). Where the regional seal is pristine the underlying sandstones have hydraulic continuity into the basin centre and form large pressure compartments in which hard overpressure (in excess of 10's MPa) occur with pressure gradients close to the fracture gradient (Moss and others, 2003). The overpressure is mainly generated via a combination of chemical diagenesis and lateral pressure transfer. By analogy with the PGIC, we infer that vertical fluid and pressure transfer from underlying overpressured aquifers is the main cause for the regional sand remobilisation and injection observed in the Tertiary strata. Overpressure release from depth along faults and/or hydrofractures, established and maximised pressure gradients, and caused extensive remobilization of sand into the shallower section, a model concurring with that of Wild and Briedis (2010). At present, in the North Sea, some areas of overpressure are preserved below the regional seal hence a fault-valve behaviour (Sibson, 1990) and/or cementation along faults and hydrofractures are invoked to explain the build-up of residual overpressure post-dating sand injection.

Because hydrofractures initiate and propagate when pore fluid pressure is in excess of the minimum stress, if the principal stress is vertical and the minimum stress lies in the horizontal plane the deeper portion of injection complexes, as observed in the PGIC, is characterized by sparse near-vertical dikes. These form the lower dike zone (LDZ) and are unlikely to be imaged by seismic surveys. It follows that in these cases the connection to deeper parent units (the source for both fluids and sand) cannot be resolved and consequently injection complexes may be misinterpreted as the result of sand remobilisation and injection from within the same stratigraphic section where intrusions occur. In some cases, the connection to a deeper source can be inferred from the presence of exotic clasts with mineralogical or paleontological characteristics indicative of origins from deeper parts of the stratigraphy (Hurst and others, 2016) or from subsurface pressure data where unexpected pressure support is observed and associated with deeper aquifers (Satur and others, 2021). Dikes are proven migration pathways for hydrocarbons (Jenkins, 1930; Hurst and others, 2003a; Jonk and others, 2005; Minisini and Schwartz, 2007; Blouet and others, 2017) into the shallower sandstone-rich parts of sand injection complexes, or any other shallower reservoir that they may transect. Such migration pathways, in the absence of direct geophysical evidence, are difficult to predict however, depth of potential parent units can be estimated if a sill zone and the location of the paleo-seafloor at the time of injection are constrained (Vigorito and Hurst

2010). Discordant intrusive elements are generally mapped in seismic above large sill complexes (saucers) and as wings emanating from depositional sandstone. These may cross-cut 100's m of stratigraphy but, by analogy with the PGIC and other injection complexes, are likely to represent only the lower part of an UDZ with the upper part potentially consisting of near-vertical dikes invisible to seismic.

CONCLUSIONS

Detailed description of the regionally developed (~4500 km^2) and excellently exposed (>300 km^2) Panoche Giant Injection Complex (PGIC) enables unique insight into the shallow crustal processes by which a giant sand injection complex forms. At least 25 km^3 of sand were injected in a single regional hydrofracturing event that was geologically instantaneous, the entire PGIC estimated to have formed in a minimum of several days to weeks. Fluidised sand flow is inferred to be pervasively turbulent with dilute grain concentration and velocity similar to that of the rate of hydrofracture propagation (0.1 to 10 m/s). Hydrofractures are present in varying abundance and density throughout the PGIC but are most common in the sill zone. Probably less than 1% of hydrofractures host sandstone intrusions.

Temperature-driven chemical diagenesis and lateral transfer of fluid from contiguous strata deeper in the basin is the causal process that maximised pressure gradients and released the large volume of fluid that promoted hydrofracturing and sand injection to form the PGIC. Pressure transfer occurred laterally over at least 80 km, possibly ~150 km, and through a vertical section of ~700 m from the deep basin to the location of the PGIC. The pore-fluid volume to fluidize and inject the estimated granular volume of sand in the PGIC is equivalent to ~1% reduction of the gross rock volume in the regional aquifer. Minor pressure drops in the aquifer would release the requisite fluid volumes. Estimates of fluid volume evolved from chemical diagenesis are more than an order of magnitude greater than the volume required to form the PGIC. Compressional tectonics is rejected as a significant cause of the overpressure that drove emplacement of the PGIC, marking a significant change in the understanding of regional subsurface fluid flow. However, it created the basin physiography that controlled variations in subsidence and heating of strata and the consequent chemical diagenesis.

Major dike trends are controlled by the regional stress field at the time of injection. Persistence of two dominant groups of dikes, TO and TP formed simultaneously throughout the PGIC. The more abundant TO dikes opened against the minimum horizontal stress and parallel to the main compressive vector along the margin of North Pacific subduction. TP dikes opened against the maximum horizontal stress and were controlled by local shallow extensional processes associated with uplift of the subduction complex and, tilting to the east and landward gravitational collapse of the forearc basin. Analogous structural and *in-situ* stress relationships are known from the modern Kumano forearc basin. Regional development of lower and upper dike zones below and above the intrusion-rich sill zone records that during formation of the PGIC supra-lithostatic fluid pressure was pervasive only in the sill zone.

Pervasive bedset scale liquefaction typifies in the Uhalde Sst parent units and formed at a burial depth of at least 600 m, but most likely at depths between 1 and 1.8 km below the paleo-seafloor. This is more than an order of magnitude deeper than previously recorded examples of large scale sand liquefaction. Although laterally and vertically discontinuous, evidence of continuous vertical disruption by liquefaction in places pervades >600 m of section. A genetic association exists between dewatering, hydrofracturing and sand intrusion of overlying mudstone.

Increase of overpressure in response to a combination of chemical diagenesis and lateral pressure transfer is a common characteristic of sedimentary basins and

explains the widespread occurrence of sand injection complexes globally in a wide range of geodynamic and sedimentary settings. Because sand injection complexes are often likely to be undetected or unidentified, they present a significant uncertainty when evaluating subsurface geology and specifically with respect to past and present fluid flow; "invisible" conduits for fluid escape through otherwise poorly transmissive strata.

ACKNOWLEDGMENTS

We are grateful to reviewer John Wakabayashi for a wonderfully thorough review of the paper and also acknowledge a helpful review by Lydia Lonergan. Mark Brandon provided constructive feedback and suggestions which helped to improve the manuscript.

Specials thanks goes to Bureau of Land Management in California for their continuous support. Financial support for this research provided by the companies sponsoring Phase 2 of the Sand Injection Research Group (SIRG) of the University of Aberdeen: Equinor, Lundin, Marathon, Total.

Data acquisition and mapping, outcrop interpretation, definition of PGIC geographic and stratigraphic framework and architecture, and petrological analyses performed by SIRG (all authors). Additional data acquisition, remote mapping, structural analysis, review and analysis of subsurface data, Petrel modeling and volume calculations performed by Mario Vigorito in Equinor.

SUPPLEMENTARY DATA

https://earth.eps.yale.edu/%7eajs/SupplementaryData/2022/Vigorito

REFERENCES

Ahmadi, Z. M., Sawyers, M., Kenyon-Roberts, S., Stanworth, C. W., Kugler, K. A., Kristensen, J., and Fugelli, E. M. G., 2003, Palaeocene, *in* Evans, D., Graham, C., Armour, A., and Bathurst, P., editors, The Millennium Atlas: Petroleum Geology of the Central and Northern North Sea: Geological Society, London, p. 235–259.

Allen, J. R. L., 1982, Liquidization, Liquidized Sediment, and the Sedimentation of Dense Particle Dispersions, *in* Allen, J. R. L., editor, Developments in Sedimentology: Elsevier, v. 30, Part B, p. 293–342, https://doi.org/10.1016/S0070-4571(08)71018-5

Almgren, A. A., 1986, Benthic foraminiferal zonation and correlations of Upper Cretaceous strata of the Great Valley of California—A modification, *in* Abbott, P. L., editor, Cretaceous Stratigraphy: Western North America: Pacific Section, Society of Economic Paleontologists and Mineralogists, Book 46, p. 137–152.

Anderson, R., and Pack, R. W., 1915, Geology and oil resources of the west border of the San Joaquin Valley north of Coalinga, California: United States Geological Survey Bulletin, v. 603, 220 p.

Atwater, T., 1970, Implications of plate tectonics for the Cenozoic tectonic evolution of western North America: Geological Society of America Bulletin, v. 81, n. 12, p. 3513–3536, https://doi.org/10.1130/0016-7606(1970)81[3513:IOPTFT]2.0.CO;2

Bailey, E. H., Irwin, W. P., and Jones, D. L., 1964, Franciscan and related rocks, and their significance in the geology of western California: California Division of Mines and Geology Bulletin, v. 183, 177 p.

Bartow, J. A., 1991, The Cenozoic evolution of the San Joaquin Valley, California: United States Geological Survey Professional Paper, v. 1501, 40 p., https://doi.org/10.3133/pp1501

Bartow, J. A, 1996, Geologic map of the west border of the San Joaquin Valley in the Panoche Creek–Cantua Creek area, Fresno and San Benito counties, California: Miscellaneous Investigations Series, United States Geological Survey Professional Papers, v. 1713, Map, I-2430, scale 1:50,000.

Bartow, J. A., and Nilsen, T. H., 1990, Review of the Great Valley sequence, eastern Diablo Range and northern San Joaquin Valley, Central California: United States Geological Survey Professional Papers, v. 1713, Open-File Report 90-226, 25 p., https://doi.org/10.3133/ofr90226

Bell, F. G., 2000, Engineering Properties of Soils and Rocks (fourth edition): Blackwell, Oxford, 496 p.

Berry, F. A. F., 1973, High fluid potential in California Coast Ranges and their tectonic significance: American Association of Petroleum Geologists Bulletin, v. 57, n. 7, p. 1219–1249.

Bird, P., 2017, Stress field models from Maxwell stress functions: southern California, Geophysical Journal International, v. 210, n. 2, p. 951–963, https://doi.org/10.1093/gji/ggx207
Bjørkum, P. A., Walderhaug, O., and Nadeau, P. H., 2001, Thermally driven porosity reduction: impact on basin subsidence, *in* Shannon, P. M., Haughton, P. D. W., and Corcoran, D. V., editors, The Petroleum Exploration of Ireland's Offshore Basins: Geological Society, London, Special Publications, v. 188, n. 1, p. 385–392, https://doi.org/10.1144/GSL.SP.2001.188.01.23
Blouet, J. P., Imbert, P., and Foubert, A., 2017, Mechanisms of biogenic gas migration revealed by seep carbonate paragenesis, Panoche Hills, California: American Association of Petroleum Geologists Bulletin, v. 101, n. 8, p.1309–1340, https://doi.org/10.1306/10171616021
Bohem, A., and Moore, J. C., 2002, Fluidized sandstone intrusions as an indicator of paleostress orientation, Santa Cruz, California: Geofluids, v. 2, n. 2, p. 147–161, https://doi.org/10.1046/j.1468-8123.2002.00026.x
Braccini, E., De Boer, W., Hurst, A., Huuse, M., Vigorito, M., and Templeton, G., 2008, Sand Injectites: Oilfield Review, v. 20, p. 34–49.
Brenner, S. L., and Gudmundsson, A., 2004, Arrest and aperture variation of hydrofractures in layered reservoirs, *in* Cosgrove, J. W., and Engelder, T., editors, The initiation, propagation and arrest of joints and other fractures: Geological Society, London, Special Publications, v. 231, n. 1, p. 117–128. https://doi.org/10.1144/GSL.SP.2004.231.01.08[10.1144/GSL.SP.2004.231.01.08]
Briedis, N. A, Bergslien, D., Hjellbakk, A., Hill, R. E., and Moir, G. J., 2007, Recognition criteria, significance to field performance, and reservoir modelling of sand injections in the Balder Field, North Sea, *in* Hurst, A., and Cartwright, J., editors, Sand Injectites: Implications for hydrocarbon exploration and production: American Association of Petroleum Geologists Memoir, v. 87, p. 91–102, https://doi.org/10.1306/1209853M873259
Bruijn, R. H. C., and Almqvist, B. S. G., 2015, The role of stress on chemical compaction of illite shale powder, *in* Faulkner, D. R., Mariani, E., and Mecklenburgh, J., editors, Rock deformation from field, experiments and theory: A volume in honour of Ernie Rutter: Geological Society, London, Special Publication, v. 409, p. 125–147, https://doi.org/10.1144/SP409.3
Bureau, D., Mourgues, R., and Cartwright, J., 2014, Use of a new artificial cohesive material for physical modelling: Application to sandstone intrusions and associated fracture networks: Journal of Structural Geology, v. 66, p. 223–236, https://doi.org/10.1016/j.jsg.2014.05.024
Cartwright, J., and Huuse, M., 2005, 3D seismic technology: the geological 'Hubble': Basin Research, v. 17, n. 1, p. 1–20, https://doi.org/10.1111/j.1365-2117.2005.00252.x
Cartwright, J., James, D., Huuse, M., Vettel, W., and Hurst, A., 2008, The mechanics of saucer-shaped sandstone intrusions: Journal of Structural Geology, v. 30, n. 7, p. 854–867, https://doi.org/10.1016/j.jsg.2008.03.012
Chang, C., McNeill., L. C., Moore., J. C., Lin, W., Conin, M., and Yamada, Y., 2010, In situ stress state in the Nankai accretionary wedge estimated from borehole wall failures: Geochemistry, Geophysics, Geosystems, v. 11, n. 12, p. 1–17, https://doi.org/10.1029/2010GC003261
Cherven, V. B., 1983, A delta-slope-submarine fan model for Maastrichtian part of Great Valley Sequence, Sacramento and San Joaquin Basins, California: American Association of Petroleum Geologists Bulletin, v. 67, n. 5, p. 772–816, https://doi.org/10.1306/03B5B6AA-16D1-11D7-8645000102C1865D
Chuhan, F. A., Kjeldstad, A., Bjørlykke, K., and Høeg, K., 2003, Experimental compression of loose sands: relevance to porosity reduction during burial in sedimentary basins: Canadian Geotechnical Journal, v. 40, p. 995–1011, https://doi.org/10.1139/t03-050
Cobain, S. L., Peakall, J., and Hodgson, D. M., 2015, Indicators of propagation direction and relative depth in clastic injectites: implications for laminar v. turbulent flow processes: Geological Society of America Bulletin, v. 127, n. 11–12, p. 1816–1830, https://doi.org/10.1130/B31209.1
Constenius, K. N., Johnson, R. A., Dickinson, W. R., and Williams, T. A., 2014, Tectonic evolution of the Jurassic–Cretaceous Great Valley forearc, California: Implications for the Franciscan thrust-wedge hypothesis: Geological Society of America Bulletin, v. 112, n. 11, p. 1703–1723, https://doi.org/10.1130/0016-7606(2000)112<1703:TEOTJC>2.0.CO;2
Cosgrove, J. W., and Hillier, R. D., 2000, Forced fold development within the Tertiary sediments of the Alba Field, UKCS: evidence of differential compaction and post-depositional sandstone remobilization, *in* Cosgrove, J. W., and Ameen, M. S., editors, Forced Folding and Fractures: Geological Society, London, Special Publications, v. 169, p. 61–72, https://doi.org/10.1144/GSL.SP.2000.169.01.05
Deming, D., 1994, Factors necessary to define a pressure seal: American Association of Petroleum Geologists Bulletin, v. 78, n. 6, p. 1005–1009, https://doi.org/10.1306/A25FE40F-171B-11D7-8645000102C1865D
Dibblee, T. W. Jr., 2007a, Geological map of the Chounet Ranch Quadrangle, Fresno County, California: Dibblee Geology Centre Map DF-321, scale 1:24,000.
Dibblee, T. W. Jr., 2007b, Geological map of the Tumey Hills Quadrangle, Fresno County, California: Dibblee Geology Centre Map, DF-316, scale 1:24,000.
Dickinson, W. R., and Seely, D. R., 1979, Structure and stratigraphy of forearc regions: American Association of Petroleum Geologists Bulletin, v. 63, n. 1, p. 2–31, https://doi.org/10.1306/C1EA55AD-16C9-11D7-8645000102C1865D
Diggs, T. N., 2007, An outcrop study of clastic-injection structures in the Carboniferous Tesnus Formation, Marathon Basin, Trans-Pecos Texas, *in* Hurst, A., and Cartwright, J., editors, Sand injectites: Implications for hydrocarbon exploration and production, American Association of Petroleum Geologists Memoir, v. 87, p. 209–219, https://doi.org/10.1306/1209864M873266
Dickinson, W. R., 2002, Reappraisal of hypothetical Franciscan thrust wedging at Coalinga: Implications for tectonic relations along the Great Valley flank of the California Coast Ranges: Tectonics, v. 21, n. 5, p. 3-1–3-14, https://doi.org/10.1029/2001TC001315
Dixon, R. J., Schofield, K., Anderton, R., Reynolds, A. D., Alexander, R. W. S., Williams, M. C., and Davies, K. G., 1995, Sandstone diapirism and clastic intrusion in the Tertiary submarine fans of the Bruce-Beryl

embayment, quadrant 9, UKCS, *in* Hartley, A. J., and Prosser, D. J., editors, Characterization of Deep-marine Clastic Systems: Geological Society, London, Special Publications, v. 94, p. 77–94, https://doi.org/10.1144/GSL.SP.1995.094.01.07

Dong, Y., ms, 2010, Hydraulic fracture containment in sand: PhD thesis, Technische Universiteit Delft, Delft, the Netherlands, 256 p.

Duranti, D., 2007, Large-scale sand injection in the Paleogene of the North Sea: modelling of energy and flow velocities, *in* Hurst, A., and Cartwright, J., editors, Sand Injectites: Implications for Hydrocarbon Exploration and Production, American Association of Petroleum Geologists Memoir, v. 87, p. 129–139, https://doi.org/10.1306/1209857M873261

Duranti, D., and Hurst, A., 2004, Fluidisation and injection in the deep-water sandstones of the Eocene Alba Formation (UK North Sea): Sedimentology, v. 51, n. 3, p. 503–531, https://doi.org/10.1111/j.1365-3091.2004.00634.x

Duranti, D., Hurst, A., Bell, C., Groves, S., and Hanson, R., 2002, Injected and remobilised Eocene sandstones from the Alba Field, UKCS: core and wireline characteristics: Petroleum Geoscience, v. 8, n. 2, p. 99–107, https://doi.org/10.1144/petgeo.8.2.99

Fonseca-Rivera, C., ms, 1997, Late Cretaceous-early Tertiary paleoceanography and cyclic sedimentation along the California margin—Evidence from the Moreno Formation: Ph.D. thesis, Stanford University, Stanford, 449 p.

Fuller, C. W., Willett, S. D., and Brandon, M. T., 2006, Formation of forearc basins and their influence on subduction zone earthquakes: Geology, v. 3, n. 2, p. 65–68, https://doi.org/10.1130/G21828.1

Gallo, F., and Woods, A. W., 2004, On steady homogeneous sand–water flows in a vertical conduit: Sedimentology, v. 51, n. 2, p. 195–210, https://doi.org/10.1111/j.1365-3091.2004.00608.x

Gao, B., and Flemings, P. B., 2017, Pore pressure within dipping reservoirs in overpressured basins: Marine and Petroleum Geology, v. 80, p. 94–111, https://doi.org/10.1016/j.marpetgeo.2016.11.014

Germanovich, L. N., and Murdoch, L. C., 2010, Injection of solids to lift coastal areas: Proceedings of The Royal Society A: Mathematical, Physical and Engineering Sciences, v. 466, n. 2123, p. 3225–3252, https://doi.org/10.1098/rspa.2010.0033

Greene, T. J., and Surpless, K. D., 2017, Facies architecture and provenance of a boulder-conglomerate submarine channel system, Panoche Formation, Great Valley Group: A forearc basin response to middle Cretaceous tectonism in the California convergent margin: Geosphere, v. 13, n. 3, p. 838–869, https://doi.org/10.1130/GES01422.1

Grippa, A., Hurst, A., Palladino, G., Iacopini, D., Lecomte, I., and Huuse, M., 2019, Seismic imaging of complex geometry: forward modelling of sandstone intrusions: Earth and Planetary Science Letters, v. 513, p. 51–63, https://doi.org/10.1016/j.epsl.2019.02.011

Gudmundsson, A., 2011, Rock fractures in geological processes: Cambridge University Press; 560 p.

Hill, P. R., and Marsters, J. C., 1990, Controls on physical properties of Peru continental margin sediments and their relationship to deformation styles, *in* Suess, E., and von Huene, R., editors: Proceedings of the Ocean Drilling Program, Scientific Results, v. 112, p. 623–632, https://doi.org/10.2973/odp.proc.sr.112.168.1990

Hosford Scheirer, A., 2007, The three-dimensional geologic model used for the 2003 National Oil and Gas Assessment of the San Joaquin Basin Province, California, *in* Hosford Scheirer, A., editor, Petroleum Systems and Geologic Assessment of Oil and Gas in the San Joaquin Basin Province, California: United States Geological Survey, Professional Papers 1713, Ch. 7.

Hosford Scheirer, A., and Magoon, L. B., 2007a, Winters-Domengine total petroleum system — northern non-associated gas assessment unit of the San Joaquin Basin Province, *in* Hosford Scheirer, A., editor, Petroleum Systems and Geologic Assessment of Oil and Gas in the San Joaquin Basin Province, California: United States Geological Survey Professional Papers 1713, Ch. 21, https://doi.org/10.3133/pp171321

Hosford Scheirer, A., and Magoon, L. B., 2007b, Age, distribution, and stratigraphic relationship of rock units in the San Joaquin Basin Province, California, *in* Hosford Scheirer, A., editor, Petroleum Systems and Geologic Assessment of Oil and Gas in the San Joaquin Basin Province, California: United States Geological Survey Professional Papers 1713, Ch. 5, https://doi.org/10.3133/pp17135

Hurst, A., and Cartwright, J. A., 2007, Sand Injectites: Implications for Hydrocarbon Exploration and Production: American Association of Petroleum Geologists Memoir, v. 87, 288 p., https://doi.org/10.1306/M871209

Hurst, A., and Cronin, B. T., 2001, The origin of consolidation laminae and dish structures in some deep-water sandstones: Journal of Sedimentary Research, v. 71, n. 1, p. 136–143, https://doi.org/10.1306/061400710136

Hurst, A., and Vigorito, M., 2017, Saucer-shaped sandstone intrusions: an underplayed reservoir target: American Association of Petroleum Geologists Bulletin, v. 101, n. 4, p. 625–633, https://doi.org/10.1306/011817DIG17070

Hurst, A., Cartwright, J., Huuse, M., Jonk, R., Schwab, A., Duranti, D., and Cronin, B. T., 2003a, Significance of large-scale sand injectites as long-term fluid conduits: evidence from seismic data: Geofluids, v. 3, n. 4, p. 263–274, https://doi.org/10.1046/j.1468-8123.2003.00066.x

Hurst, A., Cartwright, J., and Duranti, D., 2003b, Fluidization structures in sandstone produced by upward injection through a sealing lithology, *in* van Rensbergen, P., Hillis, R. R., Maltman, A., and Morley, C. K., editors, Subsurface Sediment Remobilisation: Geological Society of London, Special Publications, v. 216, p. 123–138, https://doi.org/10.1144/GSL.SP.2003.216.01.09

Hurst, A., Cartwright, J. A., Duranti, D., Huuse, M., and Nelson, M., 2005, Sand injectites: an emerging global play in deep-water clastic environments, *in* Doré, A. G., and Vining, B. A., editors, Petroleum Geology: North-West Europe and Global Perspectives- Proceedings of the 6th Petroleum Geology Conference: Geological Society, London, v. 6, p. 133–144, https://doi.org/10.1144/0060133

Hurst, A., Cartwright, J. A., Huuse, M., and Duranti, D., 2006, Extrusive sandstones (extrudites): a new class of stratigraphic trap? *in* Allen, M. R., Goffey, G. P., Morgan, R. K., and Walker, I. M., editors, The Deliberate Search for the Stratigraphic Trap: Geological Society of London, Special Publications, v. 254, p. 289–300, https://doi.org/10.1144/GSL.SP.2006.254.01.15

Hurst, A., Scott, A., and Vigorito, M., 2011, Physical characteristics of sand injectites: Earth Science Reviews, v. 106, n. 3–4, p. 215–246, https://doi.org/10.1016/j.earscirev.2011.02.004

Hurst, A., Huuse, M., Duranti, D., Vigorito, M., Jameson, E., and Schwab, A., 2016, Application of outcrop analogues in successful exploration of a sand injection complex, Volund Field, Norwegian North Sea, *in* Bowman, M., Smyth, H. R., Good, T. R., Passey, S. R., Hirst, J. P. P., and Jordan, C. J., editors, The value of outcrop studies in reducing subsurface uncertainty and risk in hydrocarbon exploration and production: Geological Society, London, Special Publications, v. 436, p. 75–92, https://doi.org/10.1144/SP436.3

Hurst, A., Morton, A., Scott, A., Vigorito, M., and Frei, D., 2017, Heavy-mineral assemblages in sandstone intrusions: Panoche Giant Injection Complex, California, U.S.A: Journal of Sedimentary Research, v. 87, n. 4, p. 388–405, https://doi.org/10.2110/jsr.2017.22

Hurst, A., Grippa, A., Silcock, S. Y., Huuse, M., Bowman, M., and Cobain, S. L., 2021a, Introduction: subsurface sand remobilization and injection: Geological Society, London, Special Publications, v. 493, p. 1–10, https://doi.org/10.1144/SP493-2020-268

Hurst, A., Luzinski, W., Zvirtes, G., Scott, A., Vigorito, M., Morton, A., and Wu, F., 2021b, Some petrographic and mineralogical diagnostics of sandstone intrusions, *in* Silcock, S., Huuse, M., Bowman, M., Hurst, A., and Cobain, S., editors, Subsurface Sand Remobilization and Injection: Geological Society, London, Special Publication, v. 493, p. 287–302, https://doi.org/10.1144/SP493-2018-063

Hurst, A., Wilson, M. J., Grippa, A, Wilson, L., Palladino, G., Belviso, C., and Cavalcante, F., 2021c, Provenance and Sedimentary Context of Clay Mineralogy in an Evolving Forearc Basin, Upper Cretaceous-Paleogene and Eocene Mudstones, San Joaquin Valley, California: Minerals, v. 11, n. 1, 71, https://doi.org/10.3390/min11010071

Huuse, M., 2008, Sandstone intrusions: implications for exploration and production: World Oil, v. 229, n. 6, p. 87–91.

Huuse, M., and Mickelson, M., 2004, Eocene sandstone intrusions in the Tampen Spur area (Norwegian North Sea Quad 34) imaged by 3D seismic data: Marine and Petroleum Geology, v. 21, n. 2, p. 141–155, https://doi.org/10.1016/j.marpetgeo.2003.11.018

Huuse, M., Duranti, D., Steinsland, N., Guargena, C. G., Prat, P., Holm, K., Cartwright, J. A., and Hurst, A., 2004, Seismic characteristics of large-scale sandstone intrusions in the Paleogene of the South Viking Graben, UK and Norwegian North Sea, *in* Davies, R. J., Cartwright, J., Stewart, S. A, Lappin, M., and Underhill, J. R., editors, 3D Seismic technology: application to the exploration of sedimentary basins: Geological Society of London, Memoir, v. 29, p. 263–277, https://doi.org/10.1144/GSL.MEM.2004.029.01.25

Huuse, M., Cartwright, J. A., Gras, R., and Hurst, A., 2005, Km-scale sandstone intrusions in the Eocene of the Outer Moray Firth (UK North Sea): migration paths, reservoirs, and potential drilling hazards, *in* Doré, A., and Vining, B., editors, Petroleum Geology: North-West Europe and Global Perspectives – Proceedings of the 6th Petroleum Geology Conference: Geological Society London, Petroleum Geology Conference series, v. 6, p. 1577–1594, https://doi.org/10.1144/0061577

Huuse, M., Hurst, A., Cartwright, J., and Steinsland, N., 2007, Seismic characterization of large-scale sandstone intrusions, *in* Hurst, A., and Cartwright, J., editors, Sand Injectites: Implications for hydrocarbon exploration and production: American Association of Petroleum Geologists Memoir, v. 87, p.21–35, https://doi.org/10.1306/1209847M873253

Huuse, M., Jackson, C. A.-L., Van Rensbergen, P., Davies, R. J., Flemings, P. B., and Dixon, R. J., 2010, Subsurface sediment remobilization and fluid flow in sedimentary basins: an overview: Basin Research, v. 22, n. 4, p. 342–360, https://doi.org/10.1111/j.1365-2117.2010.00488.x

Huuse, M., Bureau, D., Hurst, A., and Suek, D., 2014, Saucer-shaped sandstone intrusions - a global deep-water play?, 76th EAGE Conference and Exhibition 2014: European Association of Geoscientists and Engineers, v. 2014, p. 1–5, https://doi.org/10.3997/2214-4609.20141064

Imperato, D. P., and Nilsen, T. H., 1990, Deep-Sea-Fan Channel-Levee Complexes, Arbuckle Field, Sacramento Basin, California, *in* Barwis, J. H., McPherson, J. G., and Studlick, J. R., J., editors, Sandstone Petroleum Reservoirs: Casebooks in Earth Sciences: Springer, New York, NY, 535, p., https://doi.org/10.1007/978-1-4613-8988-0_23

Ingersoll, R. V., ms, 1976, Evolution of the Late Cretaceous forearc basin, northern and central California: Ph. D. thesis, Stanford University, Stanford, 200 p.

Ingersoll, R. V., 1979, Evolution of the Late Cretaceous forearc basin, northern and central California: Geological Society of America Bulletin, v. 90, n. 9, p. 813–826, https://doi.org/10.1130/0016-7606(1979)90<813:EOTLCF>2.0.CO;2

Ingersoll, R. V., 1982, Initiation and evolution of the Great Valley forearc basin of northern and central California, USA, *in* Leggett, J. K., editor, Trench-forearc geology: sedimentation and tectonics on modern and ancient active plate margins: Geological Society, London Special Publication, v. 10, p. 459–467, https://doi.org/10.1144/GSL.SP.1982.010.01.31

Jackson, C. A. L., 2007, The geometry, distribution and development of clastic injectites in deep-marine depositional systems: examples from the Late Cretaceous Kyrre Formation, Måløy slope, Norwegian margin, *in* Hurst, A., and Cartwright, J. A., editors, Sand injectites: Implications for hydrocarbon exploration and production: American Association of Petroleum Geologists Memoir, v. 87, p. 37–48, https://doi.org/10.1306/1209848M873254

Jenkins, O. P., 1930, Sandstone dikes as conduits for oil migration through shales: American Association of Petroleum Geologists Bulletin, v. 14, n. 4, p. 411–421, https://doi.org/10.1306/3D9328C2-16B1-11D7-8645000102C1865D

Jolly, R. J. H., and Lonergan, L., 2002, Mechanisms and control on the formation of sand intrusions: Journal of the Geological Society, v. 159, n. 5, p. 605–617, https://doi.org/10.1144/0016-764902-025

Jolly, R. J. H., Cosgrove, J. W., and Dewhurst, D. N., 1998, Thickness and spatial distribution of clastic dikes, northwest Sacramento Valley, California: Journal of Structural Geology, v. 20, n. 12, p. 1663–1672, https://doi.org/10.1016/S0191-8141(98)00053-4

Jonk, R., Hurst, A., Duranti, D., Parnell, J., Mazzini, A., and Fallick, A. E., 2005, Origin and timing of sand injection, petroleum migration, and diagenesis in Tertiary reservoirs, south Viking Graben, North Sea: American Association of Petroleum Geologists Bulletin, v. 89, n. 3, p. 329–357, https://doi.org/10.1306/10260404020

Kane, I. A., 2010, Development and flow structures of sand injectites: the Hind Sandstone Member injectite complex, Carboniferous, UK: Marine and Petroleum Geology, v. 27, n. 6, p. 1200–1215, https://doi.org/10.1016/j.marpetgeo.2010.02.009

Leva, M., 1959, Fluidisation: New York, McGraw-Hill, 327 p.

Levi, T., Weinberger, R., Eyal, Y., Lyakhovsky, V., and Heifetz, E., 2008, Velocities and driving pressures of clay-rich sediments injected into clastic dikes during earthquakes: Geophysical Journal International, v. 175, n. 3, p. 1095–1107, https://doi.org/10.1111/j.1365-246X.2008.03929.x

Lewan, M. D., Dolan, M. P., and Curtis, J. B., 2014, Effects of smectite on the oil-expulsion efficiency of the Kreyenhagen Shale, San Joaquin Basin, California based on hydrous-pyrolysis experiments: American Association of Petroleum Geologists Bulletin, v. 98, n. 6, p. 1091-1109, https://doi.org/10.1306/10091313059

Lonergan, L., Borlandelli, C., Taylor, A., Quine, M., and Flanagan, K., 2007, The three-dimensional geometry of sandstone injection complexes in the Gryphon Field, United Kingdom, North Sea, *in* Hurst, A., and Cartwright, J., editors, Sand injectites: Implications for hydrocarbon exploration and production: American Association of Petroleum Geologists Memoir, v. 87, p. 103–112, https://doi.org/10.1306/1209854M873260

Løseth, H., Raulline, B., and Nygård, A., 2013, Late Cenozoic geological evolution of the northern North Sea: development of a Miocene unconformity reshaped by large-scale Pleistocene sand intrusion: Journal of the Geological Society, v. 170, p. 133–145, https://doi.org/10.1144/jgs2011-165

Lowe, D. R., 1975, Water escape structures in coarse-grained sediments: Sedimentology, v. 22, n. 2, p. 157–204, https://doi.org/10.1111/j.1365-3091.1975.tb00290.x

Lowe, D. R., 1982, Sediment gravity flows: II. Depositional models with special reference to the deposits of high-density turbidity currents: Journal of Sedimentary Petrology, v. 52, n. 1, p. 279–297, https://doi.org/10.1306/212F7F31-2B24-11D7-8648000102C1865D

Lowe, D. R., and Lopiccolo, R. D., 1974, The characteristics and origins of dish and pillar structures: Journal of Sedimentary Petrology, v. 44, n. 2, p. 484–501, https://doi.org/10.1306/74D72A68-2B21-11D7-8648000102C1865D

Lyons, W. C., Plisga, G. J., and Lorenz, M. D., 2016, Reservoir Engineering: in Lyons, W. C., Plisga, G. J., and Lorenz, M. D., editors, Standard Handbook of Petroleum and Natural Gas Engineering, Third Edition: Gulf Professional Publishing, p. 5-1–5-291.

Mahmud, H. B., Leong, V. H., and Lestariono, Y., 2020, Sand production: A smart control framework for risk mitigation: Petroleum, v. 6, n. 1, p. 1–13, https://doi.org/10.1016/j.petlm.2019.04.002

Mannu, U., Ueda, K., Willett, S. D., Gerya, T. V., and Strasser, M., 2016, Impact of sedimentation on evolution of accretionary wedges: Insights from high-resolution thermomechanical modeling: Tectonics, v. 35, n. 12, p. 2828–2846, https://doi.org/10.1002/2016TC004239

Martel, S. J., 2016, Effects of small-amplitude periodic topography on combined stresses due to gravity and tectonics: International Journal of Rock Mechanics and Mining Sciences, v. 89, p. 1–13, https://doi.org/10.1016/j.ijrmms.2016.07.026

Martin, L., 1964, Upper Cretaceous and Lower Tertiary foraminifera from Fresno County, California: Jahrbuch der Geologischen Bundesanstalt, Special Volume, v. 9, p. 1–128.

McGuire, D. J., ms, 1988a, Stratigraphy, depositional history, and hydrocarbon source-rock potential of the Upper Cretaceous-Lower Tertiary Moreno Formation, central San Joaquin Basin, California: Ph. D. thesis, Stanford University, Stanford, 231 p.

McGuire, D. J., 1988b, Depositional framework of the Upper Cretaceous-lower Tertiary Moreno Formation, central San Joaquin Basin, California, *in* Graham, S. A., and Olson, H. C., editors, Studies of the geology of the San Joaquin Basin: Pacific Section, Society of Economic Paleontologists and Mineralogists, v. 60, p. 173–188.

McPherson, B. J. O. L., and Garven, G., 1999, Hydrodynamics and overpressure mechanisms in the Sacramento Basin, California: American Journal of Science, v. 299, n. 6, p. 429–466, https://doi.org/10.2475/ajs.299.6.429

Mertz, K. A. Jr., 1988, Diagenetic events and development and occlusion of secondary porosity in Upper Cretaceous feldspathic sandstones: northern Sacramento Basin, California: Society of Economic Paleontologists and Mineralogists, Midyear Meeting Abstracts, v. 5, p. 35–36.

Minisini, D., and Schwartz, H., 2007, An early Palaeocene cold seep system in the Panoche and Tumey Hills, Central California (United States), *in* Hurst, A., and Cartwright, J., editors, Sand Injectites: Implications for hydrocarbon exploration and production: American Association of Petroleum Geologists Memoir, v. 87, p. 185–197, https://doi.org/10.1306/1209862M873264

Mitchell, C., Graham, S. A., and Suek, D. H., 2010, Subduction complex uplift and exhumation and its influence on Maastrichtian forearc stratigraphy in the Great Valley Basin, northern San Joaquin Valley, California: Geological Society of America Bulletin, v. 122, n. 11–12, p. 2063–2078, https://doi.org/10.1130/B30180.1

Mondol, N. H., Bjørlykke, K., and Jahren, J., 2008, Experimental compaction of clays: relationship between permeability and petrophysical properties in mudstones: Petroleum Geoscience, v. 14, p. 319–337, https://doi.org/10.1144/1354-079308-773

Monnier, D., Gay, A., Imbert, P., Cavailhes, T., Soliva, R., and Lopez, M., 2015, Sand injectites network as a marker of the palaeoestress field, the structural framework and the distance to the sand source: example in the Vocontian Basin, SE France: Journal of Structural Geology, v. 79, p. 1–18, https://doi.org/10.1016/j.jsg.2015.07.001

Montenat, C., Barrier, P., Ott d'Estevou, P., and Hibsch, C., 2007, Seismites: an attempt at critical analysis and classification: Sedimentary Geology, v. 196, n. 1–4, p. 5–30, https://doi.org/10.1016/j.sedgeo.2006.08.004

Moore, G. F., Boston, B. B., Sacks, A. F., and Saffer, D. M., 2013, Analysis of normal fault populations in the Kumano Forearc Basin, Nankai Trough, Japan: 1. Multiple orientations and generations of faults from 3-D coherency mapping: Geochemistry, Geophysics, Geosystems, v. 14, n. 6, p. 1989– 2002, https://doi.org/10.1002/ggge.20119

Moretti, M., and Ronchi, A., 2011, Liquefaction features interpreted as seismites in the Pleistocene fluvio-lacustrine deposits of the Neuquén Basin (Northern Patagonia): Sedimentary Geology, v. 235, n. 3–4, p. 200–209, https://doi.org/10.1016/j.sedgeo.2010.09.014

Morton, A. C., and Hallsworth, C., 2007, Stability of detrital heavy minerals during burial diagenesis, *in* Mange, M. A., and Wright, D. T., editors, Heavy Minerals in Use: Developments in Sedimentology, v. 58, p. 215–245, https://doi.org/10.1016/S0070-4571(07)58007-6

Moss, B., Barson, D., Rakhit, K., Dennis, H., and Swarbrick, R., 2003, Formation pore pressures and formation waters: *in* Evans, D., Graham, C., Armour, A., and Bathurst, P., The Millennium Atlas: Petroleum Geology of the Central and Northern North Sea: Geological Society of London, p. 317–329.

Murchison, R. I., 1827, On the coal field of Bora in Sutherlandshire and some other stratified deposits in the North of Scotland: Transactions of the Geological Society of London, v. S2, n. 2, p. 293–326, https://doi.org/10.1144/transgslb.2.2.293

Nadeau, P. H., 2011, Earth's energy "Golden Zone": a synthesis from mineralogical research: Clay Minerals, v. 46, n. 1, p. 1–24, https://doi.org/10.1180/claymin.2011.046.1.1

Nadeau, P. H., Peacor, D. R., Yan, J., and Hillier, S., 2002a, I-S precipitation in pore space as the cause of geopressuring in Mesozoic mudstones, Egersund Basin, Norwegian continental shelf: American Mineralogist, v. 87, n. 11–12, p. 1580–1589, https://doi.org/10.2138/am-2002-11-1208

Nadeau, P. H., Walderhaug, O., Bjørkum, P. A., and Hay, S., 2002b, Clay diagenesis, shale permeability, and implications for petroleum systems analysis: EAGE Annual Meeting, Florence, Program Abstract G003.

Nilsen, T. H., 1987, Paleogene tectonics and sedimentation of coastal California, *in* Ingersoll, R. V., and Ernst, W. G., editors, Cenozoic basin development of coastal California: Englewood Cliffs, New Jersey, Prentice-Hall, Rubey volume 6, p. 81–123.

Nilsen, T. H., and Moore, D. W., 1997, Regional upper Cretaceous stratigraphy and depositional systems of the northern San Joaquin Basin, California, *in* Knauer, L. C., editor, Geology of the northern San Joaquin Basin gas province: Pacific Section, American Association of Petroleum Geologists, v. MP 43, p. 1–12, https://doi.org/10.32375/1997-MP43.1

Newman, M. St. J., Reeder, M. L., Woodruff, A. H. W., and Hatton, I. R., 1993, The geology of the Gryphon Oil Field, *in* Parker, J., editor, Petroleum Geology of North-West Europe: Proceedings of the 4th Conference. Geological Society, London, Petroleum Geology Conference series, v. 4, p. 123−133, https://doi.org/10.1144/0040123

Obermeier, S. F., 1989, The New Madrid Earthquakes: An Engineering-Geologic Interpretation of Relict Liquefaction Features: United States Geological Survey Professional Paper 1336-B, https://doi.org/10.3133/pp1336B

Obermeier, S. F., 1996, Use of liquefaction-induced features for paleoseismic analysis – An overview of how seismic liquefaction features can be distinguished from other features and how their regional distribution and properties of source sediment can be used to infer the location and strength of Holocene paleo-earthquakes: Engineering Geology, v. 44, 1–4, p. 1–76, https://doi.org/10.1016/S0013-7952(96)00040-3

Oelkers, E. H., Bjørkum, P. A., Walderhaug, O., Nadeau, P. H., and Murphy, W. M., 2000, Making diagenesis obey thermodynamics and kinetics: the case of quartz cementation in sandstones from offshore mid-Norway: Applied Geochemistry, v. 15, n. 3, p. 295–309, https://doi.org/10.1016/S0883-2927(99)00047-5

Owen, G., Moretti, M., and Alfaro, P., 2011, Recognising triggers for soft-sediment deformation: Current understanding and future directions: Sedimentary Geology, v. 235, n. 3–4, p. 133–140, https://doi.org/10.1016/j.sedgeo.2010.12.010

Palladino, G., Grippa, A., Bureau, D., Alsop, G. I., and Hurst, A., 2016, Emplacement of sandstone intrusions during contractional tectonics: Journal of Structural Geology, v. 89, p. 230–249, https://doi.org/10.1016/j.jsg.2016.06.010

Palladino, G., Alsop, G. I., Grippa, A., Zvirtes, G., Phillip, R. P., and Hurst, A., 2018, Sandstone-filled normal faults: a case study from central California: Journal of Structural Geology, v. 110, p. 86–111, https://doi.org/10.1016/j.jsg.2018.02.013

Parize, O., 1988, Sills et dikes gréseux sédimentaires: paléomorphologie, fracturation préocce, injection et compaction: Ecole des Mines de Paris, Mémoires des Sciences de la Terre, v. 7, 355 p.

Parize, O., Beaudoin, B., Eckert, S., Hadj-Hassen, F., Tijani, M., de Fouquet, C., Vandromme, R., Friès, G., Schneider, F., Su, K., and Trouiller, A., 2007, The Vocontian Aptian and Albian syndepositional clastic sills and dikes: a field-based mechanical approach to predict and model the early fracturing of marly-limy sediments, *in* Hurst, A., and Cartwright, J. A., editors, Sand injectites: Implications for

hydrocarbon exploration and production: American Association of Petroleum Geologists Memoir, v. 87, p. 163–172, https://doi.org/10.1306/1209860M873262
Payne, M. B., 1951, Type Moreno Formation and overlying Eocene strata on the west side of the San Joaquin Valley, Fresno and Merced Counties: California Division of Mines and Geology, Special Report, v. 9, 17 p.
Payne, M. B., 1962, Type Panoche Group (Upper Cretaceous) and overlying Moreno and Tertiary strata on the west side of the San Joaquin Valley, *in* Bowen, O.E. editor, Geologic guide to the gas and oil fields of northern California: California Division of Mines and Geology Bulletin, v. 181, p. 165–175.
Peters, K. E., Magoon, L. B., Lampe, C., Scheirer, H. A., Lillis, P. G., and Gautier, D. L., 2008, A four-dimensional petroleum systems model for the San Joaquin Basin Province, California, *in* Scheirer, H. A., editor, Petroleum Systems and Geologic Assessment of Oil and Gas in the San Joaquin Basin Province, California: United States Geological Survey, Professional Papers 1713-12, https://doi.org/10.3133/pp171312
Pollard, D. D., Muller, O. H., and Dockstader, D. R., 1975, The form and growth of fingered sheet intrusions: Geological Society of America Bulletin, v. 86, n. 3, p. 351–363, https://doi.org/10.1130/0016-7606(1975)86<351:TFAGOF>2.0.CO;2
Ramseyer, K., and Boles, J. R., 1986, Mixed-layer illite/smectite minerals in Tertiary sandstone and shales, San Joaquin basin, California: Clays and Clay Minerals, v. 34, p. 115–124, https://doi.org/10.1346/CCMN.1986.0340202
Ravier, E., Guiraud, M., Guillien, A., Vennin, E., Buoncristiani, J. F., and Portier, E., 2015, Micro- to macroscale internal structures, diagenesis and petrophysical evolution of injectite networks in the Vocontian Basin (France): Implications for fluid flow: Marine and Petroleum Geology, v. 64, p. 125–151, https://doi.org/10.1016/j.marpetgeo.2015.02.040
Robertson, J., Goulty, N. R., and Swarbrick, R. E., 2013, Overpressure distributions in Palaeogene reservoirs of the UK Central North Sea and implications for lateral and vertical fluid flow: Petroleum Geoscience, v. 19, p. 223–236, https://doi.org/10.1144/petgeo2012-060
Rodrigues, N., Cobbold, P. R., and Løseth, H., 2009, Physical modelling of sand injectites: Tectonophysics, v. 474, n. 3–4, p. 610–632, https://doi.org/10.1016/j.tecto.2009.04.032
Rodríguez-Pascua, M. A., Silva, P. G., Pérez-López, R., Giner-Robles, J. L., Martín-González, F., and Del Moral, B., 2015, Polygenetic sand volcanoes: on the features of liquefaction processes generated by a single event (2012 Emilia Romagna 5.9 Mw earthquake, Italy): Quaternary International, v. 357, p. 329–335, https://doi.org/10.1016/j.quaint.2014.09.020
Ross, J. A., Peakall, J., and Keevil, G. M., 2014, Facies and flow regimes of sandstone-hosted columnar intrusions: insights from the pipes of Kodachrome Basin State Park: Sedimentology, v. 61, n. 6, p. 1764–1792, https://doi.org/10.1111/sed.12115
Rubin, A. M., 1995, Propagation of magma-filled cracks: Annual Review of Earth and Planetary Sciences, v. 23, p. 287–336, https://doi.org/10.1146/annurev.ea.23.050195.001443
Sacks, A., Saffer, D. M., and Fisher, D., 2013, Analysis of normal fault populations in the Kumano forearc basin, Nankai Trough, Japan: 2. Principal axes of stress and strain from inversion of fault orientations: Geochemistry, Geophysics, Geosystems, v. 14, n. 6, p. 1973–1988, https://doi.org/10.1002/ggge.20118
Saffer, D. M., Flemings, P. B., Boutt, D., Doan, M. L., Ito, T., McNeill, L., Byrne, T., Conin, M., Lin, W., Kano, Y., Araki, E., Eguchi, N., and Toczko, S., 2013, In situ stress and pore pressure in the Kumano Forearc Basin, offshore SW Honshu from downhole measurements during riser drilling: Geochemistry, Geophysics, Geosystems, v. 14, n. 5, p. 1454–1470, https://doi.org/10.1002/ggge.20051
Satur, N., Hurst, A., Bang, A., Skjærpe, I., and Muehlboeck, S. A., 2021, Characteristics of a wing-like sandstone intrusion, Volund Field, *in* Silcock, S., Huuse, M., Bowman, M., Hurst, A., and Cobain, S., editors, Subsurface sand remobilisation and injection: Geological Society, London, Special Publication, v. 493, https://doi.org/10.1144/SP493-2017-309
Schneider, F., Nadeau, P. H., and Hay, S., 2003, Model of shale permeability as a function of the temperature: application to Mesozoic mudstones, Norwegian Continental Shelf: European Association of Geoscientists and Engineers, Annual Meeting, 65th EAGE Conference & Exhibition, Program Abstract C26, https://doi.org/10.3997/2214-4609-pdb.6.C26
Schofield, N., Jerram, D. A., Holford, S., Archer, S., Mark, N., Hartley, A., Howell, J., Muirhead, D., Green, P., Hutton, D., and Stevenson, C., 2016, Sills in sedimentary basins and petroleum systems, *in* Breitkreuz, C., and Rocchi, S., editors, Physical Geology of Shallow Magmatic Systems: Springer, Advances in Volcanology, p. 273–294, https://doi.org/10.1007/11157_2015_17
Schwab, A. M., Jameson, E. W., and Townsley, A., 2015, Volund field: development of an Eocene sandstone injection complex, offshore Norway, *in* McKie, T., Rose, P. T. S., Hartley, A. J., Jones, D. W., and Armstrong, T. L., editors, Tertiary deep-marine reservoirs of the North Sea region: Geological Society, London, Special Publications, v. 403, p. 247–260, https://doi.org/10.1144/SP403.4
Schwartz, H., Sample, J., Weberling, K. D., Minisini, D., and Moore, J. C., 2003, An ancient linked fluid migration system: cold-seep deposits and sandstone intrusions in the Panoche Hills, California, USA: Geo-Marine Letters, v. 23, p. 340–350, https://doi.org/10.1007/s00367-003-0142-1
Scott, A. J. S., ms, 2009, Processes of sand injection: relationships with host strata, internal structures, and permeability implications: Ph.D. thesis, University Aberdeen, Aberdeen, United Kingdom, 299 p.
Scott, A., Vigorito, M., and Hurst., A., 2009, The process of sand injection: internal structures and relationships with host strata (Yellowbank Creek Injectite Complex, California, USA): Journal of Sedimentary Research, v. 79, n. 8, p. 568–583, https://doi.org/10.2110/jsr.2009.062
Scott, A., Hurst, A., and Vigorito, M., 2013, Outcrop-based reservoir characterization of a kilometer-scale sand-injectite complex: American Association of Petroleum Geologists Bulletin, v. 97, p. 309–343, https://doi.org/10.1306/05141211184

Seed, H. B., 1968, Landslides during earthquakes due to soil liquefaction: American Society of Civil Engineers, Journal of Soil Mechanics and Foundations Division, v. 94, n. 5, p. 1055–1122, https://doi.org/10.1061/JSFEAQ.0001182

Seed, H. B., and Idriss, I. M., 1971, Simplified procedure for evaluating soil liquifaction potential: American Society of Civil Engineers, Journal of Soil Mechanics and Foundations Division, v. 97, n . 9, p. 1249–1273, https://doi.org/10.1061/JSFEAQ.0001662

Serié, C., and Pemberton, E., 2021, A new hydrocarbon exploration play: Upper Cretaceous-Palaeocene sand injection complexes in the Austral-Magallanes Basin, *in* Silcock, S., Huuse, M., Bowman, M., Hurst, A., and Cobain, S., editors, Subsurface sand remobilisation and injection: Geological Society, London, Special Publication, v. 493, https://doi.org/10.1144/SP493-2018-179

Shanmugam, G., 2016, The seismite problem: Journal of Palaeogeography, v. 5, n. 4, p. 318–362, https://doi.org/10.1016/j.jop.2016.06.002

Shoulders, S. J., ms, 2005, The mechanics of large-scale sandstone intrusions: Ph.D. thesis, University of Cardiff, Wales, 295 p.

Shoulders, S. J., and Cartwright, J., 2004, Constraints on the timing and depth of intrusion of giant conical sandstone intrusions: Geology, v. 32, n. 8, p. 661–664, https://doi.org/10.1130/G20654.1

Sibson, R., 1990, Conditions for fault-valve behaviour, *in* Knipe, R. J., and Rutter, E. H., editors, Deformation mechanisms, rheology and tectonics, Geological Society, London, Special Publication, v. 54, p. 15–28, https://doi.org/10.1144/GSL.SP.1990.054.01.02

Silcock, S., Huuse, M., Bowman, M., Hurst, A., and Cobain, S., 2021, Subsurface Sand Remobilization and Injection: Geological Society, London, Special Publications, v. 493, 328 p.,10.1144/SP493

Skjærpe, I., Tøllefsen, I., and Endresen, T., 2018, Developing Viper-Kobra: maximizing recovery by exploiting the unique characteristics of the sand injectite environment: European Association of Geoscientists and Engineers, 80th EAGE Conference and Exhibition, v. 2018, p. 1–5, https://doi.org/10.3997/2214-4609.201801426

Smith, C. A., and Berry, R. W., 1988, Smectite dehydration and gas production in Forbes Formation, Sacramento Valley, California: American Association of Petroleum Geologists Bulletin, AAPG-SEPM-SEG Pacific Sections and SPWLA Annual Convention, Santa Barbara, California, 17–19 April 1988, v. 72.

Smyers, N. B., and Peterson, G. L., 1971, Sandstone dikes and sills in the Moreno Shale, Panoche Hills, California: Geological Society of America Bulletin, v. 82, n. 11, p. 3201–3208, https://doi.org/10.1130/0016-7606(1971)82[3201:SDASIT]2.0.CO;2

Sneddon, I. N., and Lowengrub, M., 1969, Crack problems in the classical theory of elasticity: New York, Wiley, 221 p.

Stanzione, O., Hurst, A., Vigorito, M., Scott, A., Vettel, W., Cartwright, J., and Moreau, J., 2008, An example from the Panoche Formation (California, USA) of post-depositional deformations of turbidite channels and lobes through liquefaction-fluidisation processes: implications for reservoir modelling: 70th European Association of Geoscientists and Engineers Congress and Exhibition, Rome, May 2008 - extended abstract - A037.

Stewart, D., and Knox, R., 1995, What is the Maximum Depth Liquefaction Can Occur?: 3rd International Conference on Recent Advances in Geotechnical Earthquake Engineering and Soil Dynamics, 27, Paper 3.55, p. 1157–1161.

Strongin, O., 1981, Identification of geopressured occurrences outside of the Gulf Coast: US Department of Energy, Science Applications, Inc., DOE/NV/10133-2, 114 p., https://doi.org/10.2172/6481456

Surlyk, F., and Noe-Nygaard, N., 2003, A Giant Sand Injection Complex: The Upper Jurassic Hareelv Formation of East Greenland: Geologia Croatica, v. 56, n. 1, p. 69–81, https://doi.org/10.4154/GC.2003.04

Surlyk, F., Noe-Nygaard, N., and Gjelberg, J., 2007, The Upper Jurassic Harleev Formation of East Greenland: A giant sedimentary injection complex, *in* Hurst, A., and Cartwright, J., editors, Sand injectites: implications for hydrocarbon exploration and production: American Association of Petroleum Geologists Memoir, v. 87, p. 141–150, https://doi.org/10.1306/1209858M871101

Swarbrick, R. E., and Osborne, M. J., 1998, Mechanisms which generate abnormal pressures: an overview, *in* Law, B. E., Ulmishek, G. F., and Slavin, V. I., editors, Abnormal pressures in hydrocarbon environments: American Association of Petroleum Geologists Memoir, v. 70, p. 13–34.

Taylor, B. J., 1982, Sedimentary dykes, pipes and related structures in the Mesozoic sediments of south-eastern Alexander Island: British Antarctic Survey Bulletin, v. 51, p. 1–42.

Terzaghi, K., 1925, Principles of Soil Mechanics: Engineering News-Record, v. 95, p. 19–27.

Tingay, M., 2010, Anatomy of the 'Lusi' Mud Eruption, East Java: ASEG Extended Abstracts, v. 2010, n. 1, p. 1–6, https://doi.org/10.1081/22020586.2010.12042009

Tuttle, M. P., Hartleb, R., Wolf, L., and Mayne, P. W., 2019, Paleoliquefaction Studies and the Evaluation of Seismic Hazard: Geosciences, v. 9, n. 7, 311, https://doi.org/10.3390/geosciences9070311

Valkó, P., and Economides, M. J., 1995, Hydraulic Fracture Mechanics: Wiley, New York, v. 28, 318 p.

Van Oorschot, L. A., Pyle, J. R., Byerley, G. W., and Rose, P. T. S., 2021, Development of the Brimmond sand, airway: *in* Silcock, S., Huuse, M., Bowman, M., Hurst, A., and Cobain, S., editors, Subsurface Sand Remobilization and Injection: Geological Society of London, Special Publication, v. 493, p. 167–180, https://doi.org/10.1144/SP493-2017-350

Van Loon, A. J., and Maulik, P., 2011, Abraded sand volcanoes as a tool for recognizing paleoearthquakes, with examples from the Cisuralian Talchir formation near Angul (Orissa, eastern India): Sedimentary Geology, v. 238, n. 1–2, p. 145–155, https://doi.org/10.1016/j.sedgeo.2011.04.009

Van Rensbergen, P., Hillis, R. R., Maltman, A., and Morley, C. K., 2003, Subsurface Sediment Mobilization, Geological Society, London, Special Publications, v. 216, 522 p., https://doi.org/10.1144/GSL.SP.2003.216.01.01

Vétel, W., and Cartwright, J. A., 2010, Emplacement mechanics of sandstone intrusions: insights from the Panoche Giant Injection Complex, California: Basin Research, v. 22, n. 5, p. 783–807, https://doi.org/10.1111/j.1365-2117.2009.00439.x

Vigorito, M., and Hurst, A., 2007, Outcrop analogues for reservoir-scale conical intrusions: European Association of Geoscientists and Engineers, 69th EAGE Conference and Exhibition, 11 June 2007, extended abstract P131, https://doi.org/10.3997/2214-4609.201401822

Vigorito, M., and Hurst, A., 2010, Regional sand injectite architecture as a record of pore-pressure evolution and sand redistribution in the shallow crust: insights from the Panoche Giant Injection Complex, California: Journal of the Geological Society, v. 167, p. 889–904., https://doi.org/10.1144/0016-76492010-004

Vigorito, M., Hurst, A., Scott, A., and Cartwright, J., 2007, Seismic Modelling of Large-Scale Conical Intrusions: American Association of Petroleum Geologists Convention, Long Beach, 2007, Abstract Book.

Vigorito, M., Hurst, A., Cartwright, J., and Scott, A., 2008, Regional-scale subsurface crustal sediment remobilization: geometry and architecture: Journal of the Geological Societt, v. 165, n. 3, p. 609–612, https://doi.org/10.1144/0016-76492007-096

Villemure, M., Wilson, T. M., Bristow, D., Gallagher, M., Giovinazzi, S., and Brown, C., 2012, Liquefaction ejecta clean-up in Christchurch during the 2010-2011 earthquake sequence: Annual NZSSE Conference, New Zealand Society for Earthquake Engineering, 131.

Walderhaug, O., 1994, Precipitation rates for quartz cement in sandstones determined by fluid-inclusion microthermometry and temperature-history modeling: Journal of Sedimentary Research, v. 64, n. 2a, p. 324–333, https://doi.org/10.2110/jsr.64.324

Walderhaug, O., 1996. Kinetic modeling of quartz cementation and porosity loss in deeply buried sandstone reservoirs: American Association of Petroleum Geologists Bulletin, v. 80, n. 5, p. 731–745, https://doi.org/10.1306/64ED88A4-1724-11D7-8645000102C1865D

Walderhaug, O., Bjørkum, P. A., Nadeau, P. H., and Langnes, O., 2001, Quantitative modelling of basin subsidence caused by temperature-driven silica dissolution and reprecipitation: Petroleum Geoscience, v. 7, p. 107–113, https://doi.org/10.1144/petgeo.7.2.107

Weberling, K. D., ms, 2002, Clastic intrusions and cold seeps in the Late Cretaceous-early Tertiary Great Valley forearc basin. Panoche Hills, CA: Structural context of a linked fluid system: Master Thesis, University of California, Santa Cruz, 48 p.

Wentworth, C. M., Blake, M. C. Jr., Jones, D. L., Walter, A. W., and Zoback, M. D., 1984, Tectonic wedging associated with emplacement of the Franciscan Assemblage, California Coast Ranges, *in* Blake, M. C Jr., editor, Franciscan geology of northern California: Pacific Section, Society of Economic Paleontologists and Mineralogists Book, v. 43, p. 163–173.

Wild, J., and Briedis, N., 2010, Structural and stratigraphic relationships of the Palaeocene mounds of the Utsira High: Basin Research, v. 22, n. 4, p. 533–547, https://doi.org/10.1111/j.1365-2117.2010.00479.x

Wilson, A. M., Garven, G., and Boles, J. R., 1999, Paleohydrogeology of the San Joaquin Basin, California: Geological Society of America Bulletin, v. 111, n. 3, p. 432–449, https://doi.org/10.1130/0016-7606(1999)111<0432:POTSJB>2.3.CO;2

Wu, F., Hurst, A., and Grippa, A., 2018, Grain and pore microtexture in sandstone sill and depositional sandstone reservoirs: preliminary insights: Petroleum Geoscience, v. 24, n. 2, p. 236–243, https://doi.org/10.1144/petgeo2017-027

Yeseul, K., Changyeol, L., and Young, L. E., 2018, Numerical analysis of sedimentary compaction: implications for porosity and layer thickness variation: Journal of the Geological Society of Korea, v. 54, n. 6, p. 631–640. https://doi.org/10.14770/jgsk.2018.54.6.631

Zvirtes, G., Hurst, A., Philipp, R. P., Palladino, G., and Grippa, A., 2021, The Tumey Giant Injection Complex, Tumey Hill, California (USA), in Silcock, S., Huuse, M., Bowman, M., Hurst, A., and Cobain, S., editors, Subsurface Sand Remobilization and Injection: Geological Society of London, Special Publication, v. 493, p. 181-214, https://doi.org/10.1144/SP493-2019-3